colloids and interfaces

MDPI

Review

Comprehensive Rheology of Dilute Emulsions

Rajinder Pal

Department of Chemical Engineering, University of Waterloo, Waterloo, ON N2L 3G1, Canada; rpal@uwaterloo.ca

Abstract

The rheology of dilute emulsions is reviewed comprehensively. The fundamental equations governing the flow fields inside and outside the droplets are discussed, along with the boundary conditions. The rheological constitutive law for dilute emulsions with pure interfaces characterized by interfacial tension is developed using the flow field external to the droplets. Both zero-order and first-order deformations of droplets are considered. Dilute emulsions exhibit non-Newtonian behavior. The influences of surface charge and surfactants on the emulsion rheology are covered in detail. The rheology of emulsions of double droplets and droplets covered with elastic membranes is covered as well. Finally, a significant section of the review is focused on the dynamic rheology of dilute emulsions. Emulsions with pure interfaces and additive-laden interfaces are considered. The theories developed for the dynamic rheology of emulsions consisting of different types of interfaces are reviewed, including purely viscous interfaces, purely elastic interfaces, viscoelastic interfaces, and interfaces possessing bending rigidity. In general, the theory for dilute emulsion rheology is well developed. Our current understanding of dilute emulsion rheology is good from a theoretical point of view. A priori predictions of dilute emulsion rheology are possible using the existing theories. However, serious gaps in the existing knowledge on dilute emulsion rheology remain. This review identifies the gaps in existing knowledge and points out future directions in research related to dilute emulsion rheology.

Keywords: emulsions; droplets; rheology; non-Newtonian; dynamic rheology; viscosity; shear-thinning; storage modulus; loss modulus; normal stress

1. Introduction

Emulsions are blends of two immiscible liquids. Emulsions can generally be categorized into two classes: (a) oil-in-water (denoted O/W) emulsions, and (b) water-in-oil (denoted W/O) emulsions. Oil droplets form the dispersed phase in the case of O/W emulsions, whereas water droplets are dispersed in W/O emulsions.

Crude oil is often produced as an emulsion [1–7]. Emulsions find widespread usage in oil-well drilling [8] and oil-well fracturing and acidizing processes [9] for one reason or another. In some oil production applications, emulsions can be intentionally produced from the oil well. For example, when the crude oil being produced is highly viscous in nature, it is desirable to transform the viscous oil into an O/W emulsion as a low-viscosity fluid by injection of an appropriate surfactant solution into the oil well [10–13].

Dilute emulsions find applications as sprays in crop protection. The spraying of dilute emulsions instead of water produces coarser sprays compared to water when atomized. This reduces the drift risk of agricultural chemicals [14]. Dilute emulsions can also be used in boiling applications. They produce high heat flux and are, therefore, useful in the efficient cooling of electronics [15].

Check for updates

Academic Editors: Reinhard Miller and Ramón G. Rubio

Received: 26 March 2026
Revised: 25 April 2026
Accepted: 6 May 2026
Published: 8 May 2026

Copyright: © 2026 by the author. Licensee MDPI, Basel, Switzerland. This article is an open access article distributed under the terms and conditions of the Creative Commons Attribution (CC BY) license.

Emulsion technology could be applied in the pipeline transportation of highly viscous crude oils by first converting crude oils into O/W emulsions [16–21] and then transporting the emulsions instead of crude oil through the pipeline. The viscosity of O/W emulsions is generally very low in comparison to that of the crude oil alone [21]. The energy required to pump emulsions is only a fraction of that required to pump the crude oil alone. A pipeline 21 km in length and 20 cm in diameter in California and a pipeline 238 km in length and 51 cm in diameter in Indonesia [16–21] are in use for the transportation of oil in emulsion form. Emulsions are also used in enhanced oil recovery processes as oil displacement fluids [22,23]. They can also act as blocking agents to alter the permeability of reservoirs [24].

Emulsions find applications in many other industries [25–46] such as food and medicine. Many creams and cosmetics are produced and sold in emulsion form [36,38,39]. Emulsions are used as insecticides [29,40,41]. Certain explosives are produced in emulsion form [42]. Emulsions are used as fat liquors to treat leather [29]. The antistatic agents used in the textile industry are often in the form of emulsions [29].

Emulsions are equally important in the paints industry [29,44]. Emulsion paints are superior compared to solvent-based paints. Emulsions are extensively used as lubricants for drilling and cutting tools [45]. The construction of roads utilizes bitumen emulsions [29,43]. Emulsions can also be used for the transportation of hazardous materials such as liquid explosives.

Dense emulsions are suitable as printing inks in 3D printing, as they exhibit shear-thinning, storage modulus, and yield stress, characteristics ideally suitable for 3D printing inks [46]. Emulsions are also used widely in the production of a variety of porous materials [46].

The rheology of emulsions is important in most of the applications discussed above. For instance, the key rheological property required in the estimation of pumping energy for the pipeline transportation of emulsion is emulsion viscosity and its variation with shear rate. In practical applications, the dispersed-phase concentration of emulsion may vary from a few volume percent to very concentrated systems where the droplets are jam-packed against each other. However, this review is focused on the rheology of dilute emulsions where the volume fraction of droplets (φ) is typically less than 0.05. Understanding the rheology of dilute emulsions is important from both theoretical and practical points of view. Due to the diluteness of emulsions and the consequent lack of any interactions between the droplets, it is possible to develop exact rheological constitutive laws for dilute emulsions using rigorous single-droplet mechanics.

2. Influence of Flow Field on Deformation and Breakup of Droplets

The droplet deforms when it is subjected to shear [47–64]. The shape and orientation of the droplet are governed by the viscosity ratio λ (ratio of η_d to η_c, where η_d is dispersed-phase viscosity and η_c is matrix viscosity) and capillary number N_{Ca}, given as:

$$N_{Ca} = \frac{\eta_c \dot{\gamma} R}{\gamma} \quad (1)$$

where $\dot{\gamma}$, R, and γ are the shear rate, undeformed droplet radius, and interfacial tension, respectively. The droplet deforms as shown in Figure 1. The deformation parameter D of the droplet is given as:

$$D = \frac{L - B}{L + B} \quad (2)$$

where L and B are the lengths of the major and minor axes, respectively, of the deformed droplet (see Figure 1). With the increase in N_{Ca}, the droplet deforms and becomes more

stretched (D increases) and oriented with the flow direction. The angle θ between the droplet's major axis and flow direction decreases toward zero (see Figure 1) with the increase in N_{Ca}. For small deformations ($D \leq 0.30$; $N_{Ca} \ll 1$):

$$D = \left(\frac{19\lambda + 16}{16\lambda + 16}\right) N_{Ca} \tag{3}$$

$$\theta = \frac{\pi}{4} - \left(\frac{2\lambda + 3}{5}\right)\left(\frac{19\lambda + 16}{16\lambda + 16}\right) N_{Ca} \tag{4}$$

For large deformations, the following model developed by Maffetone and Minale is applicable [65]:

$$D = \frac{\sqrt{f_1^2 + N_{Ca}^2} - \sqrt{f_1^2 + N_{Ca}^2 - f_2^2 N_{Ca}^2}}{f_2 N_{Ca}} \tag{5}$$

$$f_1 = \frac{40(\lambda + 1)}{(2\lambda + 3)(19\lambda + 16)} \tag{6}$$

$$f_2 = \frac{5}{(2\lambda + 3)} + \frac{3N_{Ca}^2}{2 + 6N_{Ca}^2} \tag{7}$$

$$\theta = \frac{1}{2} arctan\left(\frac{f_1}{N_{Ca}}\right) \tag{8}$$

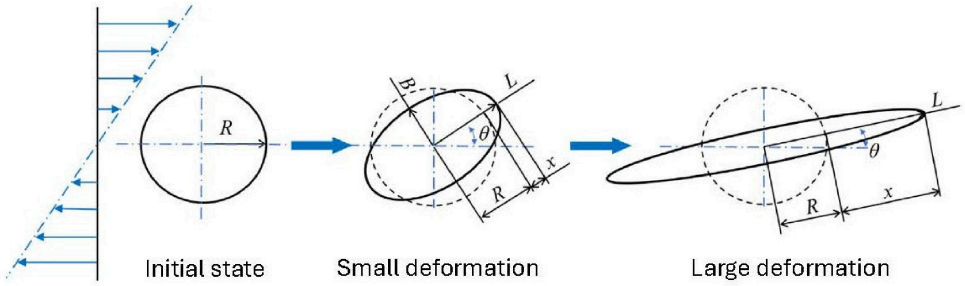


Figure 1. Droplet deformation in shear flow. Adapted from [65].

Figure 2 shows the variations in droplet deformation D and orientation angle θ with the capillary number. As expected, both Taylor and Maffetone and Minale (MM) models predict an increase in D and a decrease in θ; that is, the droplets become elongated and oriented in the flow direction with the increase in N_{Ca}. However, the two models deviate from each other when $N_{Ca} > 0.2$. The experimental data follows the MM model more closely at high N_{Ca}.

The emulsion exhibits pseudoplastic rheological behavior; that is, the viscosity decreases with the increase in N_{Ca}, due to the elongation (increase in D) and streamlining of droplets (decrease in angle θ) with the flow as illustrated in Figure 2. The emulsions also exhibit normal stresses in shear flows and strain thickening in elongational flows [66–72] due to the elasticity of the shape of the droplets.

It is important to recognize that the droplets do not continue to elongate and orient with the increase in capillary number. When $N_{Ca} > N_{Ca,crit}$, no stable droplet shape is possible, and the droplet undergoes breaking. The breakup of droplets is shown schematically in Figure 3. The breakup usually occurs with two different modes. When N_{Ca} is just above $N_{Ca,crit}$, a simple breakup of deformed droplets occurs, resulting in two smaller droplets. If N_{Ca} is much larger than $N_{Ca,crit}$, the so-called Rayleigh breakup of a deformed droplet into many droplets occurs [73,74]. The $N_{Ca,crit}$ depends on λ [56] for a given type of flow field.

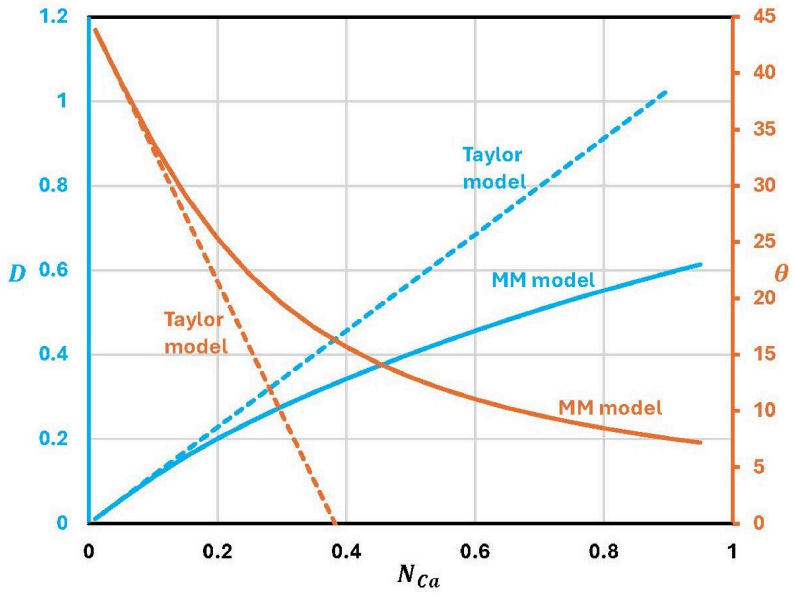


Figure 2. Variations in deformation parameter D and orientation angle θ with capillary number for $\lambda = 3$.

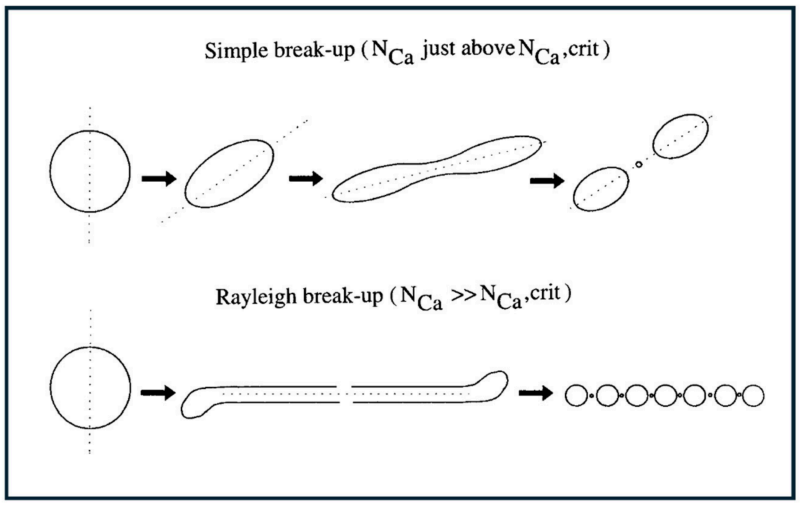


Figure 3. Simple and Rayleigh breakups of droplets in simple shear.

Grace [56] conducted extensive experimental work on the breakup of droplets covering a broad range of λ. The variations in $N_{Ca,crit}$ with λ are shown in Figure 4. The droplet breakup is easy in shear flow if $0.1 < \lambda < 1$. However, the $N_{Ca,crit}$ tends to rise sharply when $\lambda > 4$. As a result, the breaking up of droplets is difficult in shear flow when $\lambda > 4$. If the viscosity ratio $\lambda < 0.01$, the droplet undergoes a large deformation without any breakup in shear flow, as the $N_{Ca,crit}$ is large. The experimental data fits the following criterion for low-viscosity droplets ($\lambda < 0.01$) [55]:

$$N_{Ca,crit} = 0.054\lambda^{-2/3} \tag{9}$$

The experimental $N_{Ca,crit}$ data in shear flow over the viscosity range of $10^{-3} < \lambda < 10$ can be described as [75]:

$$logN_{Ca,crit} = a + blog\lambda + c(log\lambda)^2 + \frac{d}{log\lambda - log\lambda_c} \tag{10}$$

where $a = -0.506$, $b = -0.0994$, $c = 0.124$, $d = -0.115$, and $\lambda_c = 4.08$. However, the picture is different in elongational flow. Now, the $N_{Ca,crit}$ is usually small (Figure 4) for all viscosity ratios, and, therefore, the breakup of droplets is easier.

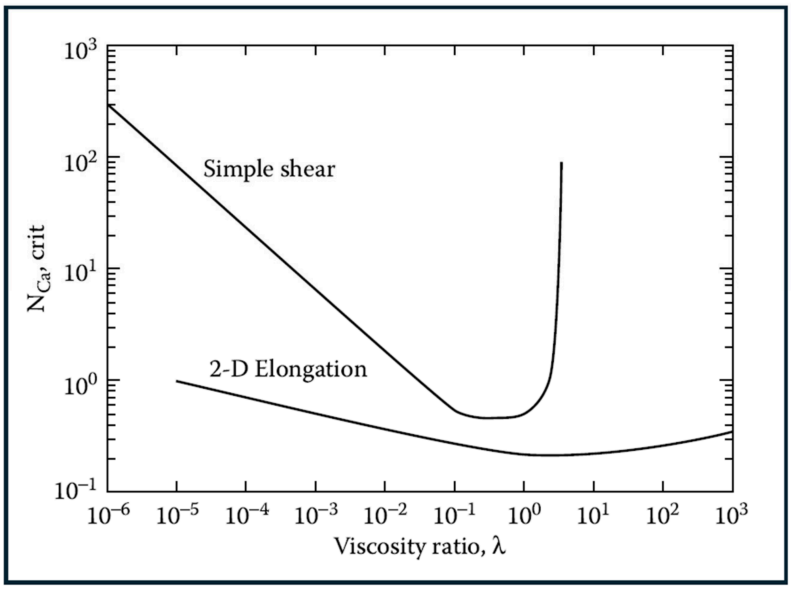


Figure 4. $N_{Ca,crit}$ versus λ in shear and elongational flows.

The effect of surfactants is not considered in the preceding discussion on the deformation and breakup of droplets. Surfactant-laden droplets behave differently from surfactant-free pure droplets [60,74]. Surfactant-free droplets and surfactant-laden droplets do not deform in the same way even at the same λ and N_{Ca}. The surfactant reduces the interfacial tension and leads to the generation of Marangoni stresses. The Marangoni stresses act against surface deformation and tend to immobilize the droplet interface.

Modeling emulsion rheology is difficult, as the droplets are deformable. It is not easy to satisfy the boundary conditions on the surface of the droplet as it is deforming. Droplet shape and flow fields need to be determined at the same time. Such "free-surface type" problems can be solved using a domain perturbation method [63,64,69,76].

3. Microhydrodynamics of Emulsion: Governing Equations and Boundary Conditions

Consider a droplet spherical in shape of radius R suspended in a liquid of viscosity η_c. The droplet is neutrally buoyant. The liquid inside the droplet is assumed to be of viscosity $\lambda\eta_c$. Furthermore, the two liquids are treated as incompressible. When the droplet suspended in matrix liquid is subjected to flow, it deforms. The equation of the droplet surface with respect to a set of axes fixed at the center of the droplet can be written as:

$$r = \left(x_1^2 + x_2^2 + x_3^2\right)^{1/2} = f(x_1, x_2, x_3) \tag{11}$$

where r is the distance from the droplet center of mass to the interface. Assuming creeping flow, the system can be described by the following equations with respect to a reference frame fixed on the droplet's center:

$$\eta_c \nabla^2 \vec{u} - \nabla P = 0 \qquad \nabla \bullet \vec{u} = 0 \qquad for\, r > f \tag{12}$$

$$\lambda\eta_c \nabla^2 \vec{u}^* - \nabla P^* = 0 \qquad \nabla \bullet \vec{u}^* = 0 \qquad for\, r < f \tag{13}$$

where $\vec{u}$ is the fluid velocity vector, P is pressure, η_c is the continuous-phase viscosity, λ is the viscosity ratio, and the starred quantities refer to the inside of the droplet.

The boundary conditions are:

(i)

$$\vec{u} \rightarrow \vec{u}_\infty \; as \; r \rightarrow \infty \tag{14}$$

(ii) There is a continuity of tangential and normal velocities at the interface

$$(\vec{u} - \vec{u} \bullet \hat{n}\hat{n}) = (\vec{u}^* - \vec{u}^* \bullet \hat{n}\hat{n}) \tag{15}$$

$$\vec{u} \bullet \hat{n} = \vec{u}^* \bullet \hat{n} = u_{\text{interface}} \tag{16}$$

where $u_{\text{interface}}$ is the interface velocity.

(iii) There is a continuity of tangential and normal stresses at the interface

$$(\bar{\bar{\sigma}} \bullet \hat{n} - \hat{n} \bullet \bar{\bar{\sigma}} \bullet \hat{n}\hat{n}) = (\bar{\bar{\sigma}}^* \bullet \hat{n} - \hat{n} \bullet \bar{\bar{\sigma}}^* \bullet \hat{n}\hat{n}) \tag{17}$$

$$\hat{n} \bullet (\bar{\bar{\sigma}} - \bar{\bar{\sigma}}^*) \bullet \hat{n} = -(\nabla_s \bullet \bar{\bar{P}}_s) \bullet \hat{n} \tag{18}$$

where $\nabla_s = \left(\bar{\bar{\delta}} - \hat{n}\hat{n}\right) \bullet \nabla$ and $\bar{\bar{P}}_s$ is the surface stress tensor given as:

$$\bar{\bar{P}}_s = \gamma(\bar{\bar{\delta}} - \hat{n}\hat{n}) \tag{19}$$

where γ is the interfacial tension.

The flow fields outside and inside the droplet are obtained through the solution of Equations (12) and (13), respectively, subject to the above-listed boundary conditions. This problem is not easy to solve as the surface of the droplet is deforming. Analytical results are possible only for a small degree of drop deformation. An iterative technique referred to as "domain perturbation" is applied. In the first iteration, the flow fields are obtained using the continuity of velocity and tangential stress at the undeformed, spherical interface. This gives the zero-order deformation solution for the flow fields. The deviation of the interface from sphericity is then obtained using the normal stress boundary condition. In the second iteration, the flow fields are obtained by satisfying the boundary conditions at the deformed interface.

4. Bulk Stress in Emulsion

The bulk stress tensor in emulsions is the volume-average stress tensor $\left\langle \bar{\bar{\sigma}} \right\rangle$ defined as:

$$\left\langle \bar{\bar{\sigma}} \right\rangle = \frac{1}{V} \iiint \bar{\bar{\sigma}} dV \tag{20}$$

where V is the volume of the emulsion, which consists of a statistically significant number of droplets, but $V^{1/3}$ is smaller than the characteristic macroscale over which the bulk properties of the emulsion change appreciably. For an emulsion, the bulk stress tensor could be split as:

$$\left\langle \bar{\bar{\sigma}} \right\rangle = \left\langle \bar{\bar{\sigma}}_o \right\rangle + \left\langle \bar{\bar{\sigma}}^p \right\rangle \tag{21}$$

where $\left\langle \overline{\overline{\sigma}}_o \right\rangle$ is the stress tensor in the matrix (continuous phase) of the emulsion and $\left\langle \overline{\overline{\sigma}}^p \right\rangle$ is the average contribution of droplets to the bulk stress tensor. For an emulsion of identical droplets, $\left\langle \overline{\overline{\sigma}}^p \right\rangle$ could be further expressed as:

$$\left\langle \overline{\overline{\sigma}}^p \right\rangle = \frac{N}{V} \left\langle \overline{\overline{s}} \right\rangle \tag{22}$$

where N/V is the number density of droplets and $\left\langle \overline{\overline{s}} \right\rangle$ is the average value of the so-called dipole strength of a single droplet. For a very dilute emulsion, $\left\langle \overline{\overline{s}} \right\rangle$ is simply the dipole strength of a single droplet $\overline{\overline{S}}^o$, given as:

$$\overline{\overline{S}}^o = \int_{A_0} \left[\overline{\overline{\sigma}} \bullet \hat{n} \vec{x} - \frac{1}{3} \left(\vec{x} \bullet \overline{\overline{\sigma}} \bullet \hat{n} \right) \overline{\overline{\delta}} - \eta_c \left(\hat{n} \vec{u} + \vec{u} \hat{n} \right) \right] dA \tag{23}$$

where A_0, $\hat{n}$, $\vec{u}$, $\overline{\overline{\sigma}}$, and $\vec{x}$ are the surface area of the droplet, unit outward normal, fluid velocity at the droplet surface, stress tensor at the droplet surface, and position vector, respectively.

The tensor $\overline{\overline{S}}^o$ is also referred to as the Landau–Batchelor tensor in the literature. It depends on the surface traction and velocity distribution over the droplet surface [77]. Thus, $\left\langle \overline{\overline{\sigma}}^p \right\rangle$ could be expressed as:

$$\left\langle \overline{\overline{\sigma}}^p \right\rangle = \frac{3\varphi}{4\pi R^3} \overline{\overline{S}}^o \tag{24}$$

where φ is the volume fraction of droplets in the emulsion and R is the droplet radius. Obviously, knowledge of the flow fields (velocity, stress tensor) is required for the calculation of $\overline{\overline{S}}^o$ and, hence, $\left\langle \overline{\overline{\sigma}}^p \right\rangle$.

The stress tensor in the continuous phase (assuming it is Newtonian) is given as:

$$\left\langle \overline{\overline{\sigma}}_o \right\rangle = -\langle P \rangle \overline{\overline{\delta}} + 2\eta_c \left\langle \overline{\overline{E}} \right\rangle \tag{25}$$

where $\left\langle \overline{\overline{E}} \right\rangle$ is the bulk rate of the strain tensor. Combining Equations (21), (24) and (25), the bulk stress for a dilute emulsion of identical droplets is given as:

$$\left\langle \overline{\overline{\sigma}} \right\rangle = -\langle P \rangle \overline{\overline{\delta}} + 2\eta_c \left\langle \overline{\overline{E}} \right\rangle + \frac{3\varphi}{4\pi R^3} \overline{\overline{S}}^o \tag{26}$$

The velocity and stress distributions around the droplet are needed to evaluate the dipole strength $\overline{\overline{S}}^o$. Thus, we need to solve the governing Equations (12) and (13) subject to the given boundary conditions, that is, Equations (14)–(18).

4.1. Zero-Order Deformation

The zero-order deformation solution of Equations (12) and (13) is obtained by neglecting the deformation of the droplet. Excluding the normal stress discontinuity, that is, Equation (18), all other boundary conditions (Equations (14)–(17)) are satisfied. It is also assumed that $u_{\text{interface}} = 0$.

The solution for the velocity in the continuous phase (matrix) is [76,78–80]:

$$\vec{u}(\vec{x}) = \overline{\overline{E}}_{\infty}\bullet\vec{x} + \vec{\omega}_o \times \vec{x} - \left(\frac{\lambda}{1+\lambda}\right)\left(\frac{R}{r}\right)^5\left(\overline{\overline{E}}_{\infty}\bullet\vec{x}\right) + \frac{\vec{x}\left(\vec{x}\bullet\overline{\overline{E}}_{\infty}\bullet\vec{x}\right)}{r^2}\left[-\left(\frac{2+5\lambda}{2+2\lambda}\right)\left(\frac{R}{r}\right)^3 + \left(\frac{5\lambda}{2+2\lambda}\right)\left(\frac{R}{r}\right)^5\right] \quad (27)$$

where $\overline{\overline{E}}_{\infty}$ is the rate of strain tensor of the undisturbed flow and $\vec{\omega}_o$ is half the vorticity of the undisturbed flow. The pressure distribution in the matrix is:

$$P = P_{\infty} - \left(\frac{2+5\lambda}{1+\lambda}\right)\eta_c\left(\frac{R}{r}\right)^3\left(\frac{\vec{x}\bullet\overline{\overline{E}}_{\infty}\bullet\vec{x}}{r^2}\right) \quad (28)$$

From the knowledge of the velocity field, $\overline{\overline{E}}$ in the continuous phase is obtained as [76,78]:

$$\begin{aligned}\overline{\overline{E}}\left(\vec{x}\right) = \overline{\overline{E}}_{\infty}\left[1 - \left(\tfrac{\lambda}{1+\lambda}\right)\left(\tfrac{R}{r}\right)^5\right] + \left[\frac{\left(\overline{\overline{E}}_{\infty}\bullet\vec{x}\right)\vec{x}+\vec{x}\left(\overline{\overline{E}}_{\infty}\bullet\vec{x}\right)}{r^2}\right]\left[-\left(\tfrac{2+5\lambda}{2+2\lambda}\right)\left(\tfrac{R}{r}\right)^3 + \left(\tfrac{5\lambda}{1+\lambda}\right)\left(\tfrac{R}{r}\right)^5\right]\\ + \left[\left(\tfrac{\vec{x}\vec{x}}{r^2}\right)\left(\tfrac{\vec{x}\bullet\overline{\overline{E}}_{\infty}\bullet\vec{x}}{r^2}\right)\right]\left[\tfrac{5}{2}\left(\tfrac{2+5\lambda}{1+\lambda}\right)\left(\tfrac{R}{r}\right)^3 - \tfrac{35}{2}\left(\tfrac{\lambda}{1+\lambda}\right)\left(\tfrac{R}{r}\right)^5\right] + \left[\left(\tfrac{5\lambda}{2+2\lambda}\right)\left(\tfrac{\vec{x}\bullet\overline{\overline{E}}_{\infty}\bullet\vec{x}}{r^2}\right)\left(\tfrac{R}{r}\right)^5\overline{\overline{\delta}}\right] - \left[\left(\tfrac{2+5\lambda}{2+2\lambda}\right)\left(\tfrac{R}{r}\right)^3\left(\tfrac{\vec{x}\bullet\overline{\overline{E}}_{\infty}\bullet\vec{x}}{r^2}\right)\overline{\overline{\delta}}\right]\end{aligned} \quad (29)$$

The stress tensor in the continuous phase can now be obtained from Equations (28) and (29) by making use of the following equation:

$$\overline{\overline{\sigma}} = -P\overline{\overline{\delta}} + 2\eta_c\overline{\overline{E}} \quad (30)$$

Thus, the stress tensor in the continuous phase is [76]:

$$\begin{aligned}\overline{\overline{\sigma}} = -P_{\infty}\overline{\overline{\delta}} + 2\eta_c\overline{\overline{E}}_{\infty}\left[1 - \left(\tfrac{\lambda}{1+\lambda}\right)\left(\tfrac{R}{r}\right)^5\right] + 2\eta_c\left[\frac{\left(\overline{\overline{E}}_{\infty}\bullet\vec{x}\right)\vec{x}+\vec{x}\left(\overline{\overline{E}}_{\infty}\bullet\vec{x}\right)}{r^2}\right]\left[-\left(\tfrac{2+5\lambda}{2+2\lambda}\right)\left(\tfrac{R}{r}\right)^3 + \left(\tfrac{5\lambda}{1+\lambda}\right)\left(\tfrac{R}{r}\right)^5\right]\\ + 2\eta_c\left[\left(\tfrac{\vec{x}\vec{x}}{r^2}\right)\left(\tfrac{\vec{x}\bullet\overline{\overline{E}}_{\infty}\bullet\vec{x}}{r^2}\right)\right]\left[\tfrac{5}{2}\left(\tfrac{2+5\lambda}{1+\lambda}\right)\left(\tfrac{R}{r}\right)^3 - \tfrac{35}{2}\left(\tfrac{\lambda}{1+\lambda}\right)\left(\tfrac{R}{r}\right)^5\right] + \left[2\eta_c\left(\tfrac{5\lambda}{2+2\lambda}\right)\left(\tfrac{\vec{x}\bullet\overline{\overline{E}}_{\infty}\bullet\vec{x}}{r^2}\right)\left(\tfrac{R}{r}\right)^5\overline{\overline{\delta}}\right]\end{aligned} \quad (31)$$

The dipole strength $\overline{\overline{S}}^{o}$ can now be evaluated from the Landau-Batchelor tensor, Equation (23), using velocity distribution, Equation (27), and stress tensor, Equation (31). Equation (23) yields:

$$\overline{\overline{S}}^{o} = \frac{4}{3}\pi R^3\eta_c\left[\frac{2+5\lambda}{1+\lambda}\right]\overline{\overline{E}}_{\infty} \quad (32)$$

We can equate $\overline{\overline{E}}_{\infty}$ to the imposed rate of strain tensor $\left\langle\overline{\overline{E}}\right\rangle$, as the emulsion is dilute. Therefore, the rheological constitutive law or bulk stress for a dilute emulsion (Equation (26)) can be expressed as:

$$\left\langle\overline{\overline{\sigma}}\right\rangle = -\langle P\rangle\overline{\overline{\delta}} + 2\eta_c\left\langle\overline{\overline{E}}\right\rangle + \varphi\eta_c\left[\frac{2+5\lambda}{1+\lambda}\right]\left\langle\overline{\overline{E}}\right\rangle \quad (33)$$

Dropping off the angular brackets $\langle\ \rangle$ from Equation (33) to simplify the notation, we obtain:

$$\overline{\overline{\sigma}} = -P\overline{\overline{\delta}} + 2\eta_c\left[1 + \frac{2+5\lambda}{2(1+\lambda)}\varphi\right]\overline{\overline{E}} \quad (34)$$

Upon comparing Equation (34) with the Newtonian constitutive law,

$$\bar{\bar{\sigma}} = -P\bar{\bar{\delta}} + 2\eta\bar{\bar{E}} \tag{35}$$

the relative viscosity η_r of a dilute emulsion of spherical droplets can be expressed as:

$$\eta_r = \frac{\eta}{\eta_c} = \left[1 + \frac{2+5\lambda}{2(1+\lambda)}\varphi\right] = 1 + [\eta]\varphi \tag{36}$$

where $[\eta]$ is the intrinsic viscosity. Equation (36) is the well-known Taylor equation [81] for η_r of a dilute emulsion. Figure 5 shows the plot of [η], defined as $(\eta_r - 1)/\varphi$, versus λ. The $[\eta]$ is unity initially at low values of λ, increases with the increase in λ at intermediate values of λ, and finally becomes equal to the Einstein value of 2.5 at high values of λ. Note that the Einstein equation for rigid inclusions is given as [82–84]:

$$\eta_r = 1 + \frac{5}{2}\varphi \tag{37}$$

Figure 6 shows η_r versus φ plots for dilute emulsions. The Taylor equation, Equation (36), is used to generate the plots. The slope of the plot gives the intrinsic viscosity $[\eta]$ that increases with the increase in λ. The $[\eta]$ is 2.5 when $\lambda \to \infty$ and 1.0 when $\lambda \to 0$.

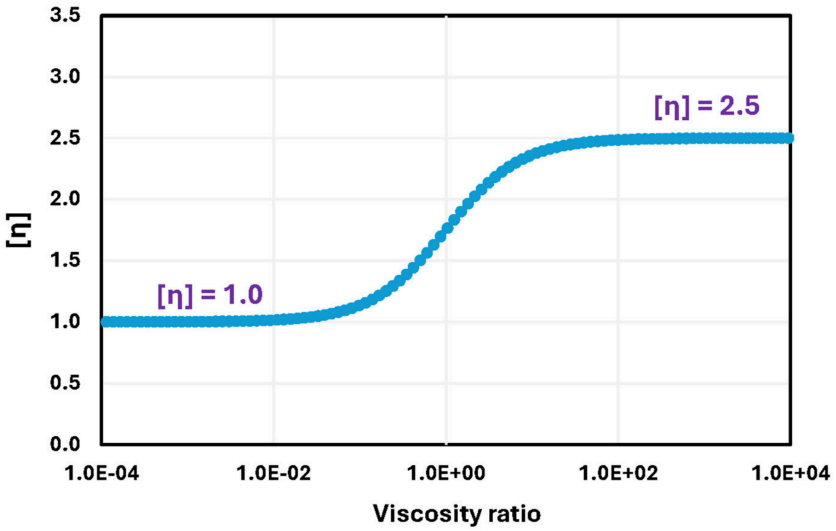


Figure 5. Emulsion $[\eta]$ as a function of λ.

Figure 7 compares experimental viscosity data for emulsions with theoretical predictions. The emulsions tested are toluene-in-glycerol [85] with a viscosity ratio λ of 8.66×10^{-4}. The experimental data show excellent agreement with Equation (36) when $\varphi \leq 0.05$. Equation (36) underestimates η_r at higher concentrations of droplets, as expected. The Taylor equation is developed using single-droplet mechanics and is restricted to very dilute emulsions.

Figure 8 compares the predictions of Equation (37) with experimental data for disperse systems of rigid spheres. The agreement between the data and the predictions is good for $\varphi \leq 0.03$. When $\varphi > 0.03$, the theory underpredicts relative viscosity.

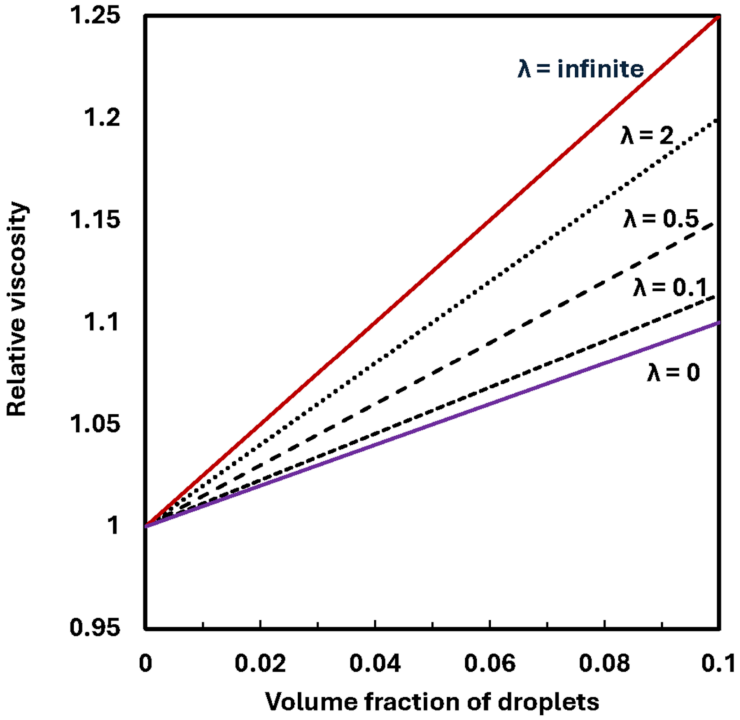


Figure 6. η_r versus φ for different values of λ predicted from the Taylor viscosity equation, Equation (36).

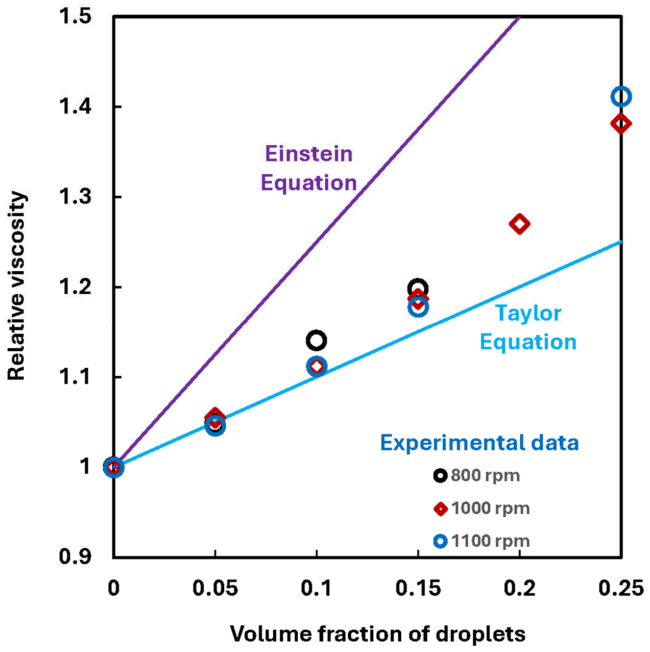


Figure 7. Comparison between experimental η_r and theoretical predictions for emulsions.

The deformation of the droplets is neglected in the zero-order solution of the fundamental equations (Equations (12) and (13)). In the absence of droplet deformation, the emulsion is found to be Newtonian (Equation (34)). The $[\eta]$ does not depend on shear rate and depends only on λ. The $[\eta]$ is equal to unity at low λ (see Figure 5). It increases with the increase in λ at intermediate values of λ, and at high values of λ, it becomes constant, equal to 2.5, corresponding to the Einstein value [83,84] for disperse systems of rigid inclusions.

The rheological constitutive law for dilute emulsions given by Equation (34) is valid under the condition that the deformation of droplets is negligible. Thus, it is valid at

very low rates of deformation. Consequently, Equation (36) is valid in the limit of zero shear rate.

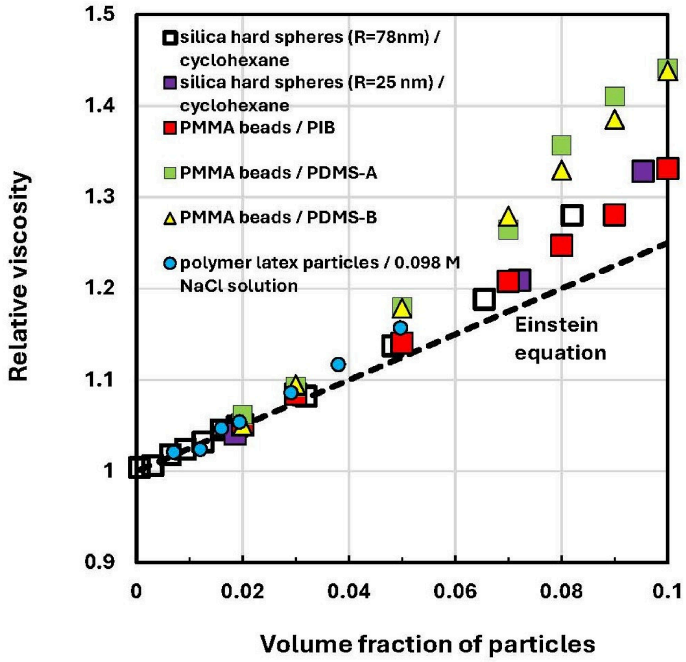


Figure 8. Comparison between experimental η_r and predictions of Equation (37).

Schowalter et al. [66] and, later, Frankel and Acrivos [67] developed a more general constitutive law for dilute emulsions considering the small (first-order) deformation of droplets. The constitutive laws developed by Schowalter et al. [66] and Frankel and Acrivos [67] are described in the following section.

4.2. First-Order Deformation

The small deformation solution is obtained by solving the fundamental equations, that is, Equations (12) and (13), with the boundary conditions now applied at the deformed interface. For the first-order deformation of droplets, the droplet shape can be expressed as:

$$S_i = r^{i+1}\overbrace{\nabla.....\nabla}^{i\ \ times}\left(\frac{1}{r}\right) \tag{38}$$

where S_i is the *ith* surface spherical harmonic. Only the second-order harmonics are sufficient for the first-order deformation of droplets. Thus, the shape of a deformed droplet can be expressed as:

$$\frac{r}{R} = 1 + \varepsilon g \tag{39}$$

where r is the distance to the droplet surface from the droplet center of mass and g is given as:

$$g = \overset{=\prime}{F}(t) : S_2 \tag{40}$$

where $\overset{=\prime}{F}(t)$ is a dimensionless tensor that describes the instantaneous shape of a droplet, and ε is the deformation parameter ($\varepsilon \ll 1$).

In the weak shear flow case ($N_{Ca} << 1$), ε is taken equal to N_{Ca}. Thus, Equation (39) can be re-written as:

$$\frac{r}{R} = 1 + N_{Ca}\left[\overset{=\prime}{F}(t) : S_2\right] \tag{41}$$

According to Schowalter et al. [66], $\overline{\overline{F}}'(t) : S_2$ should be set equal to (in order to satisfy Equation (18)):

$$\overline{\overline{F}}'(t) : S_2 = \left[\frac{19\lambda + 16}{8(1+\lambda)}\right]\left(\frac{\overline{\overline{E}}'_\infty : \vec{r}\,\vec{r}}{r^2}\right) \tag{42}$$

where $\overline{\overline{E}}'_\infty$ is the dimensionless rate-of-strain tensor far away from the droplet. From Equations (41) and (42), it follows that:

$$\frac{r}{R} = 1 + N_{Ca}\left[\frac{19\lambda + 16}{8(1+\lambda)}\right]\left(\frac{\overline{\overline{E}}'_\infty : \vec{r}\,\vec{r}}{r^2}\right) \tag{43}$$

Equation (43) represents the first-order deformation of droplets, originally obtained by Taylor [47], and leads to the following expressions for D and angle θ (see Figure 1):

$$D = N_{Ca}\left(\frac{19\lambda + 16}{16\lambda + 16}\right); \theta = \pi/4 \tag{44}$$

where the deformation parameter D is defined in Equation (2).

Using the first-order flow fields, Schowalter et al. [66] developed the following expression for $\overline{\overline{S}}^o$:

$$\overline{\overline{S}}^o = \frac{4}{3}\pi R^3 \eta_c \left\{ \left(\frac{5\lambda + 2}{1+\lambda}\right)\overline{\overline{E}}_\infty + \left(\frac{\eta_c R}{\gamma}\right)\left[\begin{array}{l} \frac{3(19\lambda+16)\left(25\lambda^2+41\lambda+4\right)}{140(1+\lambda)^3}\left(\overline{\overline{E}}_\infty \bullet \overline{\overline{E}}_\infty - \frac{\overline{\overline{\delta}}}{3}\left(\overline{\overline{E}}_\infty : \overline{\overline{E}}_\infty\right)\right) \\ -\frac{1}{40}\left(\frac{19\lambda+16}{\lambda+1}\right)^2 \frac{D\overline{\overline{E}}_\infty}{Dt} \end{array} \right] \right\} \tag{45}$$

where $D\overline{\overline{E}}_\infty/Dt$ is the Jaumann time derivative of $\overline{\overline{E}}_\infty$. Using Equation (26), the rheological equation for dilute emulsions can be expressed as:

$$\overline{\overline{\sigma}} = -P\overline{\overline{\delta}} + 2\eta_c\overline{\overline{E}} + \varphi\eta_c \left\{ \left(\frac{5\lambda + 2}{1+\lambda}\right)\overline{\overline{E}} + \left(\frac{\eta_c R}{\gamma}\right)\left[\begin{array}{l} \frac{3(19\lambda+16)\left(25\lambda^2+41\lambda+4\right)}{140(1+\lambda)^3}\left(\overline{\overline{E}} \bullet \overline{\overline{E}} - \frac{\overline{\overline{\delta}}}{3}\left(\overline{\overline{E}} : \overline{\overline{E}}\right)\right) \\ -\frac{1}{40}\left(\frac{19\lambda+16}{\lambda+1}\right)^2 \frac{D\overline{\overline{E}}}{Dt} \end{array} \right] \right\} \tag{46}$$

where $\overline{\overline{\sigma}}$, P, and $\overline{\overline{E}}$ are average quantities. This equation is valid for steady or weak time-dependent flows for arbitrary λ and small N_{Ca}. Equation (46) predicts emulsion to be non-Newtonian in that it exhibits non-zero normal stresses, although the viscosity is still independent of the shear rate [66,75,86], that is:

$$\eta = \eta_c\left[1 + \frac{5\lambda + 2}{2\lambda + 2}\varphi\right] \tag{47}$$

$$N_1 = \tau_{11} - \tau_{22} = \frac{\eta_c^2\dot{\gamma}^2 R}{40\gamma}\left(\frac{19\lambda + 16}{1+\lambda}\right)^2\varphi \tag{48}$$

$$N_2 = \tau_{22} - \tau_{33} = -\frac{\eta_c^2\dot{\gamma}^2 R}{280\gamma}\left[\frac{(19\lambda + 16)(29\lambda^2 + 61\lambda + 50)}{(1+\lambda)^3}\right]\varphi \tag{49}$$

where N_1 is the first normal stress difference, N_2 is the second normal stress difference, and τ_{11}, τ_{22}, and τ_{33} are normal stresses, where subscript 1 denotes the direction of flow, subscript 2 denotes the direction of the velocity gradient, and subscript 3 denotes the neutral direction. Interestingly, the ratio $N_1/N_2 = -2.24$ when $\lambda \to 0$ and $N_1/N_2 = -4.586$ when $\lambda \to \infty$. As expected, N_1 is larger in magnitude than N_2, and N_2 is negative.

Frankel and Acrivos [67] have developed a more general constitutive law for dilute emulsions, with no restriction on time dependence, based on the first-order deformation of droplets. Their constitutive equation is:

$$\bar{\bar{\sigma}} = -P\bar{\bar{\delta}} + 2\eta_c\bar{\bar{E}} + \eta_c\varphi\left[\frac{10(\lambda-1)}{2\lambda+3}\bar{\bar{E}} + \frac{24}{2\lambda+3}\bar{\bar{F}} + \frac{360(\lambda-1)^2}{7(2\lambda+3)^2}\left(\frac{R\eta_c}{\gamma}\right)Sd\left(\bar{\bar{F}}\bullet\bar{\bar{E}}\right) + \frac{288(\lambda-6)}{7(2\lambda+3)^2}\left(\frac{R\eta_c}{\gamma}\right)Sd\left(\bar{\bar{F}}\bullet\bar{\bar{F}}\right)\right] \quad (50)$$

where $\bar{\bar{F}}$ is a tensor that describes the shape of the droplet. The time evolution of the $\bar{\bar{F}}$ is given as:

$$\bar{\bar{F}} + \left(\frac{R\eta_c}{\gamma}\right)\frac{(2\lambda+3)(19\lambda+16)}{40(\lambda+1)}\frac{D\bar{\bar{F}}}{Dt} = \frac{19\lambda+16}{24(\lambda+1)}\bar{\bar{E}} + \frac{(4\lambda-9)(19\lambda+16)}{28(2\lambda+3)((\lambda+1)}\left(\frac{R\eta_c}{\gamma}\right)Sd\left(\bar{\bar{F}}\bullet\bar{\bar{E}}\right) + \frac{36(137\lambda^3+624\lambda^2+741\lambda+248)}{35(2\lambda+3)(19\lambda+16)(\lambda+1)}\left(\frac{R\eta_c}{\gamma}\right)Sd\left(\bar{\bar{F}}\bullet\bar{\bar{F}}\right) \quad (51)$$

In Equations (50) and (51), *Sd* refers to the symmetric and traceless part of the indicated tensor. For any tensor $\bar{\bar{B}}$, *Sd* is given as:

$$Sd\left(\bar{\bar{B}}\right) = \frac{1}{2}\left[\bar{\bar{B}} + \bar{\bar{B}}^T - \frac{2}{3}tr\left(\bar{\bar{B}}\right)\bar{\bar{\delta}}\right] \quad (52)$$

where $\bar{\bar{B}}^T$ is the transpose of the tensor $\bar{\bar{B}}$, *tr* is the trace of the tensor, and $\bar{\bar{\delta}}$ is the unit tensor.

For weak time-dependent or steady flows, Equation (51) can be solved by a method of successive substitutions to obtain the following result:

$$\bar{\bar{F}} = \frac{19\lambda+16}{24(1+\lambda)}\left[\bar{\bar{E}} - \frac{(2\lambda+3)(19\lambda+16)}{40(1+\lambda)}\left(\frac{\eta_c R}{\gamma}\right)\frac{D\bar{\bar{E}}}{Dt} + \frac{1202\lambda^3+3589\lambda^2+3191\lambda+768}{140(2\lambda+3)(\lambda+1)^2}\left(\frac{\eta_c R}{\gamma}\right)Sd\left(\bar{\bar{E}}\bullet\bar{\bar{E}}\right)\right] \quad (53)$$

Using Equation (53), the constitutive equation (Equation (50)) can be re-written as:

$$\bar{\bar{\sigma}} = -P\bar{\bar{\delta}} + 2\eta_c\left[1 + \frac{5\lambda+2}{2(1+\lambda)}\varphi\right]\bar{\bar{E}} + \varphi\eta_c\left(\frac{\eta_c R}{\gamma}\right)\left[\frac{-(19\lambda+16)^2}{40(1+\lambda)^2}\frac{D\bar{\bar{E}}}{Dt} + \frac{3(19\lambda+16)(25\lambda^2+41\lambda+4)}{140(1+\lambda)^3}Sd\left(\bar{\bar{E}}\bullet\bar{\bar{E}}\right)\right] \quad (54)$$

This constitutive law for weak time-dependent or steady flows of dilute emulsions is identical to Equation (46). However, it can be recast in the following form of Oldroyd's constitutive equation [67,77,86]:

$$\left[1 + \tau_o\frac{D}{Dt}\right]\bar{\bar{\tau}} = 2\eta_c\left[1 + \frac{5\lambda+2}{2(1+\lambda)}\varphi\right]\left[\bar{\bar{E}} + \tau_o\frac{D\bar{\bar{E}}}{Dt}\right] + \varphi\eta_c\left(\frac{\eta_c R}{\gamma}\right)\left[-\frac{1}{40}\left(\frac{19\lambda+16}{1+\lambda}\right)^2\frac{D\bar{\bar{E}}}{Dt} + \frac{3(19\lambda+16)(25\lambda^2+41\lambda+4)}{140(1+\lambda)^3} \times Sd\left(\bar{\bar{E}}\bullet\bar{\bar{E}}\right)\right] \quad (55)$$

where $\bar{\bar{\tau}}$ is the deviatoric stress tensor defined as $\left(\bar{\bar{\sigma}} + P\,\bar{\bar{\delta}}\right)$ and τ_o is the characteristic time constant:

$$\tau_o = \frac{(19\lambda+16)\,(2\lambda+3)}{40(1+\lambda)}\left(\frac{\eta_c R}{\gamma}\right) \quad (56)$$

In a simple shear flow, Equation (55) gives the following expressions for viscosity and normal stresses (see Appendix A for derivations):

$$\eta = \frac{\eta_c}{1+\tau_o^2\dot{\gamma}^2}\left\{1 + \left(\frac{5\lambda+2}{2\lambda+2}\right)\varphi + \tau_o^2\dot{\gamma}^2\left[1 + \left(\frac{5\lambda+2}{2\lambda+2}\right)\varphi - \frac{(19\lambda+16)}{(2\lambda+2)(2\lambda+3)}\varphi\right]\right\} \quad (57)$$

$$N_1 = \tau_{11} - \tau_{22} = \frac{\eta_c^2\dot{\gamma}^2 R}{40\gamma\left(1+\tau_o^2\dot{\gamma}^2\right)}\left(\frac{19\lambda+16}{1+\lambda}\right)^2\varphi \quad (58)$$

$$N_2 = \tau_{22} - \tau_{33} = -\frac{\eta_c^2 \dot{\gamma}^2 R}{40\gamma\left(1+\tau_o^2\dot{\gamma}^2\right)}\varphi\left\{\frac{1}{2}\left(\frac{19\lambda+16}{\lambda+1}\right)^2 - \left[\frac{3(19\lambda+16)(25\lambda^2+41\lambda+4)}{14(\lambda+1)^3}\right]\left(1+\tau_o^2\dot{\gamma}^2\right)\right\} \quad (59)$$

Interestingly, the recast form of Equation (54), that is, Equation (55), gives shear-rate-dependent viscosity, whereas Equation (54) itself gives shear-rate-independent viscosity. Furthermore, the expressions for viscosity and first and second normal stress differences given by Equations (57)–(59) reduce to the Schowalter et al. expressions (Equations (47)–(49)) if the term $\tau_o^2\dot{\gamma}^2$ is neglected.

Equations (57)–(59) could further be re-written in dimensionless forms as follows:

$$[\eta] = \underset{\varphi\to 0}{Lim}\left(\frac{\eta-\eta_c}{\varphi\eta_c}\right) = \frac{1}{1+(hN_{Ca})^2}\left\{\left(\frac{5\lambda+2}{2\lambda+2}\right)\left[1+(hN_{Ca})^2 - \frac{(19\lambda+16)}{(5\lambda+2)(2\lambda+3)}(hN_{Ca})^2\right]\right\} \quad (60)$$

$$N_{1r} = \frac{N_1}{\eta_c\dot{\gamma}} = \frac{N_{Ca}}{40\left[1+(hN_{Ca})^2\right]}\left(\frac{19\lambda+16}{1+\lambda}\right)^2\varphi \quad (61)$$

$$N_{2r} = \frac{N_2}{\eta_c\dot{\gamma}} = -\frac{N_{Ca}}{40\left(1+(hN_{Ca})^2\right)}\varphi\left\{\frac{1}{2}\left(\frac{19\lambda+16}{\lambda+1}\right)^2 - \left[\frac{3(19\lambda+16)(25\lambda^2+41\lambda+4)}{14(\lambda+1)^3}\right]\left(1+h^2N_{Ca}^2\right)\right\} \quad (62)$$

where $h = (19\lambda+16)(2\lambda+3)/[40(1+\lambda)]$ and N_{Ca} is $\eta_c\dot{\gamma}R/\gamma$.

Equation (55) predicts strain thickening in elongational flow, with elongation viscosity η_E as follows:

$$\eta_E = 3\eta_c\left\{1+\left(\frac{5\lambda+2}{2\lambda+2}\right)\varphi + \frac{\eta_c R\dot{\gamma}_E}{4\gamma}\left[\frac{3(19\lambda+16)(25\lambda^2+41\lambda+4)}{140(\lambda+1)^3}\right]\varphi\right\} \quad (63)$$

where $\dot{\gamma}_E$ is the elongation rate.

Figure 9 shows the variation in $[\eta]$ with N_{Ca} for different values of viscosity ratio λ. The plots are generated from Equation (60). The intrinsic viscosity $[\eta]$ decreases with the increase in the capillary number N_{Ca}, indicating shear-thinning behavior. $[\eta]$ decreases with the decrease in λ at any given N_{Ca}. Interestingly, $[\eta]$ becomes zero at high N_{Ca} when $\lambda = 1$, and $[\eta]$ becomes negative at high N_{Ca} when $\lambda < 1$.

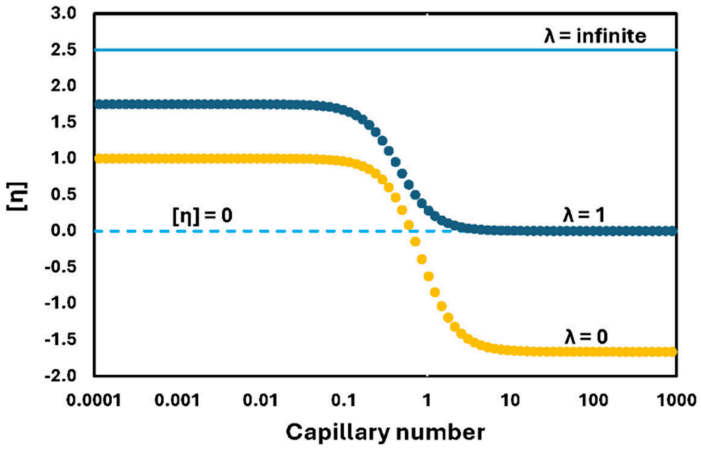


Figure 9. Variation in $[\eta]$ of emulsion with N_{Ca} for different values of λ.

The plots of N_{1r} and $-N_{2r}$ versus N_{Ca} are shown in Figure 10 for different values of λ. The N_{1r} or $-N_{2r}$ increases initially with the increase in N_{Ca}, reaches a maximum value, and then drops off with further increases in N_{Ca}.

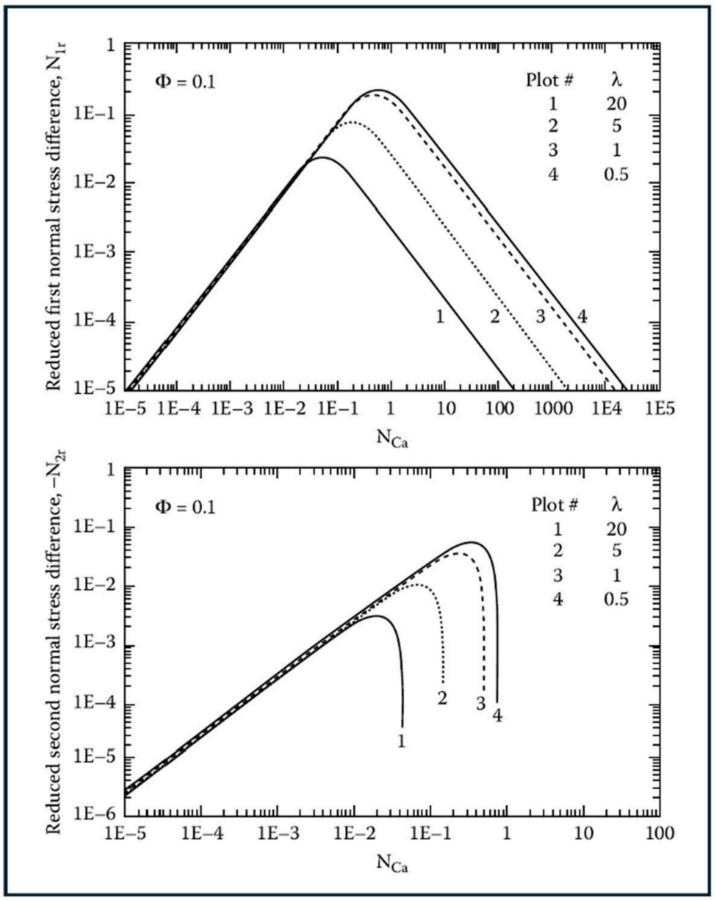


Figure 10. Variations in reduced normal stress differences (N_{1r} and $-N_{2r}$) with capillary number for different values of viscosity ratio λ.

The Frankel and Acrivos analysis assumes the first-order deformation of droplets. Therefore, Figures 9 and 10 are strictly valid for $N_{Ca} < 1$. Wetzel and Tucker [87] have extended the small deformation analysis to arbitrary deformations under the conditions of unequal viscosities and zero interfacial tension.

5. Influence of Electric Charge on Dilute Emulsion Rheology

Emulsion rheology is strongly affected by the presence of electric charge on the surface of the droplets. As shown in Figure 11, a charged droplet attracts a cloud of counter-ions and forms an *electrical double layer* consisting of a *Stern layer* of immobile ions just next to the charged droplet surface and a diffuse layer of mobile ions (*Gouy* or *Debye–Huckel layer*) [88,89] outside the Stern layer.

The viscosity of emulsion of electrically charged droplets is higher in comparison with the emulsion of neutral droplets. Maxwell stresses are generated when the motion of the fluid surrounding the charged droplet distorts the electric charge cloud from its equilibrium state. The Maxwell stresses hinder the motion of fluid in the electrical double layer, resulting in the extra dissipation of energy. This effect is referred to as the "*primary electroviscous effect*".

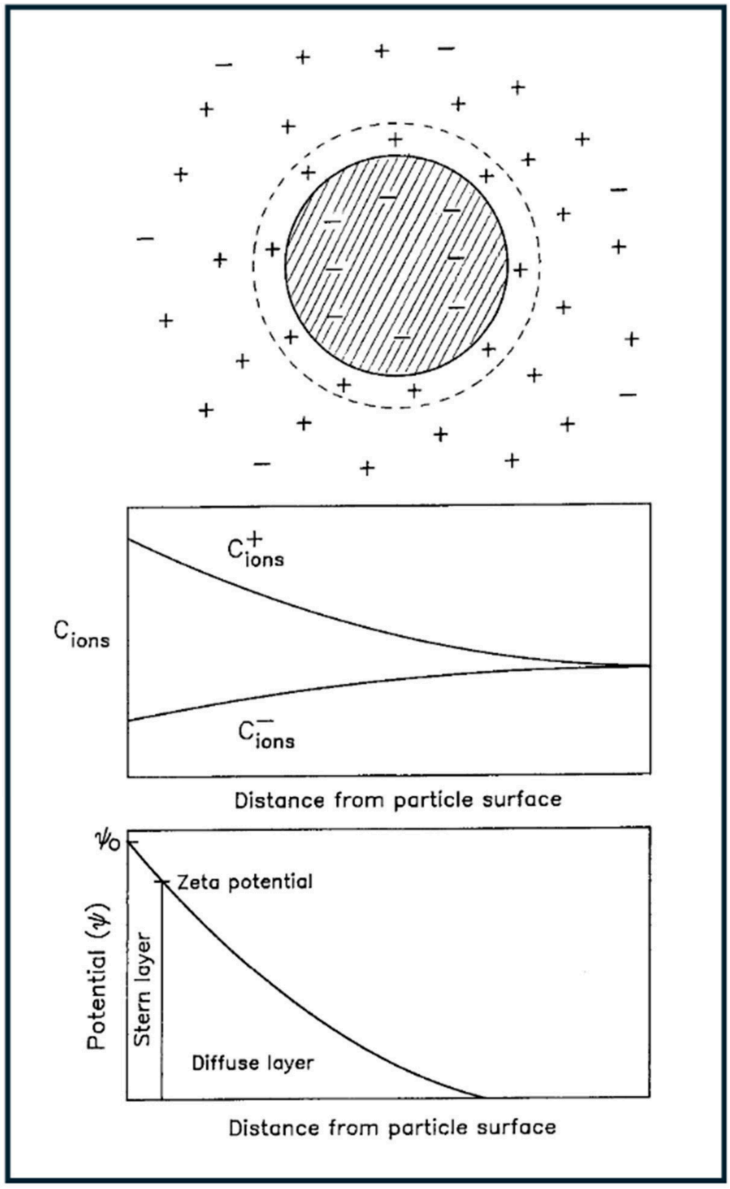


Figure 11. Charged particle surrounded by an ionic cloud. Variations in ionic concentration and electric potential are also shown.

The theory for the viscosity of electrostatically stabilized dispersions has been well established. However, the studies are mostly restricted to suspensions of solid particles. Nevertheless, they are equally relevant to emulsions. The viscosity of suspensions of charged particles is governed by four dimensionless groups [88]:

$$Ha = \left(\frac{\varepsilon\psi_0^2}{\eta_c D}\right) \text{(Hartmann number)} \tag{64}$$

$$Pe = \frac{\dot{\gamma}}{\kappa^2 D} \text{ (ion Peclet number)} \tag{65}$$

$$R\kappa = R\sqrt{e^2 I/\varepsilon kT} \text{ (ratio of particle radius to double layer thickness)} \tag{66}$$

$$\tilde{\psi}_0 = \frac{e\psi_0}{kT} \text{ (dimensionless surface potential)} \tag{67}$$

where ψ_0 is the surface potential; I is the bulk ionic strength, defined as $\sum_i^N {Z_i}^2 n_i^\infty$; Z_i is the valence of ionic species i; n_i^∞ is the number density of ionic species i far away from the

particle; N is the total number of ionic species present in the fluid; D is the ion diffusivity; ε is the permittivity of the fluid; k is the Boltzmann constant; T is the absolute temperature; R is the particle radius; η_c is the viscosity of the fluid; e is the elementary electronic charge; $\dot{\gamma}$ is the shear rate; and κ^{-1} is the Debye length $\left(\kappa^{-1}\right)$, defined as:

$$\kappa^{-1} = \sqrt{\varepsilon kT / \left(\sum Z_i^2 e^2 n_i^{\infty}\right)} \tag{68}$$

The Hartmann number Ha is the ratio of the electrical force to the viscous force acting on the fluid. It represents the rigidity of the charge cloud. When $Ha \ll 1$, the modification of the flow field around the particles caused by the electric charge is small. When $Ha \gg 1$, the fluid adjacent to the particle experiences strong electrical forces and, therefore, remains almost attached to the particle.

The ion Peclet number Pe is a measure of the extent to which the motion of the fluid relative to the particle disturbs the charge cloud. For small Pe ($Pe \ll 1$), the ionic atmosphere around the particle is distorted only slightly from its equilibrium shape because the diffusion of the ions is strong compared to the convection of the ions.

The dimensionless group $R\kappa$ is the inverse of the relative thickness of the electrical double layer (κ^{-1}/R) with respect to the particle size. The double layer extends a distance of κ^{-1} from the particle surface. The electric double layer is thin when $R\kappa \gg 1$, and it is thick when $R\kappa \ll 1$.

The dimensionless surface potential ($\widetilde{\psi}_0$) is the ratio of the electrical energy to the thermal energy of the ions. The density of the ions in the charge cloud differs only slightly from its value far away from the particle surface when $\widetilde{\psi}_0 \ll 1$.

The constitutive equation for a dilute suspension of charged particles under the condition that the distortion of charge clouds around the particles caused by fluid motion is small, that is, $Pe \ll 1$, can be expressed as:

$$\overline{\overline{\sigma}} = -P\overline{\overline{\delta}} + 2\eta_c\overline{\overline{E}} + 5(1+p)\eta_c\varphi\overline{\overline{E}} \tag{69}$$

where p is the primary electroviscous coefficient, which is, in general, a function of three dimensionless groups (assuming $Pe \to 0$), that is,

$$p = p\left(\widetilde{\psi}_0, Ha, R\kappa\right) \tag{70}$$

From Equation (69), it follows that

$$\eta_r = \left[1 + \frac{5}{2}(1+p)\varphi\right] \tag{71}$$

Several theoretical studies have been carried out to predict the primary electroviscous coefficient p. The predictive equations for p are summarized in Table 1.

Figure 12 shows the predictions of $\boldsymbol{p}$ for a dilute suspension of solid spheres under the conditions of arbitrary surface potential and a large $R\kappa$. The plots are generated using the Ohshima model [90] listed in Table 1. The electrolyte is KCl with $m_- = 0.169$ and $m_+ = 0.176$ [91]. The coefficient p decreases with the increase in $R\kappa$ at a given $\widetilde{\psi}_0$. The plot of p versus $\widetilde{\psi}_0$ exhibits a maximum at some intermediate value of $\widetilde{\psi}_0$ at any given $R\kappa$ due to the relaxation effect [90]. Also, at high $\widetilde{\psi}_0$, p levels off to a non-zero value.

Table 1. Coefficient p for dilute suspensions of solid particles.

Primary Electroviscous Coefficient, p	Comments and Restrictions
$p = 4\pi(Ha)(1+R\kappa)^2 f(R\kappa)$	$\tilde{\psi}_0 << 1$, $Ha << 1$, $Pe \ll 1$
$f(R\kappa) = \frac{1}{200\pi(R\kappa)} + \frac{11(R\kappa)}{3200\pi}$	$R\kappa << 1$
$f(R\kappa) = \frac{3}{2\pi(R\kappa)^4}$	$R\kappa >> 1$
$p = 6(Ha)(R\kappa)^{-2}$	$R\kappa >> 1$, $\tilde{\psi}_0 << 1$, $Ha << 1$, $Pe \ll 1$
$p = (Ha/50)(R\kappa)^{-1}$	$R\kappa << 1$, $\tilde{\psi}_0 << 1$, $Ha << 1$, $Pe \ll 1$
$p = \frac{72}{(R\kappa)^2}\left[m_+\left(ln\frac{1+e^{-\tilde{\psi}_0/2}}{2}\right)^2 + \left(\frac{m_-}{1+2F}\right)\left(ln\frac{1+e^{\tilde{\psi}_0/2}}{2}\right)^2\right]$ where $m_\pm = \frac{2\varepsilon kT}{3\eta_c Z^2 e^2}\lambda_\pm = \frac{2}{3}\left(\frac{Ha}{\tilde{\psi}_0^2}\right)$, $F = \frac{2}{R\kappa}(1+3m_-)\left(e^{\tilde{\psi}_0/2}-1\right)$. Note that $\lambda = kT/D$ and $\tilde{\psi}_0 = Ze\psi_0/kT$	Ohshima model [90]. Arbitrary surface potentials (no restriction on $\tilde{\psi}_0$), $R\kappa >> 1$, $Pe \ll 1$, and Z-Z symmetrical-type electrolyte where Z is the valence of the ion; $Z_1 = -Z_2 = Z$; $n_1^\infty = n_2^\infty = n^\infty$
$p = \frac{9(m_-+m_+)}{2(R\kappa)^2}\tilde{\psi}_0^2$	$\tilde{\psi}_0 << 1$, $R\kappa >> 1$, $Pe \ll 1$

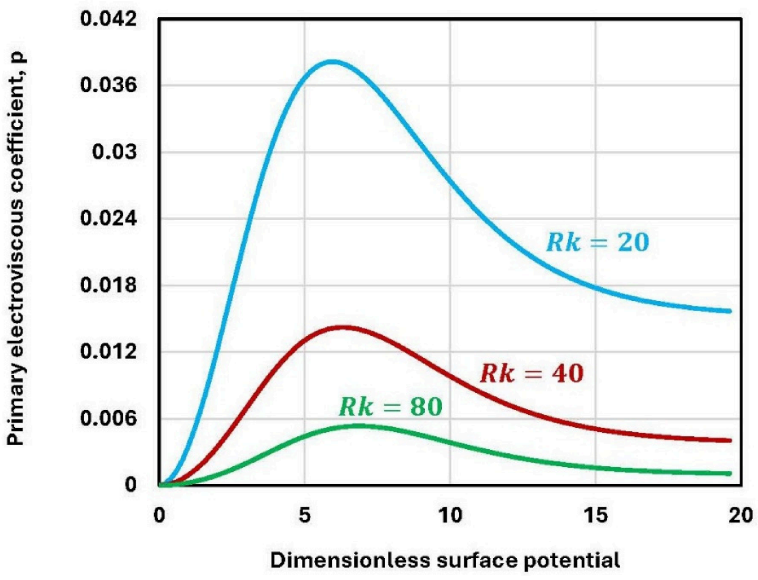


Figure 12. Variation in coefficient p with $\tilde{\psi}_0$ for different values of $R\kappa$. Adapted from [88].

The coefficient p is a strong function of the electrolyte concentration. Figure 13 shows the variation in p with the electrolyte concentration [92]. The surface charge on the particles of diameter 106 nm was -6.85 μC/cm^2, and on the particles of diameter 210 nm, it was -0.20 μC/cm^2. With the increase in electrolyte concentration, the coefficient p decreases due to a decrease in the double layer thickness.

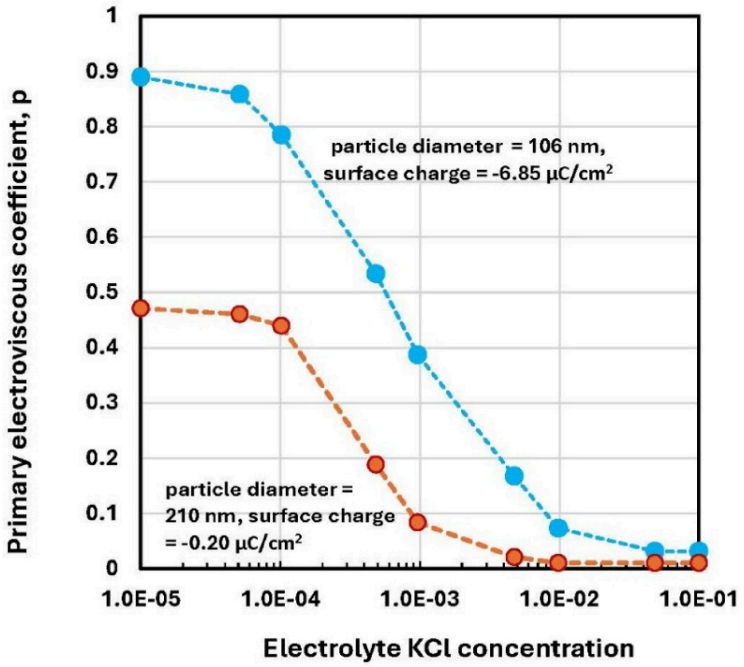


Figure 13. Variation in coefficient p with electrolyte concentration for electrically charged polystyrene latex suspensions. Adapted from [88].

Ohshimo [90] also developed equations for the coefficient p for dilute emulsions. The coefficient was now found to be a function of λ, in addition to other factors such as surface potential and Hartmann number. His expressions for p for dilute emulsions are listed in Table 2.

Table 2. Coefficient p for dilute emulsions of liquid droplets.

Primary Electroviscous Coefficient, p	Comments and Restrictions
$\eta_r = \left[1 + \frac{5}{2}\left\{\frac{5\lambda+2}{5(1+\lambda)}\right\}(1+p)\varphi\right]$	Dilute emulsions
$p = \left[\frac{18}{(5\lambda+2)}\right]\left[\frac{m_+(1-e^{-\tilde{\psi}_0/2})^2+m_-(1-e^{\tilde{\psi}_0/2})^2}{5(\lambda+1)+6\left\{m_+(1-e^{-\tilde{\psi}_0/2})^2+m_-(1-e^{\tilde{\psi}_0/2})^2\right\}}\right]$ where $m_\pm = \frac{2\varepsilon kT}{3\eta_c Z^2 e^2}\lambda_\pm = \frac{2}{3}\left(\frac{Ha}{\tilde{\psi}_0}\right)^2$ $\eta_r = \left[1 + \frac{5}{2}\left\{\frac{5\lambda+2+6\left\{m_+(1-e^{-\tilde{\psi}_0/2})^2+m_-(1-e^{\tilde{\psi}_0/2})^2\right\}}{5(1+\lambda)+6\left\{m_+(1-e^{-\tilde{\psi}_0/2})^2+m_-(1-e^{\tilde{\psi}_0/2})^2\right\}}\right\}\varphi\right]$	Ohshimo model [90]. Thin double layer (large $R\kappa$) and arbitrary surface potential, Z-Z symmetrical-type electrolyte where Z is the valence of the ion; $Z_1 = -Z_1 = Z$; $n_1^\infty = n_2^\infty = n^\infty$
$p = \frac{3}{2+5\lambda}$; $\eta_r = \left[1 + \frac{5}{2}\varphi\right]$	$R\kappa \to \infty$ and $\tilde{\psi}_0 \to \infty$
$p = \left\{\frac{6\lambda+6}{5\lambda+2}\right\}\left(\frac{\varepsilon kT}{\eta_c e^2}\right)\left(\frac{\sum_{i=1}^N z_i^2 n_i^\infty \lambda_i}{\sum_{i=1}^N z_i^2 n_i^\infty}\right)L(\kappa a,\lambda)\left(\frac{e\zeta}{kT}\right)^2$ where $L(\kappa a,\lambda)$ is a complicated function of κa and λ	arbitrary $R\kappa$ but $\tilde{\psi}_0 << 1$

For $R\kappa \to \infty$ and $\tilde{\psi}_0 \to \infty$, p approaches a value given by:

$$p = \frac{3\eta_c}{2\eta_c + 5\eta_d} \quad (72)$$

Consequently, the η_r for dilute emulsions listed in Table 2 reduces to Equation (37) for dilute suspensions. Thus, emulsion droplets with $R\kappa \to \infty$ and $\widetilde{\psi}_0 \to \infty$ act as rigid spheres regardless of λ. This effect is called the *solidification effect* [90].

Figure 14 shows p versus $\widetilde{\psi}_0$ for dilute emulsions at different values of λ. The Ohshimo model listed in Table 2 is used to generate these plots. The continuous phase is assumed to be an aqueous KCl solution. For an aqueous KCl solution at 25 °C, $m_- = 0.169$ and $m_+ = 0.176$ [91]. The coefficient p increases initially with the increase in surface potential and then levels off at a high surface potential. However, it decreases with the increase in λ. As $\lambda \to \infty$, the coefficient p approaches a value of zero, indicating that the influence of the interface becomes decreasingly important with the increase in λ.

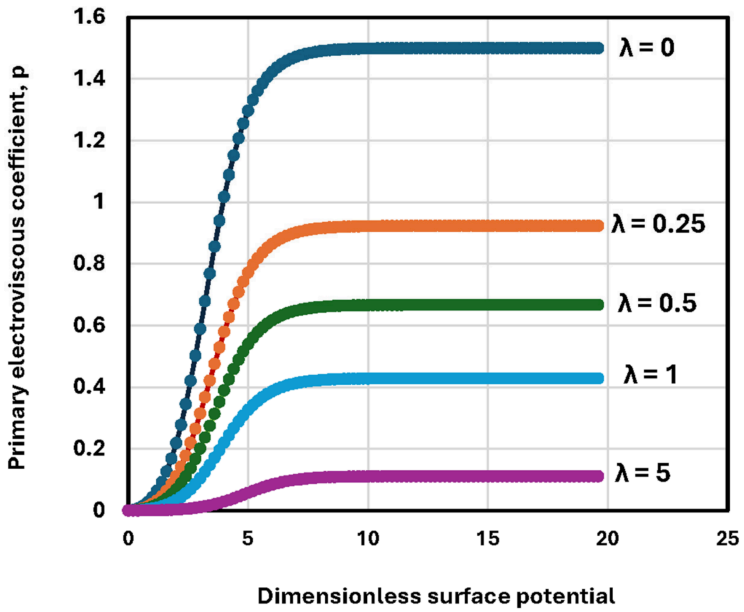


Figure 14. Coefficient p versus $\widetilde{\psi}_0$ for different values of viscosity ratio λ. Adapted from [88].

Dispersions of charged particles generally display non-Newtonian behavior. Upon increasing the shear rate, the double layer becomes streamlined with the flow as shown schematically in Figure 15. As a result, the viscosity decreases with the increase in shear rate. At high shear rates, the size of the double layer becomes negligible as the ions are convected away by the matrix fluid and the particle is now surrounded by an electroneutral matrix fluid. Thus, the viscosity of the suspension eventually becomes equal to that of a suspension of uncharged particles [89].

Russel [93] developed a constitutive equation for dilute dispersions of charged spheres under the conditions of arbitrary flow strength (arbitrary Pe), a thin double layer ($R\kappa > 1$), and a low ψ_0. His equation is as follows:

$$\left[1 + \frac{1}{(\kappa^2 D)}\frac{D}{Dt}\right]\overline{\overline{\tau}} = 2\eta_c \left[\begin{array}{c} 1 + \frac{5}{2}\varphi\left(1 + 6\frac{Ha}{(R\kappa)^2}\right)\overline{\overline{E}} + \\ \frac{\left(1+\frac{5}{2}\varphi\right)}{(\kappa^2 D)}\frac{D}{Dt}\overline{\overline{E}} \end{array}\right] \quad (73)$$

Equation (73) gives the following expression for the suspension viscosity:

$$\eta = \eta_c\left[1 + \frac{5}{2}\varphi\left\{1 + 6\frac{Ha}{(R\kappa)^2}\left(\frac{1}{1+Pe^2}\right)\right\}\right] \quad (74)$$

The intrinsic viscosity of the suspension can be expressed as:

$$[\eta] = \left[\frac{(\eta/\eta_c) - 1}{\varphi}\right] = 2.5\left[1 + 6\,\frac{Ha}{(R\kappa)^2}\left(\frac{1}{1 + Pe^2}\right)\right] \quad (75)$$

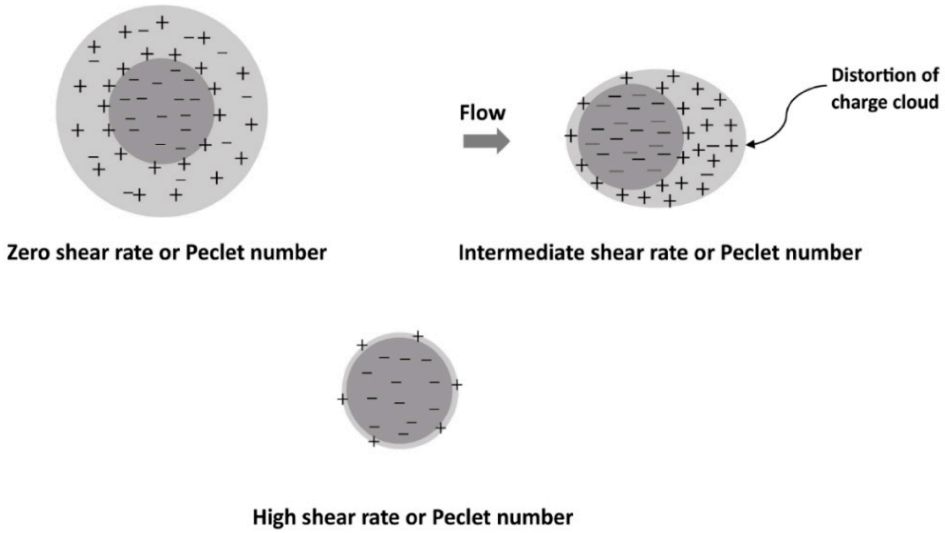


Figure 15. Influence of shear rate on the shape and size of double layer.

According to Equation (75), the suspension of charged particles is shear-thinning. For a fixed $R\kappa$, $[\eta]$ at low Pe increases with the increase in Ha, as shown in Figure 16. Also note that at high Pe, $[\eta]$ becomes equal to 2.5, corresponding to the suspension of neutral particles.

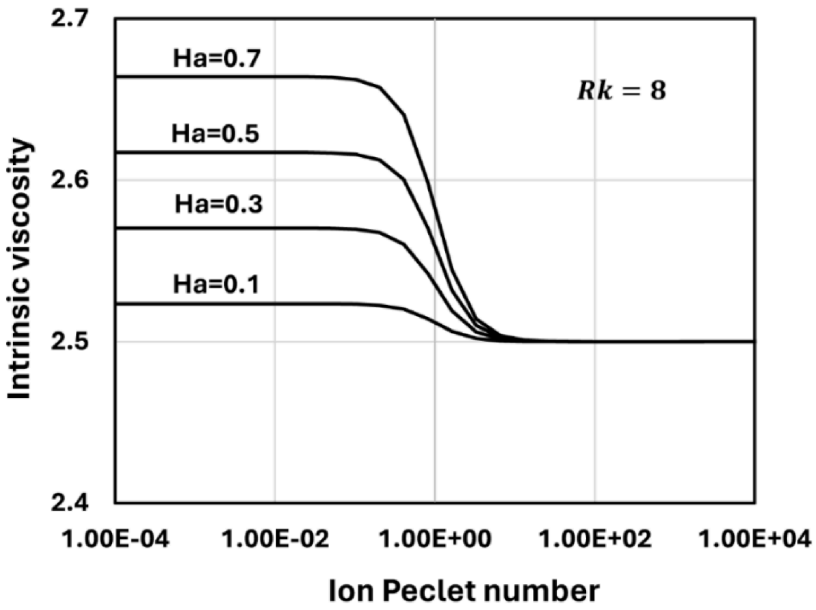


Figure 16. Variation in [η] with Pe at different values of Ha (Rk fixed at 8). Adapted from [88].

With the decrease in the value of Rk, [η] at low Pe increases at a fixed value of Ha, as can be seen in Figure 17. Once again, $[\eta]$ becomes equal to 2.5, corresponding to the suspension of neutral particles at high Pe.

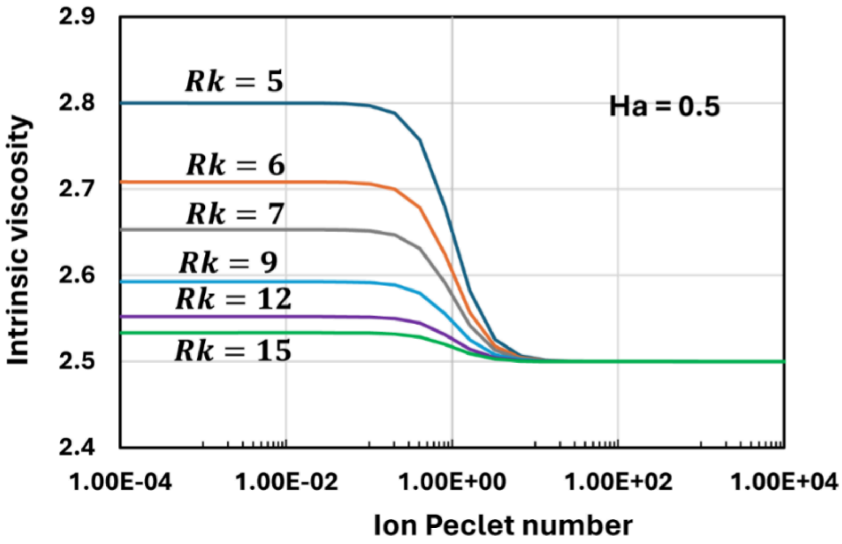


Figure 17. Variation in [η] with *Pe* at different values of *Rk* (*Ha* fixed at 0.5). Adapted from [88].

6. Influence of Surfactants on Dilute Emulsion Rheology

The presence of a surfactant on the surface of the droplets complicates the emulsion rheology. For example, dilute emulsions of surfactant-laden droplets tend to exhibit non-Newtonian rheology even when $N_{Ca} \to 0$ and the deformation of the droplets is negligible [94,95].

The flow of continuous-phase fluid around the droplet results in a non-uniform concentration of surfactants at the droplet surface (see Figure 18). The resulting inhomogeneity in the surfactant concentration generates interfacial tension gradients (Marangoni stresses). Marangoni stresses produce a jump in the tangential viscous tractions across the interface. The normal stress boundary condition is also altered due to the presence of surfactants as interfacial tension is reduced.

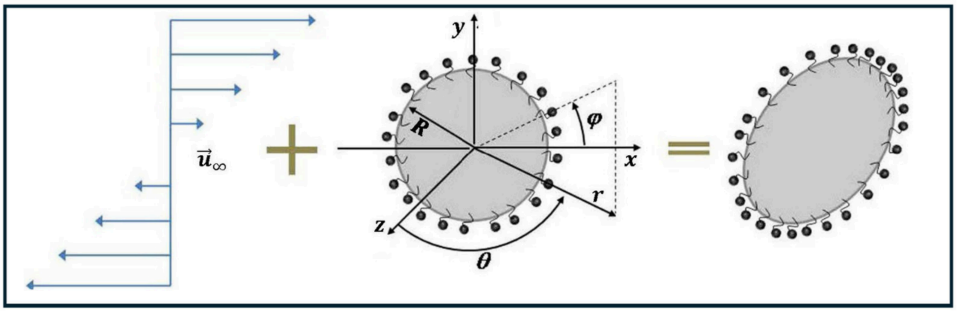


Figure 18. A droplet of radius *R* covered with surfactant placed in shear flow. Adapted from [96].

The Marangoni stresses can be neglected if $N^s_{Pe} \to 0$. The surface Peclet number is defined as:

$$N^s_{Pe} = \frac{R^2\dot{\gamma}}{D} \tag{76}$$

where D is the surface diffusivity of the surfactant. If $N^s_{Pe} \to 0$, the surfactant concentration over the droplet surface is uniform, as the diffusion of the surfactant can counteract the convection of the surfactant [97].

The interfacial film of the surfactant also possesses shear and dilational viscosities which influence the bulk rheology of the emulsion. Thus, we need to consider five dimensionless groups λ, N_{Ca}, N^k_{Bo}, N^η_{Bo}, and N_{Ma}, where N^k_{Bo} (dilational Boussinesq number) is defined as $\eta^k_s/\eta_c R$ (η^k_s is surface dilational viscosity), N^η_{Bo} (shear Boussinesq number) is

defined as $\eta_s/\eta_c R$ (η_s is surface shear viscosity), and N_{Ma} (Marangoni number) is the ratio of the interfacial tension gradient generated force to the viscous force.

The viscosity equation of a dilute emulsion of surfactant-laden droplets in the limits of $N_{Ca} \to 0$ and $N_{Ma} \to 0$ was developed by Oldroyd [98,99] as:

$$\eta = \eta_c[1 + \alpha\varphi] \tag{77}$$

where α is defined as follows:

$$\alpha = \frac{1 + \frac{5}{2}\lambda + 2N_{Bo}^{\eta} + 3N_{Bo}^{k}}{1 + \lambda + \frac{2}{5}\left(2N_{Bo}^{\eta} + 3N_{Bo}^{k}\right)} \tag{78}$$

Note that $N_{Ma} \to 0$ implies that the surfactant is uniformly distributed on the droplet surface. The interface is inviscid when $N_{Bo}^{\eta} \to 0$ and $N_{Bo}^{k} \to 0$. Equation (77) reduces to Equation (36) for the emulsion viscosity with an inviscid interface. The interface is highly viscous when $\left(2N_{Bo}^{\eta} + 3N_{Bo}^{k}\right) \gg 1$. Now, α becomes 5/2, and Equation (77) reduces to Equation (37) for the suspension of solid particles. The plots of $[\eta]$ versus $\left(2N_{Bo}^{\eta} + 3N_{Bo}^{k}\right)$ for different values of λ are shown in Figure 19. As expected, $[\eta]$ is 2.5 for large values of λ regardless of the value of $\left(2N_{Bo}^{\eta} + 3N_{Bo}^{k}\right)$. Also, $[\eta]$ increases with the increase in $\left(2N_{Bo}^{\eta} + 3N_{Bo}^{k}\right)$ at low values of λ, and for large values of $\left(2N_{Bo}^{\eta} + 3N_{Bo}^{k}\right)$, $[\eta]$ is always 2.5 regardless of λ.

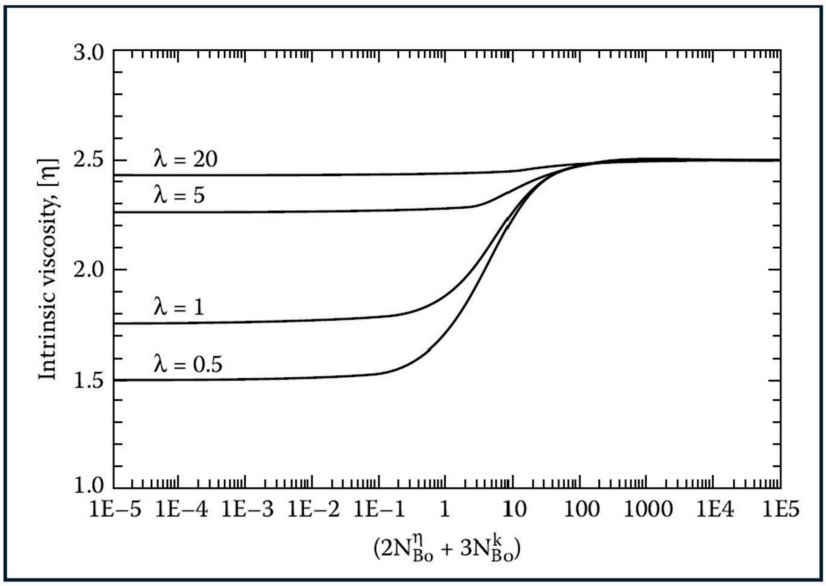


Figure 19. Variation in $[\eta]$ with $\left(2N_{Bo}^{\eta} + 3N_{Bo}^{k}\right)$ for different λ.

In Oldroyd's analysis [98,99], the Marangoni stresses are absent. This is possible only when the surfactant is uniformly distributed at the interface or $N_{Pe}^{s} \to 0$. Danov [100] developed an expression for the zero-shear viscosity of dilute emulsions considering the elasticity of the interface due to the non-uniform distribution of the surfactant. However, he assumed negligible deformation of the droplets, that is, $N_{Ca} \to 0$. His viscosity equation is given as follows:

$$\eta = \eta_c\left[1 + \left(1 + \frac{3}{2}\varepsilon_m\right)\varphi\right] \tag{79}$$

where ε_m is the interfacial mobility parameter, defined as:

$$\varepsilon_m = \left[\frac{\lambda + 0.2\left(\frac{RE_G}{\eta_c D} + 4N_{Bo}^{\eta} + 6N_{Bo}^{k}\right)}{1 + \lambda + 0.2\left(\frac{RE_G}{\eta_c D} + 4N_{Bo}^{\eta} + 6N_{Bo}^{k}\right)} \right] \tag{80}$$

where D is the diffusion coefficient of the surfactant and E_G is the Gibbs elasticity of the interface, defined as:

$$E_G = -\left(\frac{\partial \gamma}{\partial \ell n \Gamma}\right)_e \tag{81}$$

Γ in this equation is the surfactant concentration. Thus, the Gibbs elasticity E_G is the change in interfacial tension caused by perturbations of the local surfactant concentration about the equilibrium value.

The interfacial mobility parameter varies in the range of 0 to 1, that is, $0 \leq \varepsilon_m \leq 1$. The parameter ε_m is unity for interfaces with high E_G, that is, $E_G \to \infty$. In this case, Equation (79) reduces to Equation (37). For surfactant-free interfaces, the surface elasticity is zero ($E_G \to 0$) and $N_{Bo}^{\eta} \to 0$, $N_{Bo}^{k} \to 0$. Consequently, ε_m is $\lambda/(1+\lambda)$, and Equation (79) reduces to Equation (36). The variation in ε_m with $RE_G/\eta_c D$ for different λ is shown in Figure 20. Equation (80) is used to generate Figure 20. The surface viscosities are assumed to be zero, that is, $N_{Bo}^{\eta} \to 0$, $N_{Bo}^{k} \to 0$. The interfacial mobility parameter is unity independent of λ at high values of $RE_G/2\eta_c D$. ε_m increases with the increase in λ at low values of $RE_G/2\eta_c D$. Note that $RE_G/2\eta_c D$ is a dimensionless group corresponding to the ratio of Marangoni stress (E_G/R) to viscous stress ($\eta_c D/R^2$).

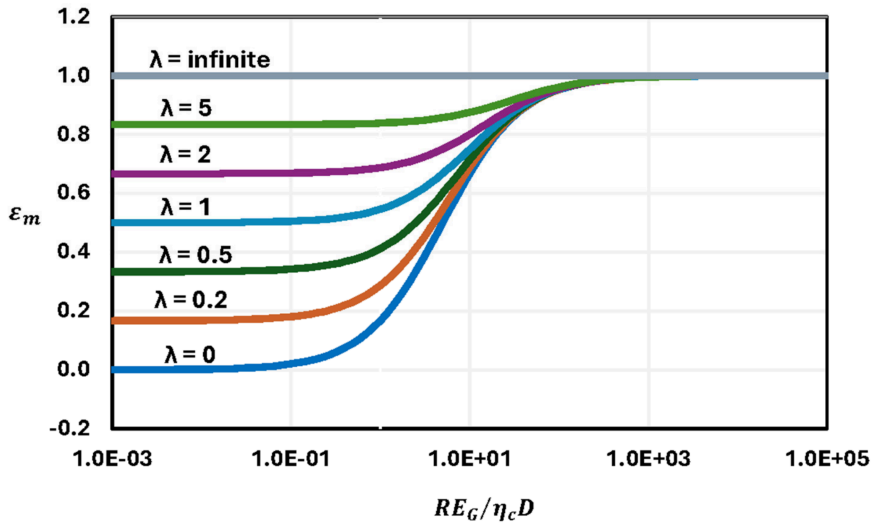


Figure 20. Variation in ε_m with $RE_G/2\eta_c D$ for different λ, $\left(4N_{Bo}^{\eta} + 6N_{Bo}^{k}\right) = 0$.

The plots of ε_m versus λ for different $4N_{Bo}^{\eta} + 6N_{Bo}^{k}$ are shown in Figure 21. The interfacial elasticity group $RE_G/2\eta_c D$ is kept at zero. Equation (80) is used to generate Figure 21. The interfacial elasticity parameter ε_m increases with the increase in the interfacial viscosities. The influence of the interfacial viscosities on ε_m is stronger at low values of the viscosity ratio λ. At high values of λ, ε_m is 1 regardless of the magnitude of the interfacial viscosities.

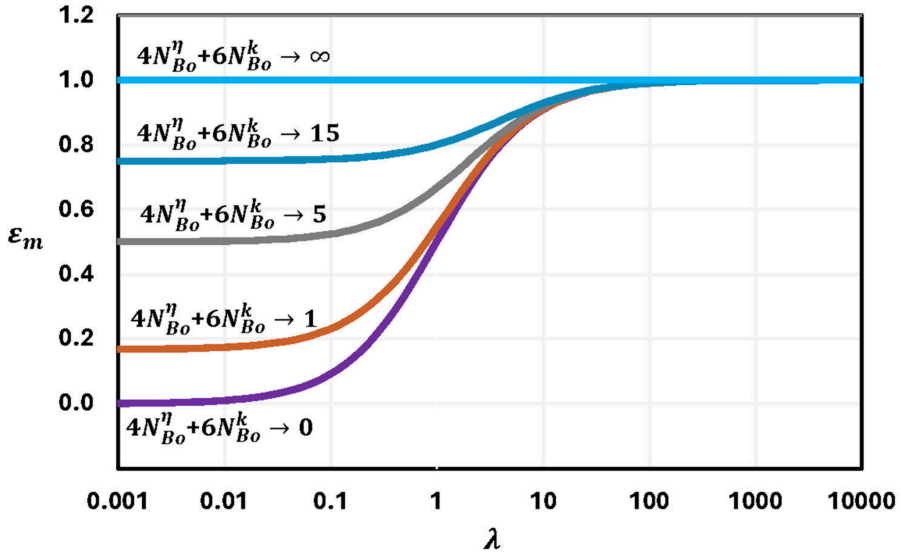


Figure 21. ε_m versus λ for different $4N_{Bo}^{\eta}+6N_{Bo}^{k}$.

Figure 22 shows $[\eta]$ versus $RE_G/2\eta_c D$ for different λ. The surface viscosities, η_s and η_s^k, are assumed to be zero; that is, the term $\left(4N_{Bo}^{\eta}+6N_{Bo}^{k}\right)$ in Equation (80) is taken as zero. $[\eta]$ is 2.5 regardless of $RE_G/2\eta_c D$ for a large value of λ, as expected. $[\eta]$ increases with $RE_G/2\eta_c D$ at low values of λ. For highly elastic films corresponding to large $RE_G/2\eta_c D$, $[\eta]$ is always 2.5 regardless of λ.

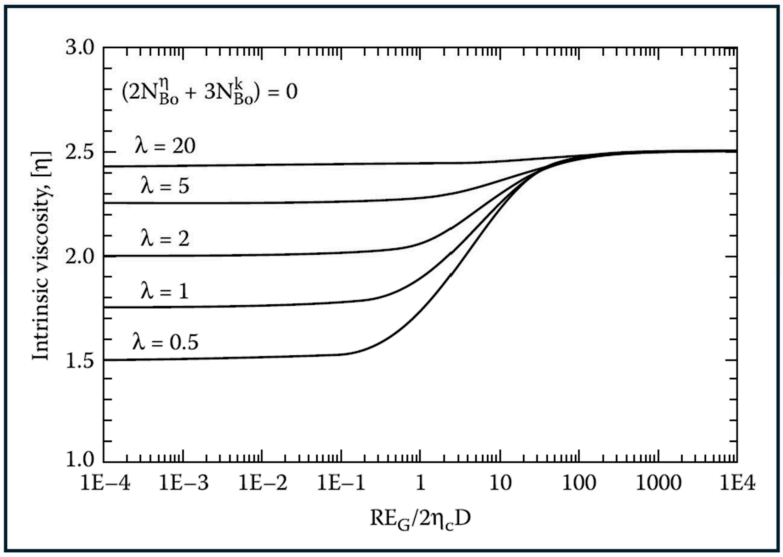


Figure 22. Variation in $[\eta]$ with $RE_G/2\eta_c D$ for different λ, $\left(4N_{Bo}^{\eta}+6N_{Bo}^{k}\right)=0$.

Blawzdziewicz et al. [95] and Vlahovska et al. [94] have studied the influence of the Marangoni phenomenon on the rheology of the dilute emulsion of surfactant-laden droplets under the condition of arbitrary flow strength but low capillary number, that is, $N_{Ca} \to 0$, so that the droplets are spherical in shape. The surfactant was assumed to be insoluble in the bulk phases. It was also assumed to be non-diffusing. The emulsion exhibited non-Newtonian rheology such as shear-thinning and non-zero normal stresses. As $N_{Ca} \to 0$ and the droplets were spherical, the non-Newtonian behavior was entirely due to the redistribution of the surfactant on the surface of the droplet.

The shear stress and normal stresses were found to be a function of λ and the Marangoni number N_{Ma}, defined as:

$$N_{Ma} = \frac{E_G/R}{\eta_c \dot{\gamma}} \tag{82}$$

N_{Ma} is the ratio of Marangoni stress (E_G/R) to viscous stress $\left(\eta_c \dot{\gamma}\right)$, where E_G is defined as in Equation (81). The effects of interfacial viscosities η_s and η_s^k, and, hence, N_{Bo}^{η} and N_{Bo}^{k}, were neglected.

Under the condition that the inverse of the Marangoni number is small, that is, $N_{Ma}^{-1} \rightarrow 0$, the interface is tangentially immobile, and the droplet behaves as a rigid sphere. With the increase in N_{Ma}^{-1}, the viscosity of emulsion decreases, indicating shear-thinning behavior. The normal stress differences (N_1 and $-N_2$) also increase with the increase in N_{Ma}^{-1}. At high N_{Ma}^{-1}, the surfactant is convected away from the droplet surface, rendering it clean and tangentially mobile. As a result, the viscosity of emulsion reduces to that of emulsions consisting of bare (clean) droplets.

Pimenta and Oliveira [101] investigated the rheology of the dilute emulsion of surfactant-covered droplets using numerical analysis. The surfactant was assumed to be insoluble in the bulk phases. However, unlike Blawzdziewicz et al. [95] and Vlahovska et al. [94], the diffusion of the surfactant at the interface was not neglected. The contributions to the bulk stress of emulsion were calculated separately for the normal stress jump (capillary effect) and tangential stress jump (Marangoni effect) across the interface. The capillary intrinsic viscosity $[\eta_C]$ due to the normal stress jump and Marangoni intrinsic viscosity $[\eta_M]$ due to the tangential stress jump were both functions of surfactant elasticity (E), surfactant coverage (X), and surface Peclet number (N_{Pe}^s). Note that the overall emulsion intrinsic viscosity $[\eta]$ is the sum of the two contributions, that is,

$$[\eta] = [\eta_C] + [\eta_M] \tag{83}$$

For a given surfactant coverage X and surfactant elasticity E, the Marangoni viscosity $[\eta_M]$ increased, whereas the capillary viscosity $[\eta_C]$ decreased with the increase in surface Peclet number N_{Pe}^s. Interestingly, the overall emulsion intrinsic viscosity $[\eta]$ also increased with the increase in N_{Pe}^s, indicating the shear-thickening behavior of the dilute emulsion. With the increase in N_{Pe}^s, the surface convection of the surfactant dominates over the surface diffusion, resulting in the generation of Marangoni stress, which opposes the motion of the surrounding fluid and increases the emulsion viscosity. Figure 23 shows the variations in $[\eta_C]$ and $[\eta_M]$ with surfactant coverage X at different values of N_{Pe}^s; Figure 23a corresponds to $E = 0.2$, and Figure 23b corresponds to $E = 0.4$. Figure 24 shows the variations in overall emulsion viscosity $[\eta]$ with surfactant coverage X at different values of N_{Pe}^s. Figure 24a corresponds to $E = 0.2$, and Figure 24b corresponds to $E = 0.4$.

The first normal stress difference N_1 increased with the increases in surfactant coverage, surfactant elasticity, and surface Peclet number. However, N_1 was found to depend only on the normal stress jump (capillary effect) and was independent of the tangential stress jump (Marangoni effect).

Mandal et al. [96] also investigated the effect of Marangoni's stress on the bulk rheology of a dilute emulsion, taking into consideration the diffusion of the surfactant. The surfactant was, however, assumed to be insoluble in the bulk phases. The problem was solved analytically. The non-uniform distribution of the surfactant on the droplet surface caused by bulk flow generated Marangoni stress, resulting in a higher effective viscosity of emulsion. The influence of surfactant redistribution due to bulk flow on the viscosity of emulsion was found to decrease with the increase in the viscosity of the droplets. Thus, the Marangoni

effect is less severe in high-viscosity droplets. The first normal stress difference was found to increase with the non-uniform distribution of the surfactant, whereas the second normal stress difference remained unaffected.

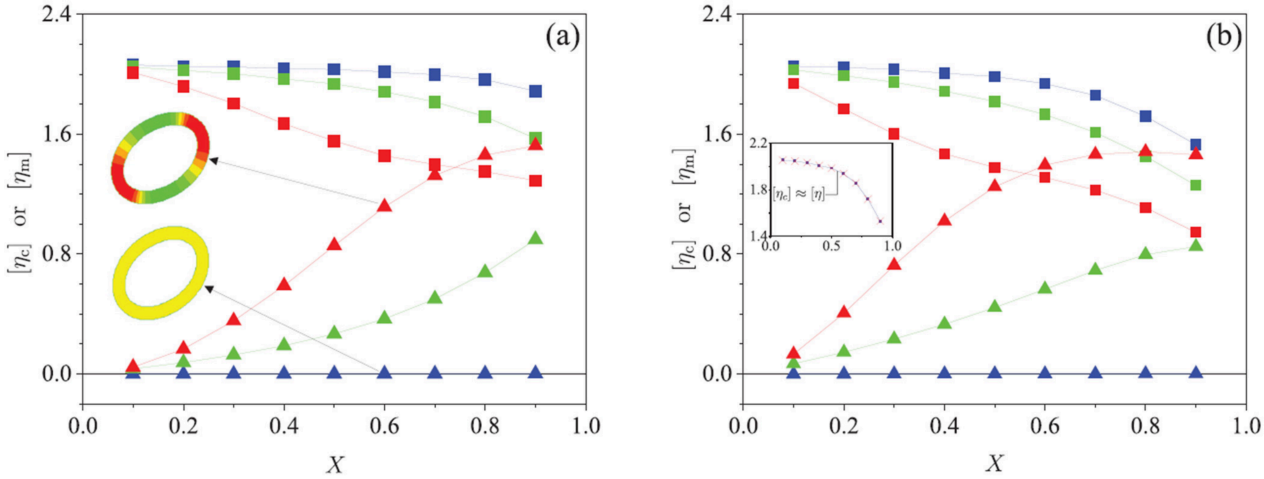


Figure 23. $[\eta_C]$ (squares) and $[\eta_M]$ (triangles) for (**a**) $E = 0.2$ and (**b**) $E = 0.4$. $N^s_{Pe} = 10^3$ (*red*), $N^s_{Pe} = 1$ (*green*), and $N^s_{Pe} = 10^{-3}$ (*blue*). Adapted from [101].

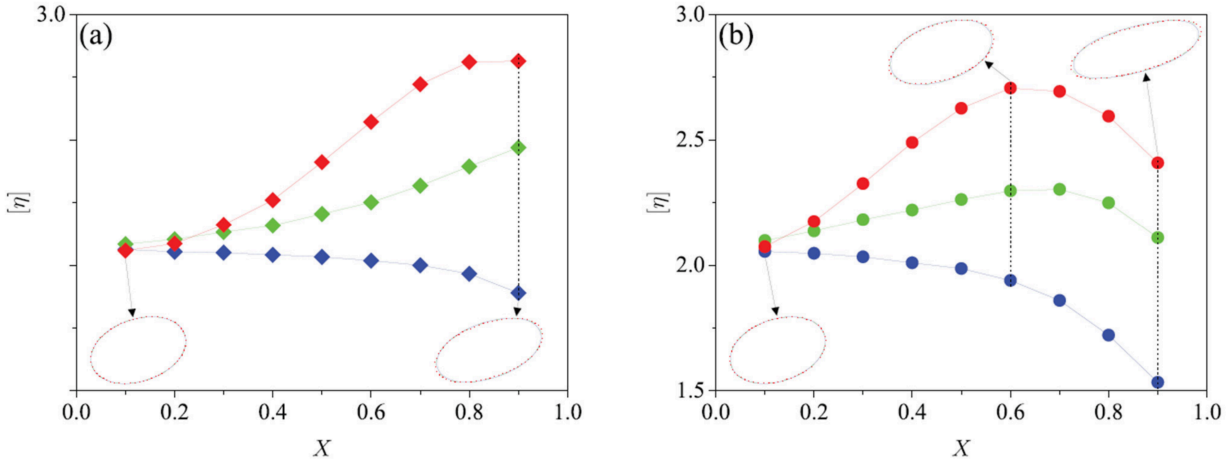


Figure 24. Overall emulsion viscosity $[\eta]$ for (**a**) $E = 0.2$ and (**b**) $E = 0.4$. $N^s_{Pe} = 10^3$ (*red*), $N^s_{Pe} = 1$ (*green*), and $N^s_{Pe} = 10^{-3}$ (*blue*). Adapted from [101].

7. Rheology of Dilute Emulsions with Droplets Covered by a Solid Elastic Membrane

Here, we consider emulsions where the liquid droplets are covered by a thin deformable elastic solid membrane. Red blood cells closely represent droplets covered by an elastic membrane [102–104] when subjected to shear.

Emulsions of droplets covered with elastic membranes exhibit non-Newtonian behavior [102–104] such as shear-thinning. A droplet covered by an elastic membrane behaves as a rigid particle at low shear rates. However, a droplet covered by an elastic membrane deforms into an ellipsoid and attains a steady-state orientation at high shear rates as shown schematically in Figure 25. Interestingly, the membrane of the droplet also undergoes a tank-treading motion which induces internal flow. With the increase in shear rate, the deformation of the coated droplet increases but the orientation remains constant, provided that the membrane is purely elastic in nature. However, in the case of droplets covered by viscoelastic membranes, the deformation of the droplet increases, and the droplet becomes more aligned with the streamlines with the increase in shear rate.

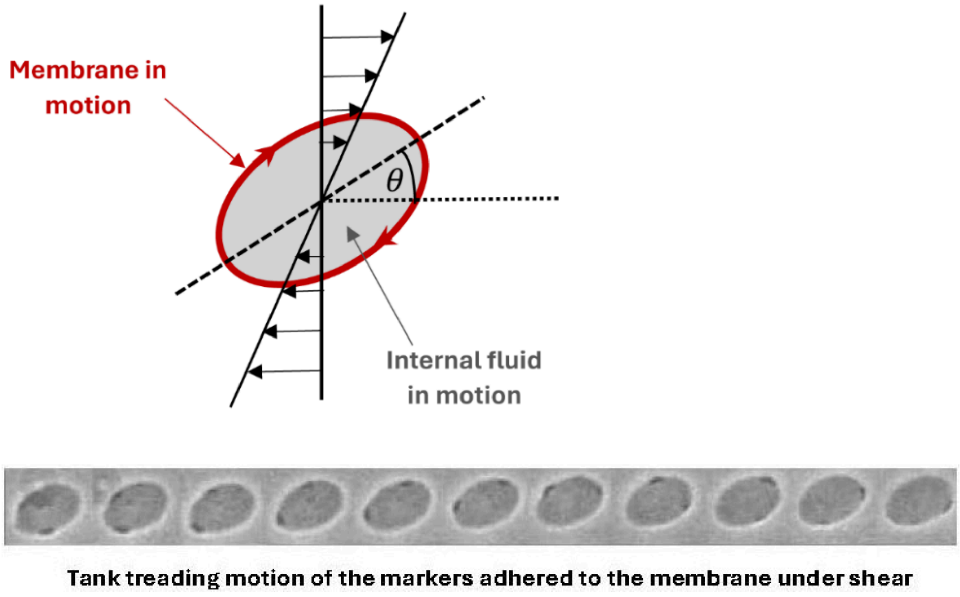


Figure 25. Deformation and orientation of initial spherical membrane-coated droplet suspended in shear flow. Also shown is the tank-treading motion of two markers adhered to the membrane.

The viscosity of emulsions of droplets enclosed by purely elastic membranes of surface elastic modulus E depends on the elastic capillary number N_{Ca}^{s}:

$$N_{Ca}^{s} = \frac{\eta_c \dot{\gamma} R}{E} \tag{84}$$

N_{Ca}^{s} could be interpreted as the ratio of viscous stress to elastic stress. The viscous force tends to elongate and orient the coated droplets in the direction of flow, and the elastic force tends to recover the original shape of the droplets. When $N_{Ca}^{s} << 1$, the coated droplets behave like rigid particles. Consequently, the viscosity is high. When $N_{Ca}^{s} >> 1$, the coated droplets become elongated and attain a steady-state orientation. Also, the membrane of the droplet exhibits a tank-treading motion. Consequently, the viscosity of emulsion is low. At high N_{Ca}^{s}, the viscosity of emulsion depends on λ due to the internal circulation effect. With the increase in λ, the viscosity of emulsion increases. At high λ, the coated droplet behaves as a rigid sphere.

The constitutive equation for a dilute emulsion of membrane-covered droplets, assuming small deformation of droplets, is given as [102–104]:

$$\bar{\bar{\tau}} = 2\eta_c \bar{\bar{E}} + 2\eta_c \varphi \left\{ \frac{5(\lambda - 1)}{2\lambda + 3} \bar{\bar{E}} - \frac{5}{2} \left(\frac{1}{2\lambda + 3} \right) \bar{\bar{L}} - \left(\frac{1}{2\lambda + 3} \right) \bar{\bar{M}} \right\} \tag{85}$$

where $\bar{\bar{L}}$ and $\bar{\bar{M}}$ are tensors that are linear functions of membrane displacement tensors $\bar{\bar{A}}$ and $\bar{\bar{B}}$:

$$\bar{\bar{L}} = 4(\alpha_2 + \alpha_3)\bar{\bar{A}} - (6\alpha_2 + 10\alpha_3)\bar{\bar{B}} \tag{86}$$

$$\bar{\bar{M}} = -4(\alpha_1 + 2\alpha_2 + 2\alpha_3)\bar{\bar{A}} + (12\alpha_2 + 16\alpha_3)\bar{\bar{B}} \tag{87}$$

In Equations (86) and (87), $\bar{\bar{A}}$ is the radial displacement tensor which specifies the radial displacement of material points of the droplet membrane, $\bar{\bar{B}}$ is the tangential displacement tensor which specifies the tangential in-plane displacement of material points of the droplet membrane, and α_i's are dimensionless elastic coefficients of the droplet membrane.

The shear stress τ_{12} in shear flow can be determined from Equation (85) as follows:

$$\tau_{12} = 2\eta_c E_{12} + 2\eta_c \varphi \left[\frac{5(\lambda-1)}{2\lambda+3} E_{12} - \frac{5}{2}\left(\frac{1}{2\lambda+3}\right) L_{12} - \left(\frac{1}{2\lambda+3}\right) M_{12} \right] \tag{88}$$

where

$$L_{12} = 4(\alpha_2+\alpha_3)A_{12} - (6\alpha_2+10\alpha_3)B_{12} \tag{89}$$

$$M_{12} = -4(\alpha_1+2\alpha_2+2\alpha_3)A_{12} + (12\alpha_2+16\alpha_3)B_{12} \tag{90}$$

The intrinsic viscosity $[\eta]$ of the emulsion can be calculated from the knowledge of the shear stress as follows:

$$[\eta] = \underset{\varphi\to 0}{Lim} \frac{(\tau_{12}/2E_{12}) - \eta_c}{\eta_c \varphi} \tag{91}$$

7.1. Droplets Covered with Mooney–Rivlin Membranes

A Mooney–Rivlin membrane is a membrane made of an infinitely thin sheet of a three-dimensional, isotropic, volume-incompressible elastomer. The values of the elastic coefficients α_i's for Mooney–Rivlin-type membranes are given as [102]:

$$\alpha_1 = 0,\ \alpha_2 = 2/3,\ \alpha_3 = 1/3 \tag{92}$$

The components A_{12} and B_{12} of Equations (89) and (90) are given as follows:

$$B_{12} = \frac{a_0}{8\delta_2}\left[1 - \frac{\left(\delta_1 + (N_{Ca}^s)^2/8\right)\left\{\beta_1 - \beta_3 + \left(\delta_1 + (N_{Ca}^s)^2/8\right)(1/4\delta_2)\right\}}{\left(\delta_2 (N_{Ca}^s)^2/16\right) + \left(\delta_1 + (N_{Ca}^s)^2/8\right)^2 (1/4\delta_2)}\right] \tag{93}$$

$$A_{12} = \frac{a_0}{16\beta_1}\left[\frac{\beta_2}{3\delta_2} - 1 + \frac{\left\{-4\beta_2\delta_1 + (3\delta_2-\beta_2)\left((N_{Ca}^s)^2/2\right)\right\}\left\{\beta_1 - \beta_3 + \left(\delta_1 + (N_{Ca}^s)^2/8\right)(1/4\delta_2)\right\}}{3\left(\delta_2^2 (N_{Ca}^s)^2/4\right) + 3\left(\delta_1 + (N_{Ca}^s)^2/8\right)^2}\right] \tag{94}$$

where

$$a_0 = 5/(2\lambda+3) \tag{95}$$

$$2\beta_1 = b_0 - 2b_1;\ 2\beta_2 = 11b_0 - 20b_1 \tag{96}$$

$$2\beta_3 = b_0 - 2b_1 - 2b_2;\ 2\beta_4 = 11b_0 - 20b_1 - 20b_2 \tag{97}$$

$$\delta_1 = \frac{4}{3}(\beta_2\beta_3 - \beta_1\beta_4);\ \delta_2 = \frac{\beta_2}{3} - 2\beta_3 \tag{98}$$

$$b_0 = 1/(2\lambda+3) \tag{99}$$

$$b_1 = 2(3\lambda+2)/[(19\lambda+16)(2\lambda+3)] \tag{100}$$

$$b_2 = 2/(19\lambda+16) \tag{101}$$

Thus, the $[\eta]$ of emulsions of droplets covered with Mooney–Rivlin membranes is:

$$[\eta] = a_0(\lambda-1) - \frac{a_0^2}{20\beta_1}\left(\frac{\beta_2}{3\delta_2} - 1\right) + \frac{a_0^2}{4\delta_2} - I \tag{102}$$

where I is given as:

$$I = \frac{a_0^2\left\{\beta_1 - \beta_3 + (1/4\delta_2)\left(\delta_1 + (N_{Ca}^s)^2/8\right)\right\}\left\{2\delta_1(15\beta_1-\beta_2) + (3\delta_2 - \beta_2 + 15\beta_1)\left((N_{Ca}^s)^2/4\right)\right\}}{30\beta_1\left[\left(\delta_2^2 (N_{Ca}^s)^2/4\right) + \left(\delta_1 + (N_{Ca}^s)^2/8\right)^2\right]} \tag{103}$$

From Equations (102) and (103), the low and high shear limits of the $[\eta]$ are as follows [98]:

$$[\eta]_0 = \frac{5}{2} \tag{104}$$

$$[\eta]_\infty = \frac{5(\lambda - 1)}{2\lambda + 3} \tag{105}$$

Figure 26 shows $[\eta]$ versus N_{Ca}^s (defined as $\eta_c \dot{\gamma} R/E$) for different values of λ. The emulsion exhibits shear-thinning as $[\eta]$ decreases with the increase in N_{Ca}^s. The coated droplets behave like rigid particles at low values of N_{Ca}^s and $[\eta] = 2.5$. At high values of N_{Ca}^s, $[\eta]$ varies from $-5/3$ to 2.5 depending upon λ.

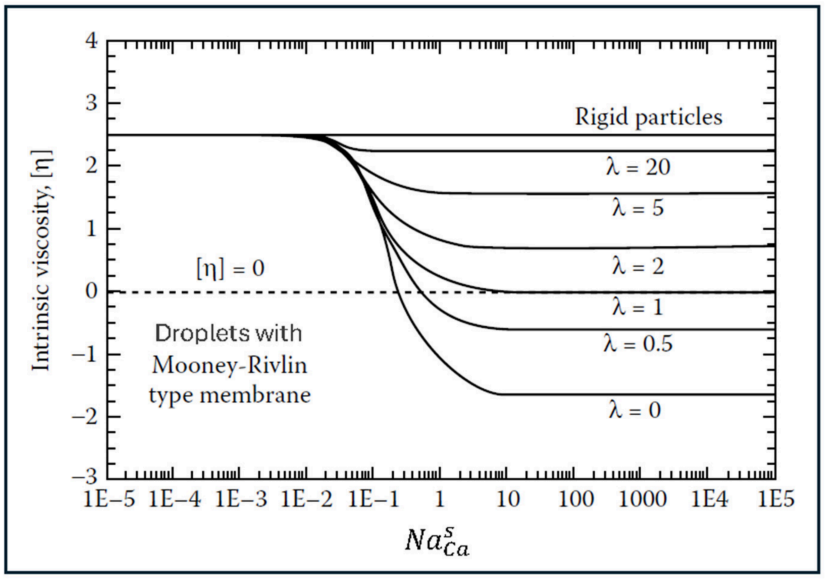


Figure 26. $[\eta]$ versus N_{Ca}^s for emulsions of droplets coated with Mooney–Rivlin membrane at different values of viscosity ratio λ. Adapted from [102].

7.2. Droplets Covered with RBC Membrane

The red blood cell (RBC) consists of a lipid bilayer lined by a protein network that imparts elasticity to its membrane. The elastic coefficients of the RBC membrane are as follows [102]:

$$\alpha_1 = 0,\ \alpha_2 = 1000,\ \alpha_3 = \frac{1}{2} \tag{106}$$

The components A_{12} and B_{12} and $[\eta]$ for emulsions with droplets covered by RBC membranes are:

$$A_{12} = \frac{3}{2} B_{12} = \frac{60}{\left[16 + (23\lambda + 32)^2 \left((N_{Ca}^s)^2/4\right)\right]} \tag{107}$$

$$[\eta] = \frac{5(23\lambda - 16)}{2(23\lambda + 32)} + \frac{7680}{(23\lambda + 32)\left[64 + (23\lambda + 32)^2 \left(N_{Ca}^s\right)^2\right]} \tag{108}$$

The low and high shear limits of [η] are as follows [102]:

$$[\eta]_0 = \frac{5}{2} \tag{109}$$

$$[\eta]_\infty = \frac{5(23\lambda - 16)}{2(23\lambda + 32)} \tag{110}$$

Figure 27 shows $[\eta]$ versus N_{Ca}^{s} plots for emulsions of droplets coated with RBC membranes. The rheological behavior is like that of emulsions of droplets coated with Mooney–Rivlin membranes (see Figure 26), although the values of $[\eta]$ are not the same. For instance, $[\eta]$ is $-5/4$ at high values of N_{Ca}^{s} when $\lambda = 0$ and the droplets are coated with RBC membranes. The corresponding value of $[\eta]$ for droplets coated with Mooney–Rivlin membranes is $-5/3$.

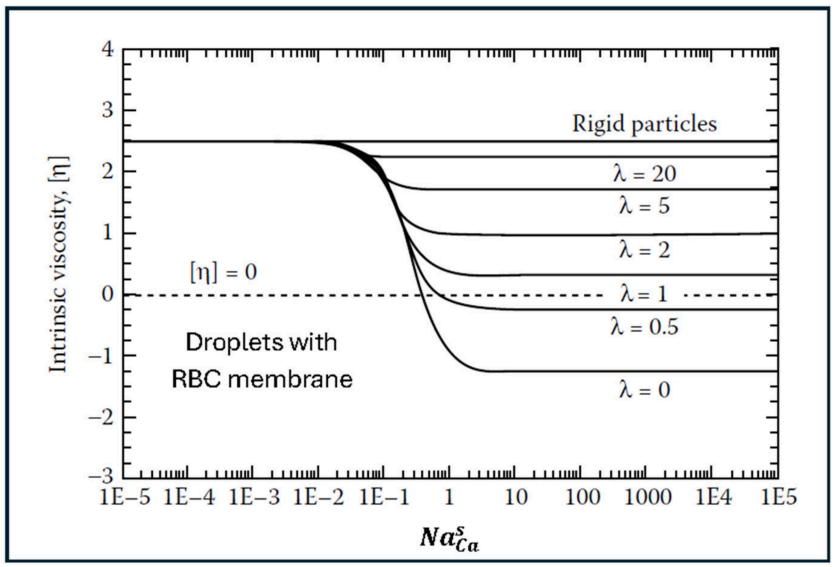


Figure 27. $[\eta]$ versus N_{Ca}^{s} for emulsions of droplets coated with RBC-type membranes at different λ. Adapted from [102].

8. Rheology of Dilute Emulsions of Double Droplets (Droplets Covered with Liquid Films)

An emulsion double droplet is a composite droplet consisting of a core liquid droplet covered by a shell of another immiscible liquid. The composite droplet is suspended in a matrix of yet another immiscible liquid as shown in Figure 28. Thus, the emulsion consists of three liquids.

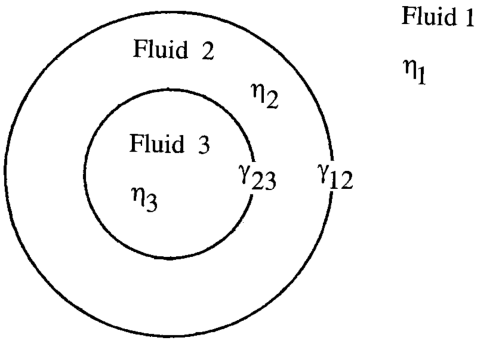


Figure 28. Emulsion double droplet.

Let a be the core droplet (fluid 3) radius, b be the radius of the composite droplet, η_1 be the viscosity of fluid 1 (matrix or continuous phase), η_2 be the viscosity of fluid 2 (shell fluid), η_3 be the viscosity of fluid 3 (core fluid), γ_{12} be the interfacial tension between fluids 1 and 2, and γ_{23} be the interfacial tensions between fluids 2 and 3, as shown in Figure 28.

When the emulsion is subjected to flow, the compound droplet deforms. The compound droplet has two interfaces: the outer interface between fluids 1 and 2 and the inner

interface between fluids 2 and 3. The shape of the outer interface between fluids 1 and 2 can be expressed as:

$$r = \left(x_1^2 + x_2^2 + x_3^2\right)^{1/2} = f_{12}(x_1, x_2, x_3) \tag{111}$$

where r is the distance from the center of the composite droplet. Likewise, the shape of the inner interface between fluids 2 and 3 can be expressed as:

$$r = \left(x_1^2 + x_2^2 + x_3^2\right)^{1/2} = f_{23}(x_1, x_2, x_3) \tag{112}$$

where r is the distance from the center of the composite droplet.

The flow field in different fluids is described by the Stokes equations (assuming that inertial effects are negligible) with respect to a co-ordinate system fixed at the center of the composite droplet. Thus,

$$\eta_1 \nabla^2 \vec{u}_1 = \nabla P_1,\ \nabla \bullet \vec{u}_1 = 0 \ \ for\, r > f_{12} \tag{113}$$

$$\eta_2 \nabla^2 \vec{u}_2 = \nabla P_2,\ \nabla \bullet \vec{u}_2 = 0 \ \ for\, f_{23} < r < f_{12} \tag{114}$$

$$\eta_3 \nabla^2 \vec{u}_3 = \nabla P_3,\ \nabla \bullet \vec{u}_3 = 0 \ \ for\, 0 \leq\ r < f_{23} \tag{115}$$

The boundary conditions to be satisfied are as follows:

(i) Far away from the compound droplet, ($r \longrightarrow \infty$),

$$\vec{u}_1 \rightarrow \vec{u}_\infty \tag{116}$$

(ii) At the interface between fluids 1 and 2, ($r = f_{12}$),

$$\vec{u}_1 = \vec{u}_2 \tag{117}$$

$$\left(\bar{\bar{\sigma}}_1 - \bar{\bar{\sigma}}_2\right) \bullet \hat{n}_2 = \gamma_{12} \hat{n}_2 (\nabla_s \bullet \hat{n}_2) \tag{118}$$

where $\hat{n}_2$ is unit normal at interface $r = f_{12}$ directed outward from fluid 2 (see Figure 28).

(iii) At the interface between fluids 2 and 3, ($r = f_{23}$),

$$\vec{u}_2 = \vec{u}_3 \tag{119}$$

$$\left(\bar{\bar{\sigma}}_2 - \bar{\bar{\sigma}}_3\right) \bullet \hat{n}_3 = \gamma_{23} \hat{n}_3 (\nabla_s \bullet \hat{n}_3\ ) \tag{120}$$

where $\hat{n}_3$ is unit normal at interface $r = f_{23}$ directed outward from fluid 3.

Stone and Leal [76] calculated the velocity and pressure distributions inside and outside the composite droplet, assuming zero- and first-order deformations of the composite droplet.

The streamline patterns in and around the compound droplet are shown in Figures 29 and 30 for $a/b = 0.2$ and 0.8 when $\eta_1 = \eta_2 = \eta_3$ when the emulsion is subjected to uniaxial flow. Interestingly, there are two vortical flow patterns interior to the double-emulsion droplet. The external continuous-phase fluid (fluid 1) motion creates a re-circulating flow in the outer shell liquid (fluid 2) that drives the motion in the inner core droplet (fluid 3) with an opposite direction of rotation. An important point to note from the streamline patterns shown in Figures 29 and 30 is that the uniaxial bulk flow tends to deform the overall compound droplet into a prolate spheroidal shape. It should be noted that although the external applied flow is a uniaxial flow, the flow generated in the outer shell liquid (fluid 2) of the compound droplet is biaxial extensional. Consequently, the inner core

droplet (fluid 3) tends to deform into an oblate spheroidal shape. The deformation of the compound droplet can be seen more clearly in Figure 31.

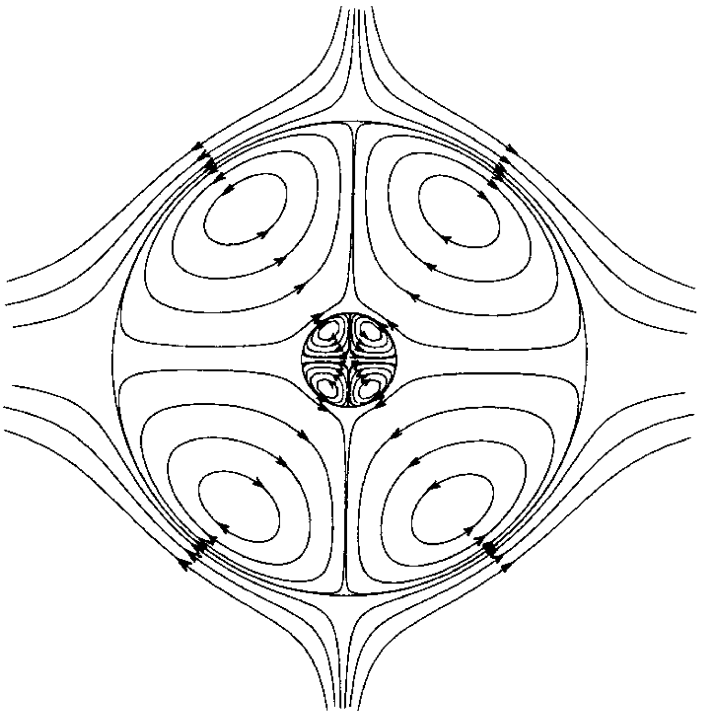


Figure 29. Streamline patterns in and around the emulsion double droplet for $a/b = 0.20$. Adapted from [76].

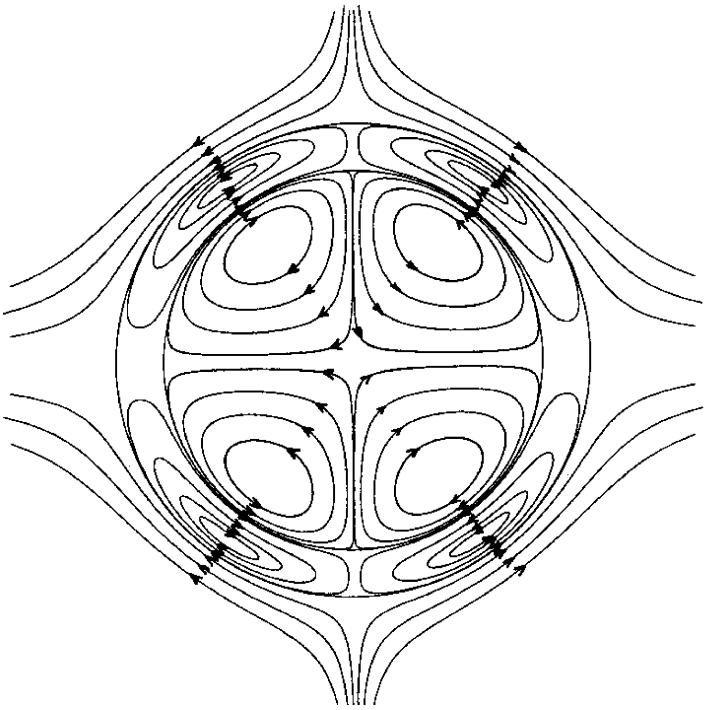


Figure 30. Streamline patterns in and around the emulsion double droplet for $a/b = 0.80$. Adapted from [76].

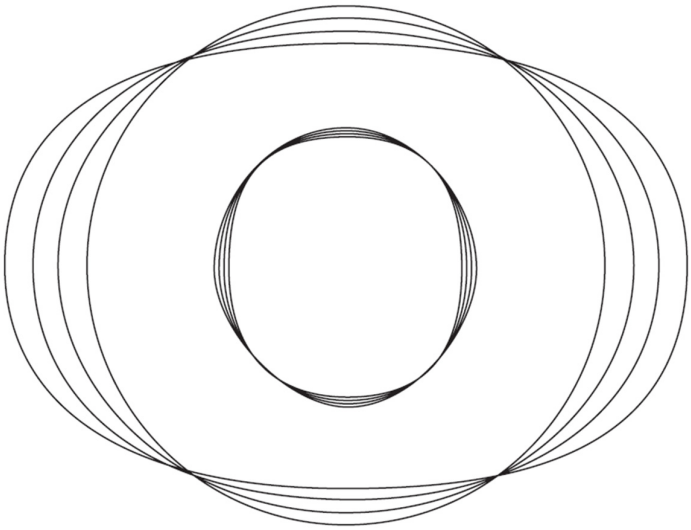


Figure 31. Deformation of an emulsion double droplet. Adapted from [76].

The dipole strength $\overline{\overline{S}}^{o}$ of a compound emulsion droplet is obtained from Equation (23) using the zero-order flow fields [76]:

$$\overline{\overline{S}}^{o} = 5\left(1 - \frac{3}{5}I\right)V_p\eta_1\overline{\overline{E}}_\infty \tag{121}$$

where $I(a/b, \lambda_{21}, \lambda_{32})$ is a function of a/b and viscosity ratios $\lambda_{21}(=\eta_2/\eta_1)$ and $\lambda_{32}(=\eta_3/\eta_2)$, V_p is the volume of a single compound droplet, and $\overline{\overline{E}}_\infty$ is the rate of deformation tensor far away from the droplet. The expression for I is:

$$I = \frac{\delta_1 + \frac{(a/b)^3}{1+\lambda_{32}}\delta_2}{\delta_1 + \lambda_{21}\delta_3 + \frac{(a/b)^3}{1+\lambda_{32}}(\delta_2 + \lambda_{21}\delta_4)} \tag{122}$$

The coefficients δ_i depend on the ratio a/b only:

$$\delta_1 = 4 - 25\left(\frac{a}{b}\right)^3 + 42\left(\frac{a}{b}\right)^5 - 25(a/b)^7 + 4(a/b)^{10} \tag{123}$$

$$\delta_2 = 15 - 42\left(\frac{a}{b}\right)^2 + 35\left(\frac{a}{b}\right)^4 - 8(a/b)^7 \tag{124}$$

$$\delta_3 = 4 - 10\left(\frac{a}{b}\right)^3 + 10\left(\frac{a}{b}\right)^7 - 4(a/b)^{10} \tag{125}$$

$$\delta_4 = 6 - 14(a/b)^4 + 8(a/b)^7 \tag{126}$$

Using Equations (26) and (121), the rheological equation for a dilute emulsion of identical double droplets is:

$$\overline{\overline{\sigma}} = -P\overline{\overline{\delta}} + 2\eta_1\,\overline{\overline{E}} + 5\left(1 - \frac{3}{5}I\right)\eta_1\varphi\overline{\overline{E}} \tag{127}$$

The relative viscosity of the emulsion of double droplets predicted from Equation (127) is:

$$\eta_r = \frac{\eta}{\eta_1} = 1 + \frac{5}{2}\left(1 - \frac{3}{5}\,I\right)\varphi \tag{128}$$

When $\lambda_{21} \longrightarrow \infty$, $I \longrightarrow 0$, Equation (128) reduces to the Einstein equation, Equation (37), valid for rigid spheres [85,86]. Equation (128) reduces to the Taylor equation, Equation (36), valid for droplets [81], in the limit $a/b \to 0$, $I \longrightarrow 1/(1 + \lambda_{21})$.

When the outer shell layer is very thin ($a/b \to 1$), I approaches zero, regardless of the core liquid viscosity. Thus, composite droplets with thin outer shells (not necessarily of high viscosity) behave like rigid particles regardless of the inner core liquid viscosity. This can be appreciated by examining the streamlines [105] shown in Figure 32. The motion of fluid 1 (continuous phase) sets up internal circulation with the streamlines as shown in Figure 32. As fluid 2's (shell liquid) thickness approaches a small value, all internal circulation within the core and shell liquid is suppressed as, otherwise, the shell liquid would have to change directions over a very short distance. Consequently, the composite droplet behaves like a rigid sphere [105].

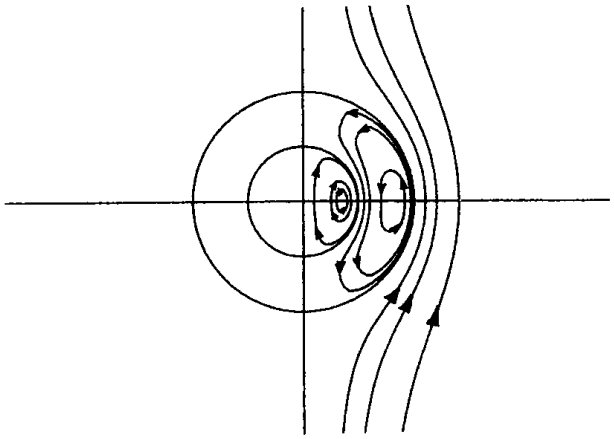


Figure 32. Streamline patterns in and around the emulsion double droplet. Adapted from [105].

Figures 33 and 34 show $[\eta]$ versus a/b plots for emulsions of double droplets. They are generated by Equation (128) under different conditions. $[\eta]$ is sensitive to λ_{21}, but λ_{32} has little effect on $[\eta]$.

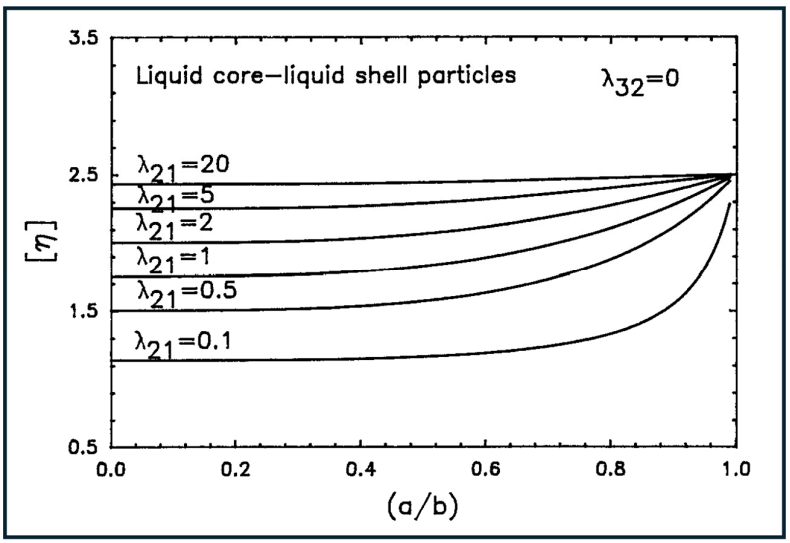


Figure 33. Intrinsic viscosity $[\eta]$ versus a/b ratio for emulsions of double droplets at different λ_{21} ($\lambda_{32} = 0$).

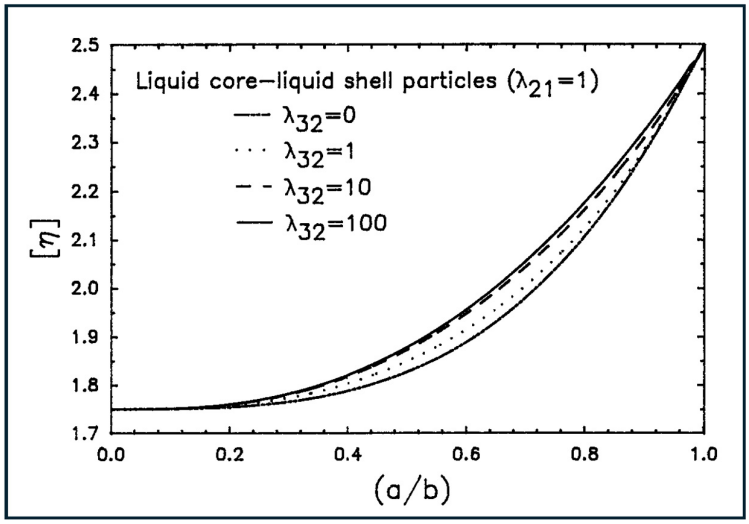


Figure 34. Intrinsic viscosity $[\eta]$ versus a/b ratio for emulsions of double droplets at different λ_{32} ($\lambda_{21} = 0$).

9. Dynamic Rheology of Dilute Emulsions

Emulsion droplets deform when subjected to viscous stresses. The interfacial tension tends to restore the droplet shape. Therefore, the droplets possess an elasticity of shape due to the restoring force of interfacial tension. When the emulsion is subjected to a variable time-dependent macroscopic rate of shear, the droplets experience variations in stress, and, therefore, the amount of elastic strain energy stored in the emulsion varies. The interchange of energy between the kinetic energy of flow and the internal potential energy manifests itself in the viscoelasticity of the emulsion.

Palierne [106] has presented a detailed analysis of the linear viscoelastic behavior of emulsions. The complex shear modulus G^* of a dilute emulsion of identical droplets is given by:

$$G^* = G_c^*(1 + 5\varphi H^*) \tag{129}$$

where G_c^* is the complex shear modulus of the continuous phase and H^* is given by:

$$H^* = \frac{(G_d^* - G_c^*)(16G_c^* + 19G_d^*) + (4\gamma/R)(2G_c^* + 5G_d^*)}{(2G_d^* + 3G_c^*)(16G_c^* + 19G_d^*) + (40\gamma/R)(G_c^* + G_d^*)} \tag{130}$$

In Equation (130), G_d^* is the complex shear modulus of the droplets, and ω is the frequency. Note that $G^* = G' + jG''$, where G' is storage modulus, G'' is loss modulus, and j is the imaginary number $\sqrt{-1}$. The Palierne model, Equation (129), could be re-written as:

$$G' = G_c' + 5\varphi(H'G_c' - G_c''H'') \tag{131}$$

$$G'' = G_c'' + 5\varphi(H''G_c' + H'G_c'') \tag{132}$$

where

$$H' = \frac{g'h' + g''h''}{\left[(g')^2 + (g'')^2\right]} \tag{133}$$

$$H'' = \frac{g'h'' - g''h'}{\left[(g')^2 + (g'')^2\right]} \tag{134}$$

$$g' = (2G_d' + 3G_c')(19G_d' + 16G_c') - (2G_d'' + 3G_c'')(19G_d'' + 16G_c'') + \left(\frac{40\gamma}{R}\right)(G_d' + G_c') \tag{135}$$

$$g'' = (2G_d' + 3G_c')(19G_d'' + 16G_c'') + (2G_d'' + 3G_c'')(19G_d' + 16G_c') + \left(\frac{40\gamma}{R}\right)(G_d'' + G_c'') \quad (136)$$

$$h' = (G_d' - G_c')(19G_d' + 16G_c') - (G_d'' - G_c'')(19G_d'' + 16G_c'') + \left(\frac{4\gamma}{R}\right)(5G_d' + 2G_c') \quad (137)$$

$$h'' = (G_d' - G_c')(19G_d'' + 16G_c'') + (G_d'' - G_c'')(19G_d' + 16G_c') + \left(\frac{4\gamma}{R}\right)(5G_d'' + 2G_c'') \quad (138)$$

Equations (131)–(138) can be used to predict the G' and G'' of the emulsion from the knowledge of G_c', G_c'', G_d', G_d'', γ and R.

Equations (129) and (130) reduce to the following expressions for emulsions composed of two Newtonian liquids:

$$G^* = j\omega\eta_c(1 + 5\varphi H^*) \quad (139)$$

$$H^* = \frac{(j\omega\eta_d - j\omega\eta_c)(16j\omega\eta_c + 19j\omega\eta_d) + (4\gamma/R)(2j\omega\eta_c + 5j\omega\eta_d)}{(2j\omega\eta_d + 3j\omega\eta_c)(16j\omega\eta_c + 19j\omega\eta_d) + (40\gamma/R)(j\omega\eta_c + j\omega\eta_d)} \quad (140)$$

Note that for Newtonian liquids:

$$G_c^* = j\omega\eta_c; G_d^* = j\omega\eta_d \quad (141)$$

where η_c and η_d are the viscosities of the continuous and dispersed phases, respectively. Equation (138) can be further re-written as:

$$H^* = \frac{j\omega\eta_c(\lambda - 1)(16 + 19\lambda) + (4\gamma/R)(2 + 5\lambda)}{j\omega\eta_c(2\lambda + 3)(16 + 19\lambda) + (40\gamma/R)(1 + \lambda)} \quad (142)$$

where $\lambda = \eta_d/\eta_c$ is the viscosity ratio.

Figure 35 shows the plots of the moduli for an emulsion of two immiscible Newtonian liquids at two different viscosity ratios λ under the conditions: $\varphi = 0.05$, $\gamma/R =$ 1000 Pa, and $\eta_c = 1000$ Pa. The Cole–Cole plot in the form of $\eta''(= G'/\omega)$ versus $\eta'(= G''/\omega)$ is also plotted. For a given viscosity ratio λ, a single relaxation domain is observed; that is, there is one G' plateau and one circular arc in the Cole–Cole plot. Increasing λ lowers the plateau value of G', whereas G'' shows a negligible change. The circular arc of the Cole–Cole plot is much bigger at a low viscosity ratio of zero due to large values of G'or η''.

Figure 36 shows the effect of interfacial stress γ/R on the G' and G'' of the emulsion. The plateau value of the storage modulus increases with the increase in interfacial stress γ/R. The frequency at which the plateau in G' begins is also shifted to higher values with the increase in γ/R. However, the effect of interfacial stress γ/R on G'' is negligible.

If the two liquids of the emulsion are not Newtonian, the emulsion does not exhibit a single relaxation behavior. For example, consider an emulsion composed of viscoelastic continuous and dispersed phases that follow the Maxwell model described as

$$G_c^* = \frac{j\omega\eta_c}{1 + j\omega\tau_c}; G_d^* = \frac{j\omega\eta_d}{1 + j\omega\tau_d} \quad (143)$$

where G_c^* and G_d^* are complex moduli of the continuous phase and dispersed phase, respectively; τ_c and τ_d are relaxation times of the continuous phase and dispersed phase, respectively; and η_c and η_d are zero shear viscosities of the continuous phase and dispersed phase, respectively. From Equation (143), it follows that:

$$G_c' = \frac{\omega^2\eta_c\tau_c}{1 + \omega^2\tau_c^2}; G_c'' = \frac{\omega\eta_c}{1 + \omega^2\tau_c^2} \quad (144)$$

$$G'_d = \frac{\omega^2 \eta_d \tau_d}{1+\omega^2\tau_d^2}; G''_d = \frac{\omega \eta_d}{1+\omega^2\tau_d^2} \quad (145)$$

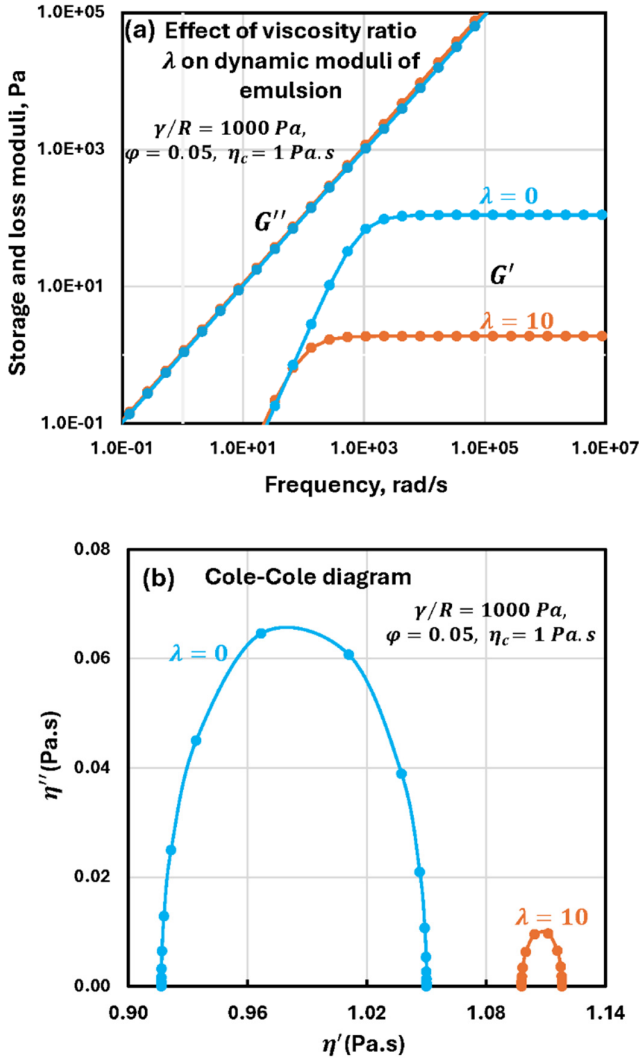


Figure 35. Effect of viscosity ratio λ on the dynamic rheology of emulsion of two immiscible Newtonian liquids.

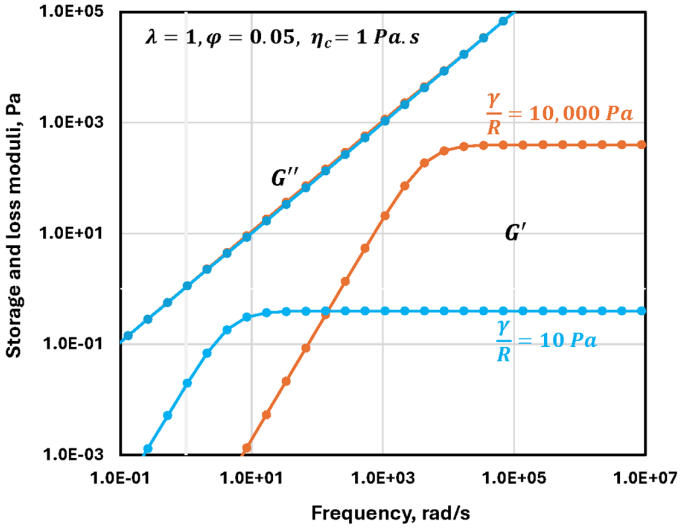


Figure 36. Effect of γ/R on the dynamic rheology of emulsion of two Newtonian liquids.

Figure 37 shows the viscoelastic behavior of a Maxwell liquid. As expected, the liquid exhibits a single relaxation behavior. The storage modulus levels off at a frequency of 10^{-3} rad/s, corresponding to τ = 1000 s. The Cole–Cole diagram shows a single circular arc corresponding to a single relaxation behavior.

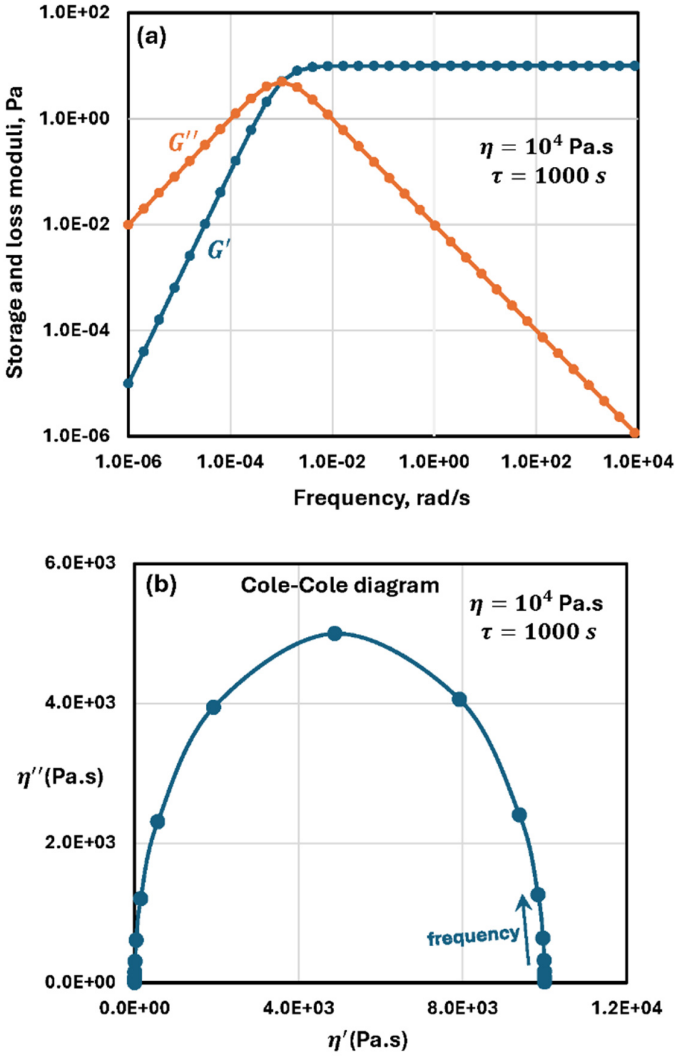


Figure 37. Viscoelastic behavior of a Maxwell liquid.

The G' and G'' of the emulsion of two viscoelastic liquids are shown in Figure 38. Equations (131)–(138) are used to generate data. The G' of the emulsion exhibits a plateau at high frequencies and a plateau at low frequencies. The Cole–Cole diagram, where $\eta''(=G'/\omega)$ is plotted as a function of $\eta'(=G''/\omega)$, shows two frequency domains: the small right-hand side circular arc corresponds to low frequencies, and the large left-hand side circular arc corresponds to high frequencies. The low-frequency domain is due to the interfacial tension effect, whereas the elastic behavior in the high-frequency domain is due to the elasticity of the matrix. At high frequencies, the upper G' plateau of the emulsion overlaps with the G' plateau of the matrix. Also, the high-frequency Cole–Cole plot of the emulsion and the matrix overlaps.

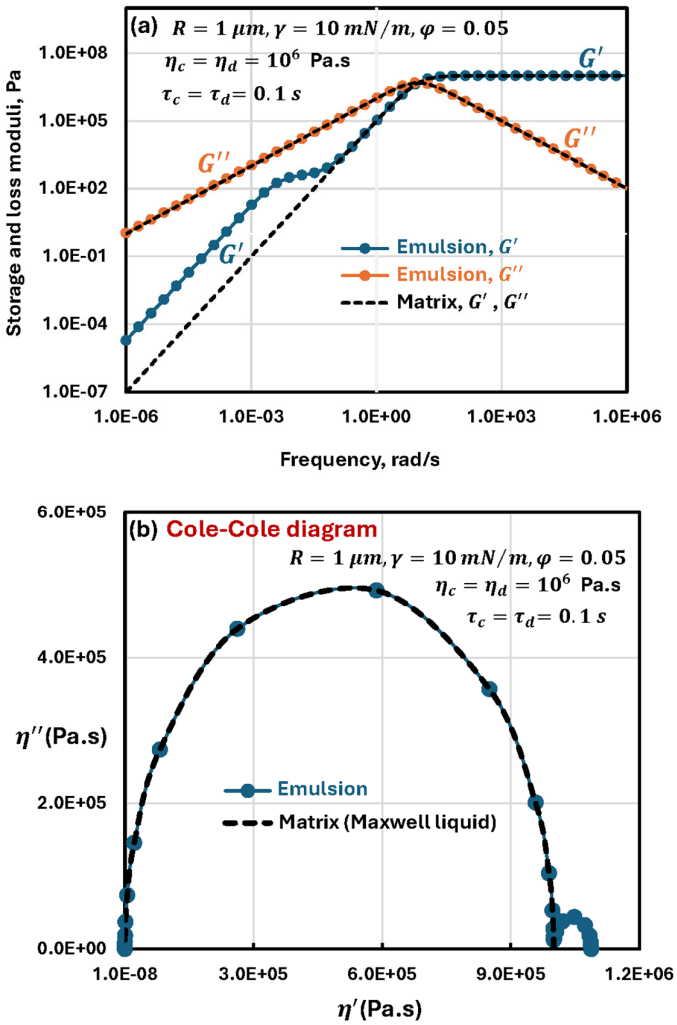


Figure 38. Dynamic rheology of an emulsion composed of Maxwellian-type viscoelastic liquids.

Figure 39 shows the effect of γ/R on the dynamic rheology of an emulsion composed of two immiscible Maxwellian-type viscoelastic liquids. With an increase in γ/R, the lower plateau value of G' increases. The high-frequency plateau in G' is unaffected by the interfacial stress. Also, the frequency at which the lower plateau in G' begins is shifted to higher values with an increase in γ/R. The effect of γ/R on the loss modulus of the emulsion is negligible.

In the Palierne model, Equation (129), the interface is treated as pure (no additives) with uniform interfacial tension. In real systems, the interface consists of additives such as surfactants, polymers, and solid nanoparticles. Examples of different types of interfacial films (interfaces) present on the droplet surface include (a) droplets coated with purely viscous film, characterized by uniform interfacial properties such as interfacial tension (γ), surface shear viscosity (η_s), and surface dilational viscosity $\left(\eta_s^k\right)$; (b) droplets coated with purely elastic film, characterized by surface shear modulus (G_s) and surface dilational modulus (K_s), in addition to interfacial tension; (c) droplets coated with viscoelastic film, characterized by complex surface shear modulus (G_s^*) and complex surface dilational modulus (K_s^*), in addition to interfacial tension (note that $G_s^* = G_s + j\eta_s\omega$ and $K_s^* = K_s + j\eta_s^k\omega$) (d) droplets with interfacial film possessing bending rigidity; and (e) droplets coated with liquid film.

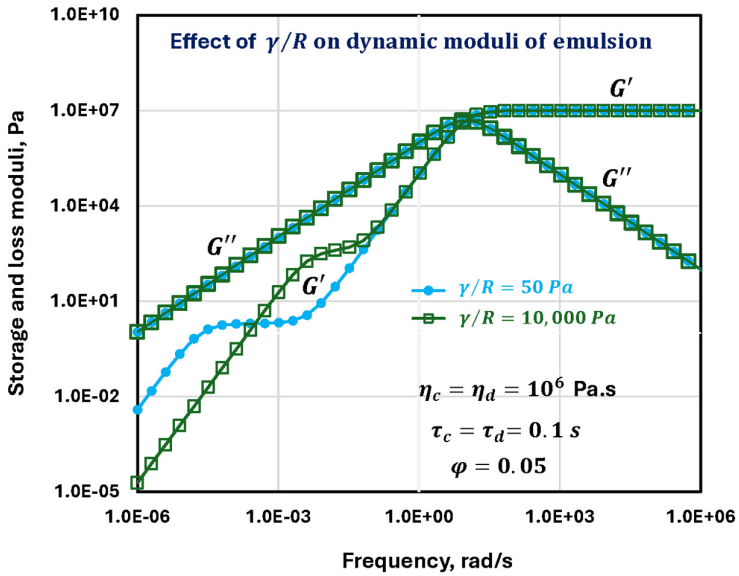


Figure 39. Effect of γ/R on the dynamic rheology of emulsion of two immiscible Maxwellian-type viscoelastic liquids.

9.1. Droplets Covered with Purely Viscous Films

The surface stress tensor $\left(\overline{\overline{P}}_s\right)$ for an infinitely thin (two-dimensional) purely viscous film is related to the surface rate-of-strain tensor $\left(\overline{\overline{E}}_s\right)$ as [98]:

$$\overline{\overline{P}}_s = \gamma\overline{\overline{\delta}}_s + 2\eta_s\overline{\overline{E}}_s + \left(\eta_s^k - \eta_s\right)\left(\overline{\overline{\delta}}_s : \overline{\overline{E}}_s\right)\overline{\overline{\delta}}_s \tag{146}$$

where γ is the interfacial tension, η_s is the surface shear viscosity, η_s^k is the surface dilational viscosity, and $\overline{\overline{\delta}}_s$ is the surface unit tensor $(= \overline{\overline{\delta}} - \hat{n}\hat{n})$. Oldroyd [98] investigated emulsions of liquid droplets coated with purely viscous films. Using the "self-consistent approach", he developed a constitutive equation to describe the viscoelastic behavior as:

$$\left(1 + \tau_1\frac{\partial}{\partial t}\right)\overline{\overline{\tau}} = 2\eta_0\left(1 + \tau_2\frac{\partial}{\partial t}\right)\overline{\overline{E}} \tag{147}$$

where η_0, τ_1 and τ_2 are given as:

$$\eta_0 = \eta_c\left[1 + 5\varphi\left\{\frac{2 + 5\lambda + (4N_{Bo}^{\eta}) + (6N_{Bo}^{k})}{10(1+\lambda) + (8N_{Bo}^{\eta}) + (12N_{Bo}^{k})}\right\}\right] \tag{148}$$

$$\tau_1 = \left(\frac{\alpha_1 - 2\varphi\alpha_2}{\beta_1 - 2\varphi\beta_2}\right)\left(\frac{\eta_c R}{4\gamma}\right) = \left(\frac{\alpha_1}{\beta_1}\right)\left[1 - 2\varphi\left(\frac{\alpha_2}{\alpha_1} - \frac{\beta_2}{\beta_1}\right)\right]\left(\frac{\eta_c R}{4\gamma}\right) \tag{149}$$

$$\tau_2 = \left(\frac{\alpha_1 + 3\varphi\alpha_2}{\beta_1 + 3\varphi\beta_2}\right)\left(\frac{\eta_c R}{4\gamma}\right) = \left(\frac{\alpha_1}{\beta_1}\right)\left[1 + 3\varphi\left(\frac{\alpha_2}{\alpha_1} - \frac{\beta_2}{\beta_1}\right)\right]\left(\frac{\eta_c R}{4\gamma}\right) \tag{150}$$

$$\alpha_1 = [(3+2\lambda)(16+19\lambda) + 4(12+13\lambda)(N_{Bo}^{\eta}) + 2(32+23\lambda)(N_{Bo}^{k}) + 32N_{Bo}^{k}N_{Bo}^{\eta}] \tag{151}$$

$$\alpha_2 = [(\lambda-1)(16+19\lambda) + 2(8+13\lambda)(N_{Bo}^{\eta}) + (23\lambda-16)(N_{Bo}^{k}) + 16N_{Bo}^{k}N_{Bo}^{\eta}] \tag{152}$$

$$\beta_1 = 10(1+\lambda) + 8N_{Bo}^{\eta} + 12N_{Bo}^{k} \tag{153}$$

$$\beta_2 = 2 + 5\lambda + 4N_{Bo}^{\eta} + 6N_{Bo}^{k} \tag{154}$$

where N_{Bo}^{η} is the shear Boussinesq number ($=\eta_s/\eta_c R$), N_{Bo}^{k} is the dilational Boussinesq number ($=\eta_s^k/\eta_c R$), and λ is the viscosity ratio. The stress boundary condition at the interface ($r=R$) was modified because of the presence of a film on the droplet. From force balance at the interface, it follows that [80]:

$$\hat{n}\bullet\left(\overline{\overline{\sigma}}_c-\overline{\overline{\sigma}}_d\right)=(\nabla_s\bullet\hat{n})\left(\hat{n}\bullet\overline{\overline{P}}_s\right)-\nabla_s\bullet\overline{\overline{P}}_s \tag{155}$$

where ∇_s is given as $\left(\overline{\overline{\delta}}-\hat{n}\hat{n}\right)\bullet\nabla$. As $\hat{n}\bullet\overline{\overline{P}}_s=0$, Equation (155) reduces to

$$\hat{n}\bullet\left(\overline{\overline{\sigma}}_c-\overline{\overline{\sigma}}_d\right)=-\nabla_s\bullet\overline{\overline{P}}_s \tag{156}$$

The normal stress discontinuity across the interface at $r=R$ is:

$$\hat{n}\bullet\left(\overline{\overline{\sigma}}_c-\overline{\overline{\sigma}}_d\right)\bullet\hat{n}=-\left(\nabla_s\bullet\overline{\overline{P}}_s\right)\bullet\hat{n} \tag{157}$$

The tangential stress discontinuity at the interface at $r=R$ is:

$$\hat{n}\bullet\left(\overline{\overline{\sigma}}_c-\overline{\overline{\sigma}}_d\right)\bullet\overline{\overline{\delta}}_s=-\left(\nabla_s\bullet\overline{\overline{P}}_s\right)\bullet\overline{\overline{\delta}}_s \tag{158}$$

where $\overline{\overline{P}}_s$ is given by Equation (146). Using Equations (147)–(154), it can be readily shown that in oscillatory shear flow:

$$\frac{G^*}{j\omega\eta_c}=1+5\varphi H^* \tag{159}$$

where H^* is given by

$$H^*=\left[\frac{(4\gamma/R)\beta_2+(j\omega\eta_c)\alpha_2}{(4\gamma/R)\beta_1+(j\omega\eta_c)\alpha_1}\right] \tag{160}$$

The effect of N_{Bo}^{η} on the G' and G'' of an emulsion is shown in Figure 40. Equations (159) and (160) are used to generate the plots.

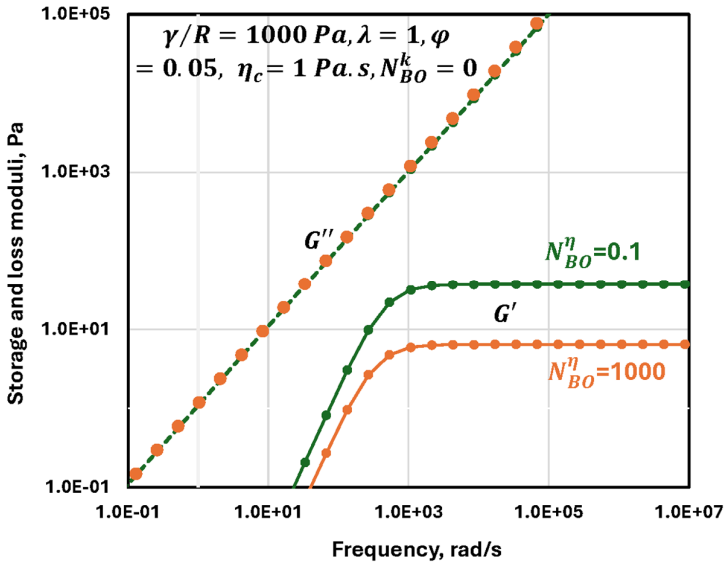


Figure 40. The effect of N_{Bo}^{η} on G' and G'' of an emulsion.

The storage modulus of the emulsion decreases significantly with the increase in N_{Bo}^{η}. The effect of N_{Bo}^{η} on the loss modulus is negligible. Note that the emulsion with purely viscous interfacial films exhibits a single relaxation domain.

Figure 41 shows the effect of N_{Bo}^{k} on the G' and G'' of emulsion. The storage modulus of the emulsion increases slightly with the increase in N_{Bo}^{k}. There is a negligible effect of N_{Bo}^{k} on G''.

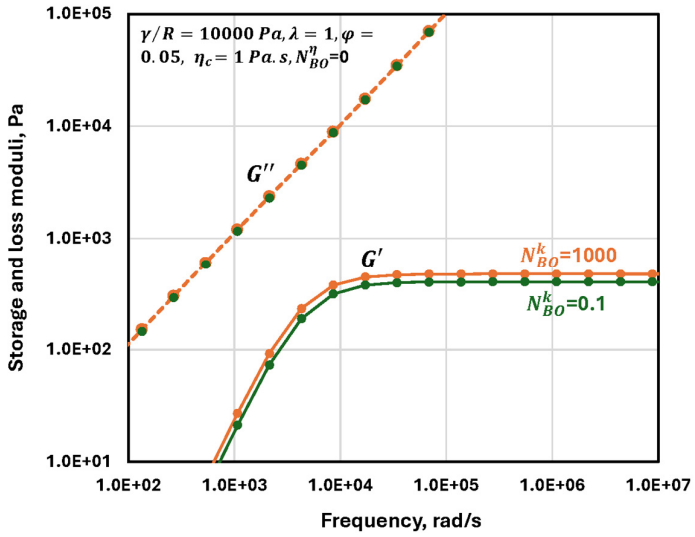


Figure 41. The effect of N_{Bo}^{k} on G' and G'' of an emulsion.

9.2. Droplets Covered with Purely Elastic Films

For purely elastic membranes, $\overline{\overline{P}}_s$ is related to the surface strain tensor $\overline{\overline{e}}_s$ as [98]:

$$\overline{\overline{P}}_s = \gamma\overline{\overline{\delta}}_s + 2G_s\overline{\overline{e}}_s + (K_s - G_s)\left(\overline{\overline{\delta}}_s : \overline{\overline{e}}_s\right)\overline{\overline{\delta}}_s \tag{161}$$

Oldroyd [98] has shown that viscoelastic behavior of emulsions coated with purely elastic films is governed by:

$$\left(1 + \tau_1\frac{\partial}{\partial t} + \nu_1\frac{\partial^2}{\partial t^2}\right)\overline{\overline{\tau}} = 2\eta_0\left(1 + \tau_2\frac{\partial}{\partial t} + \nu_2\frac{\partial^2}{\partial t^2}\right)\overline{\overline{E}} \tag{162}$$

where τ_1 and $\sqrt{\nu_1}$ are relaxation times and τ_2 and $\sqrt{\nu_2}$ are retardation times. The expressions for η_0, τ_1, τ_2, ν_1 and ν_2 are given as:

$$\eta_0 = \eta_c\left[1 + \frac{5}{2}\varphi\right] \tag{163}$$

$$\tau_1 = \left(\frac{\alpha_1 - 2\varphi\alpha_2}{\beta_1 - 2\varphi\beta_2}\right)\left(\frac{\eta_c R}{8\gamma}\right) = \left(\frac{\alpha_1}{\beta_1}\right)\left[1 - 2\varphi\left(\frac{\alpha_2}{\alpha_1} - \frac{\beta_2}{\beta_1}\right)\right]\left(\frac{\eta_c R}{8\gamma}\right) \tag{164}$$

$$\tau_2 = \left(\frac{\alpha_1 + 3\varphi\alpha_2}{\beta_1 + 3\varphi\beta_2}\right)\left(\frac{\eta_c R}{8\gamma}\right) = \left(\frac{\alpha_1}{\beta_1}\right)\left[1 + 3\varphi\left(\frac{\alpha_2}{\alpha_1} - \frac{\beta_2}{\beta_1}\right)\right]\left(\frac{\eta_c R}{8\gamma}\right) \tag{165}$$

$$\nu_1 = \left(\frac{\alpha_1' - 2\varphi\alpha_2'}{\beta_1 - 2\varphi\beta_2}\right)\left(\frac{\eta_c^2 R^2}{8\gamma}\right) = \left(\frac{\alpha_1}{\beta_1}\right)\left[1 - 2\varphi\left(\frac{\alpha_2}{\alpha_1} - \frac{\beta_2}{\beta_1}\right)\right]\left(\frac{\eta_c^2 R^2}{8\gamma}\right) \tag{166}$$

$$\nu_2 = \left(\frac{\alpha_1' + 3\varphi\alpha_2'}{\beta_1 + 3\varphi\beta_2}\right)\left(\frac{\eta_c^2 R^2}{8\gamma}\right) = \left(\frac{\alpha_1}{\beta_1}\right)\left[1 + 3\varphi\left(\frac{\alpha_2}{\alpha_1} - \frac{\beta_2}{\beta_1}\right)\right]\left(\frac{\eta_c^2 R^2}{8\gamma}\right) \tag{167}$$

$$\alpha_1 = [40(1+\lambda)\gamma + 4(12+13\lambda)G_s + 2(32+23\lambda)K_s] \tag{168}$$

$$\alpha_2 = [4(2+5\lambda)\gamma + 2(8+13\lambda)G_s + (23\lambda - 16)K_s] \tag{169}$$

$$\beta_1 = 2[2G_s + 3K_s + (2G_sK_s/\gamma)] \tag{170}$$

$$\beta_2 = [2G_s + 3K_s + (2G_sK_s/\gamma)] \tag{171}$$

$$\alpha_1' = (3+2\lambda)(16+19\lambda) \tag{172}$$

$$\alpha_2' = (\lambda - 1)(16+19\lambda) \tag{173}$$

Using Equations (162)–(173), it can be readily shown that in oscillatory shear flow:

$$\frac{G^*}{j\omega\eta_c} = 1 + 5\varphi H^* \tag{174}$$

where H^* is now given by:

$$H^* = \frac{(8\gamma/R)\beta_2 - (R\omega^2\eta_c^2)\alpha_2' + (j\omega\eta_c)\alpha_2}{(8\gamma/R)\beta_1 - (R\omega^2\eta_c^2)\alpha_1' + (j\omega\eta_c)\alpha_1} \tag{175}$$

The dynamic moduli of emulsion predicted from Equations (174) and (175) under different conditions are shown in Figures 42 and 43 along with the corresponding Cole–Cole diagrams. The emulsion exhibits two plateaus in the G' plot, and there are two frequency domains in the Cole–Cole diagram. The right-hand side arc describes low-frequency behavior, and the left-hand side arc describes high-frequency behavior. The low-frequency domain reflects elastic behavior due to interfacial relaxation, whereas the high-frequency domain reflects elastic behavior due to the shape relaxation of droplets.

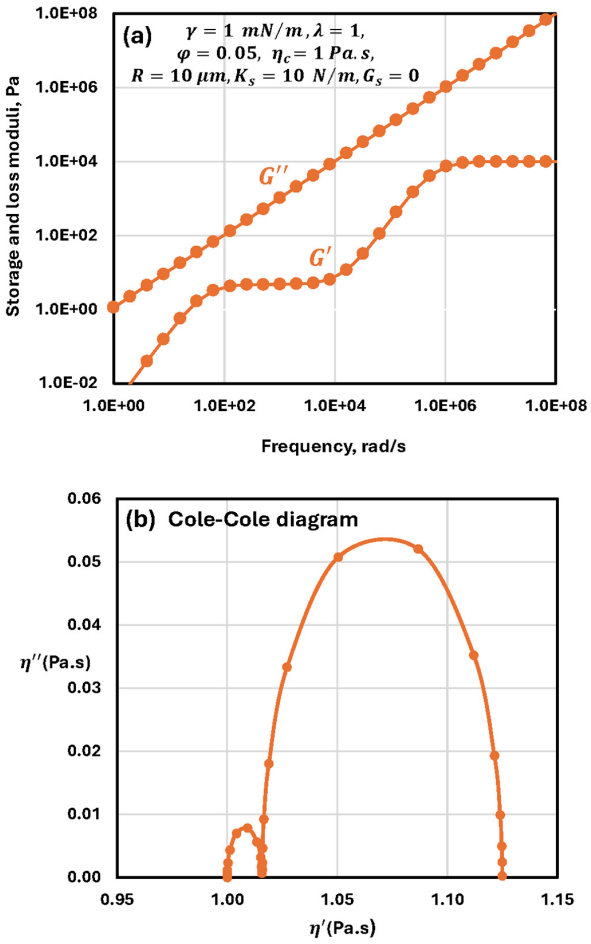


Figure 42. Dynamic rheology of an emulsion composed of droplets covered with elastic film.

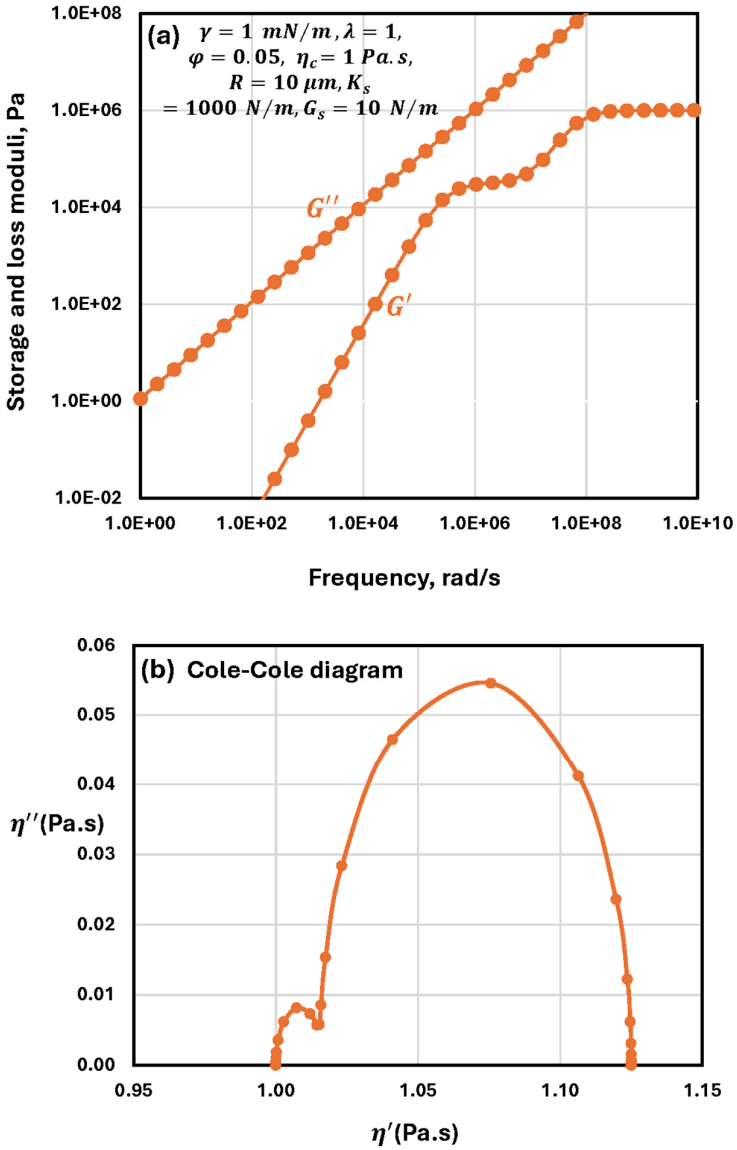


Figure 43. Dynamic moduli and Cole–Cole diagram for an emulsion composed of droplets covered with elastic film.

Figures 44–46 show the influences of different parameters on the G' and G'' of emulsion predicted from Equations (174) and (175). The upper plateau value of G' increases with the increase in G_s; also, the upper plateau shifts to a higher frequency (see Figure 44). Similar behavior is observed with the increase in K_s (see Figure 45). With the increase in the γ, the upper plateau value of G' increases (see Figure 46). Also, the Cole–Cole diagram shows two frequency domains at high γ—the low-frequency domain due to interfacial relaxation and the high-frequency domain due to shape relaxation. At a low value of γ, only one frequency domain is observed due to the overlapping of interfacial and shape relaxation processes.

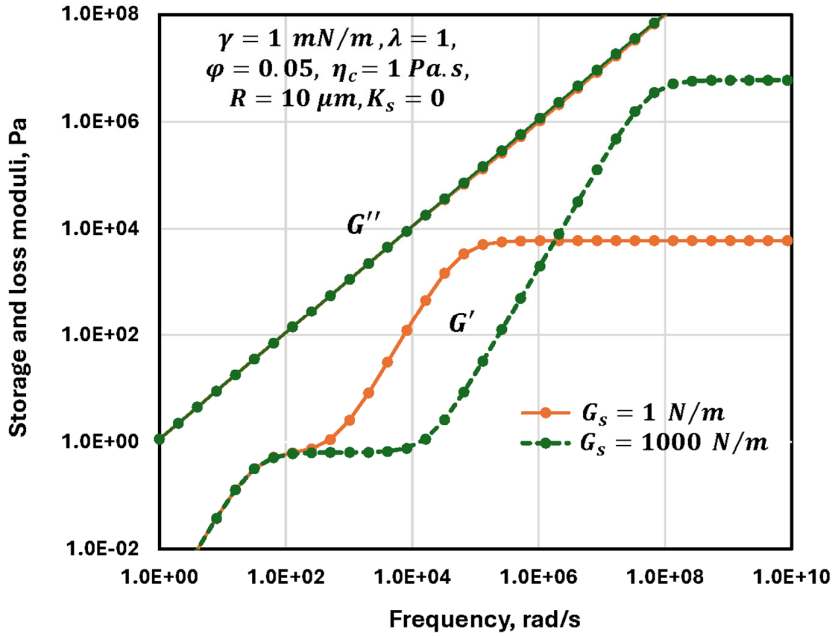


Figure 44. The effect of G_s on G' and G'' of an emulsion composed of droplets covered with elastic film.

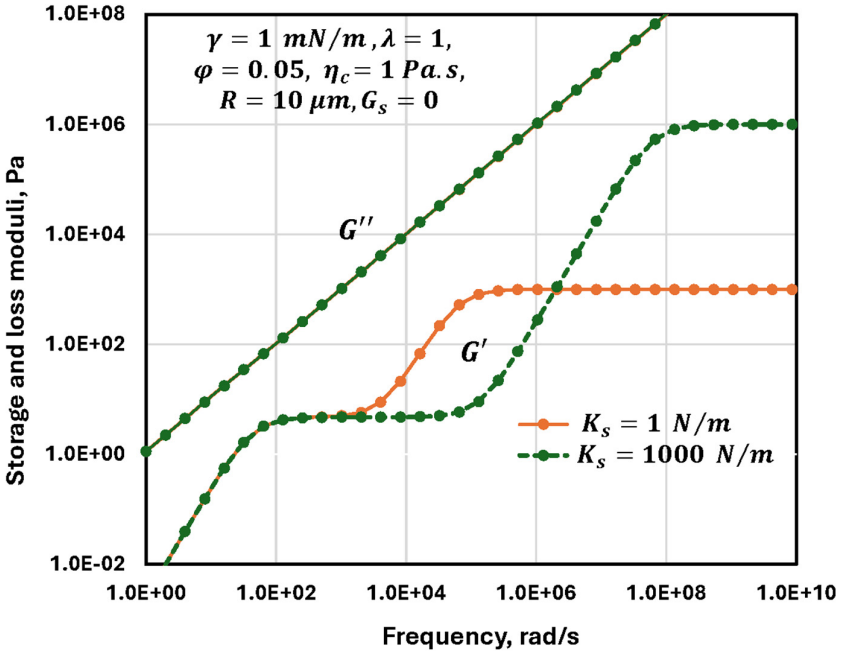


Figure 45. The effect of K_s on G' and G'' of an emulsion composed of droplets covered with elastic film.

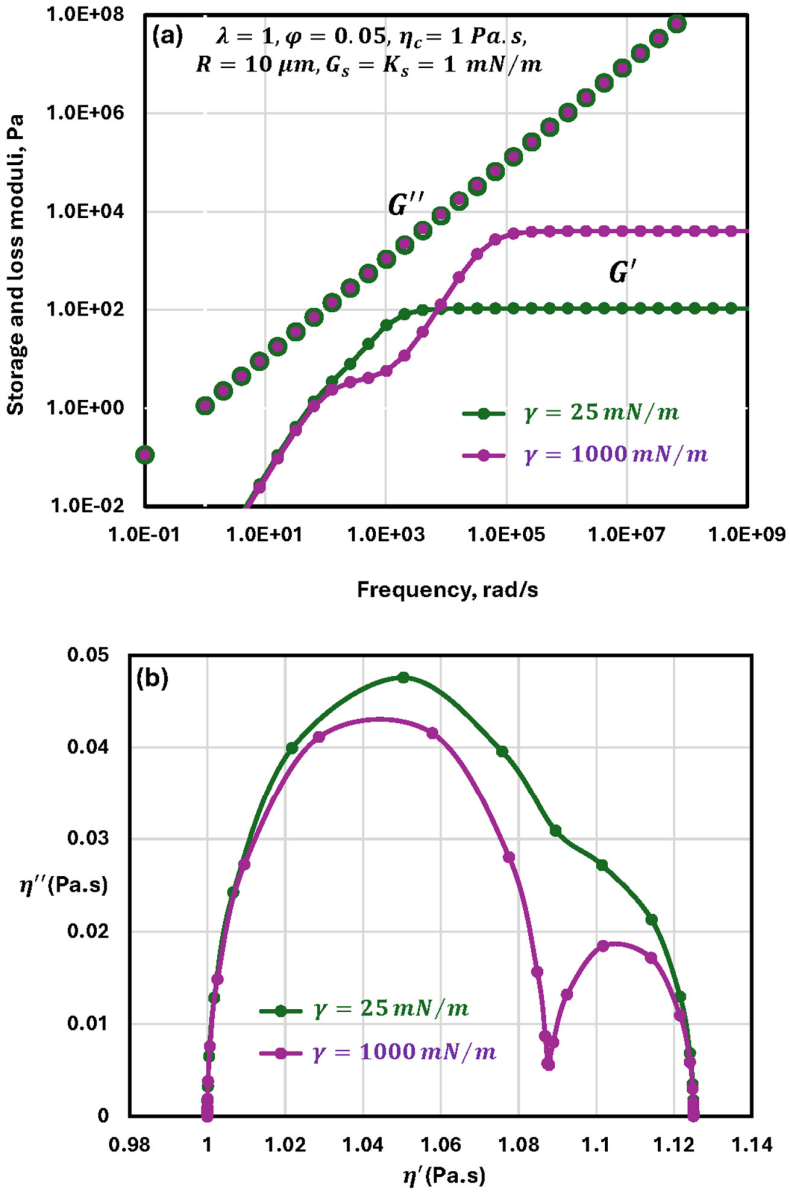


Figure 46. The effect of γ on G' and G'' and Cole–Cole diagram of an emulsion composed of droplets covered with elastic film.

9.3. Droplets Covered with Viscoelastic Films

The constitutive equation for a viscoelastic interface is as follows:

$$\overline{\overline{P}}_s^* = \gamma \overline{\overline{\delta}}_s + 2G_s^* \overline{\overline{e}}_s^* + (K_s^* - G_s^*)\left(\overline{\overline{\delta}}_s : \overline{\overline{e}}_s^*\right)\overline{\overline{\delta}}_s \tag{176}$$

where $\overline{\overline{P}}_s^*$ is complex surface stress tensor, $\overline{\overline{e}}_s^*$ is complex surface strain tensor, G_s^* is complex surface shear modulus and K_s^* is complex surface dilational modulus. G_s^* and K_s^* are defined as:

$$G_s^* = G_s + j\eta_s\omega \tag{177}$$

$$K_s^* = K_s + j\eta_s^k\omega \tag{178}$$

In general, G_s, η_s, K_s and η_s^k are functions of frequency.

The linear viscoelastic behavior of emulsions with viscoelastic interfaces can be described by the generalized Palierne model, Equation (129), with H^* defined as:

$$H^* = H' + jH'' = \frac{F^*}{D^*} \tag{179}$$

where F^* and D^* are given as:

$$\begin{aligned} F^* = F' + jF'' = {} & \left[\left(G_d^* - G_c^*\right)\left(19G_d^* + 16G_c^*\right)\right] + \left[24\gamma K_s^*/R^2\right] + \left[16G_s^*(\gamma + K_s^*)/R^2\right] + \left[(4\gamma/R)\left(5G_d^* + 2G_c^*\right)\right] \\ & + \left[(K_s^*/R)\left(23G_d^* - 16G_c^*\right)\right] + \left[(2G_s^*/R)\left(13G_d^* + 8G_c^*\right)\right] \end{aligned} \tag{180}$$

$$\begin{aligned} D^* = D' + jD'' = {} & \left[\left(2G_d^* + 3G_c^*\right)\left(19G_d^* + 16G_c^*\right)\right] + \left[(40\gamma/R)\left(G_d^* + G_c^*\right)\right] + \left[\tfrac{2K_s^*}{R}\left(23G_d^* + 32G_c^*\right)\right] \\ & + \left[\tfrac{4G_s^*}{R}\left(13G_d^* + 12G_c^*\right)\right] + \left[48K_s^*\gamma/R^2\right] + \left[32G_s^*\left(\gamma + K_s^*\right)/R^2\right] \end{aligned} \tag{181}$$

Thus, the G' and G'' of emulsions with viscoelastic interfaces can be calculated from Equations (131) and (132) using the following expressions for H' and H'':

$$H' = \frac{D'F' + D''F''}{\left[(D')^2 + (D'')^2\right]} \tag{182}$$

$$H'' = \frac{D'F'' - D''F'}{\left[(D')^2 + (D'')^2\right]} \tag{183}$$

where

$$\begin{aligned} F' = {} & G_d'(19G_d' + 16G_c') - G_d''\left(19G_d'' + 16G_c''\right) - G_c'\left(19G_d' + 16G_c'\right) + G_c''\left(19G_d'' + 16G_c''\right) + 24\gamma K_s/R^2 \\ & + \tfrac{16G_s(\gamma + K_s)}{R^2} - \tfrac{16}{R^2}\left(\eta_s\eta_s^k\omega^2\right) + \left(\tfrac{4\gamma}{R}\right)\left(5G_d' + 2G_c'\right) + \left(\tfrac{K_s}{R}\right)\left(23G_d' - 16G_c'\right) \\ & - \tfrac{\eta_s^k\omega}{R}\left(23G_d'' - 16G_c''\right) + \left(\tfrac{2G_s}{R}\right)\left(13G_d' + 8G_c'\right) - \tfrac{2\eta_s\omega}{R}\left(13G_d'' + 8G_c''\right) \end{aligned} \tag{184}$$

$$\begin{aligned} F'' = {} & G_d''\left(19G_d' + 16G_c'\right) + G_d'\left(19G_d'' + 16G_c''\right) - G_c''\left(19G_d' + 16G_c'\right) - G_c'\left(19G_d'' + 16G_c''\right) + \left(24\gamma/R^2\right)\eta_s^k\omega \\ & + \tfrac{16G_s\eta_s^k\omega}{R^2} + \tfrac{16}{R^2}(\eta_s\omega)(+K_s) + \left(\tfrac{4\gamma}{R}\right)\left(5G_d'' + 2G_c''\right) + \left(\tfrac{K_s}{R}\right)\left(23G_d'' - 16G_c''\right) \\ & + \tfrac{\eta_s^k\omega}{R}\left(23G_d' - 16G_c'\right) + \left(\tfrac{2G_s}{R}\right)\left(13G_d'' + 8G_c''\right) + \tfrac{2\eta_s\omega}{R}\left(13G_d' + 8G_c'\right) \end{aligned} \tag{185}$$

$$\begin{aligned} D' = {} & \left(2G_d' + 3G_c'\right)\left(19G_d' + 16G_c'\right) - \left(2G_d'' + 3G_c''\right)\left(19G_d'' + 16G_c''\right) + \left(\tfrac{40\gamma}{R}\right)\left(G_d' + G_c'\right) \\ & + \left(\tfrac{4G_s}{R}\right)\left(13G_d' + 12G_c'\right) + \left(\tfrac{2K_s}{R}\right)\left(23G_d' + 32G_c'\right) - \tfrac{2\eta_s^k\omega}{R}\left(23G_d'' + 32G_c''\right) \\ & - \tfrac{4\eta_s^k\omega}{R}\left(13G_d'' + 12G_c''\right) + \left(\tfrac{48\gamma K_s}{R^2}\right) + 32G_s\left(\tfrac{\gamma + K_s}{R^2}\right) - \tfrac{32\eta_s\eta_s^k\omega^2}{R^2} \end{aligned} \tag{186}$$

$$\begin{aligned} D'' = {} & \left(2G_d' + 3G_c'\right)\left(19G_d'' + 16G_c''\right) + \left(2G_d'' + 3G_c''\right)\left(19G_d' + 16G_c'\right) + \left(\tfrac{40\gamma}{R}\right)\left(G_d'' + G_c''\right) + \\ & \left(\tfrac{4G_s}{R}\right)\left(13G_d'' + 12G_c''\right) + \left(\tfrac{2K_s}{R}\right)\left(23G_d'' + 32G_c''\right) + \tfrac{2\eta_s^k\omega}{R}\left(23G_d' + 32G_c'\right) \\ & + \tfrac{4\eta_s\omega}{R}\left(13G_d' + 12G_c'\right) + \tfrac{48\gamma\eta_s^k\omega}{R^2} + 32G_s\left(\tfrac{\eta_s^k\omega}{R^2}\right) + \tfrac{32\eta_s\omega(\gamma + K_s)}{R^2} \end{aligned} \tag{187}$$

Equations (184)–(187) follow from Equations (180) and (181). When γ is the only non-zero mechanical property of the interface, the expression for H^* given by Equations (179)–(181) reduces to Equation (130).

Figures 47 and 48 show the G' and G'' and Cole–Cole plot of emulsion obtained from the Palierne model. There are two frequency domains (see Figure 47). The high-frequency domain is due to the shape relaxation of droplets, and the low-frequency domain is due to interfacial relaxation. Upon increasing G_s or K_s, only one frequency domain is observed.

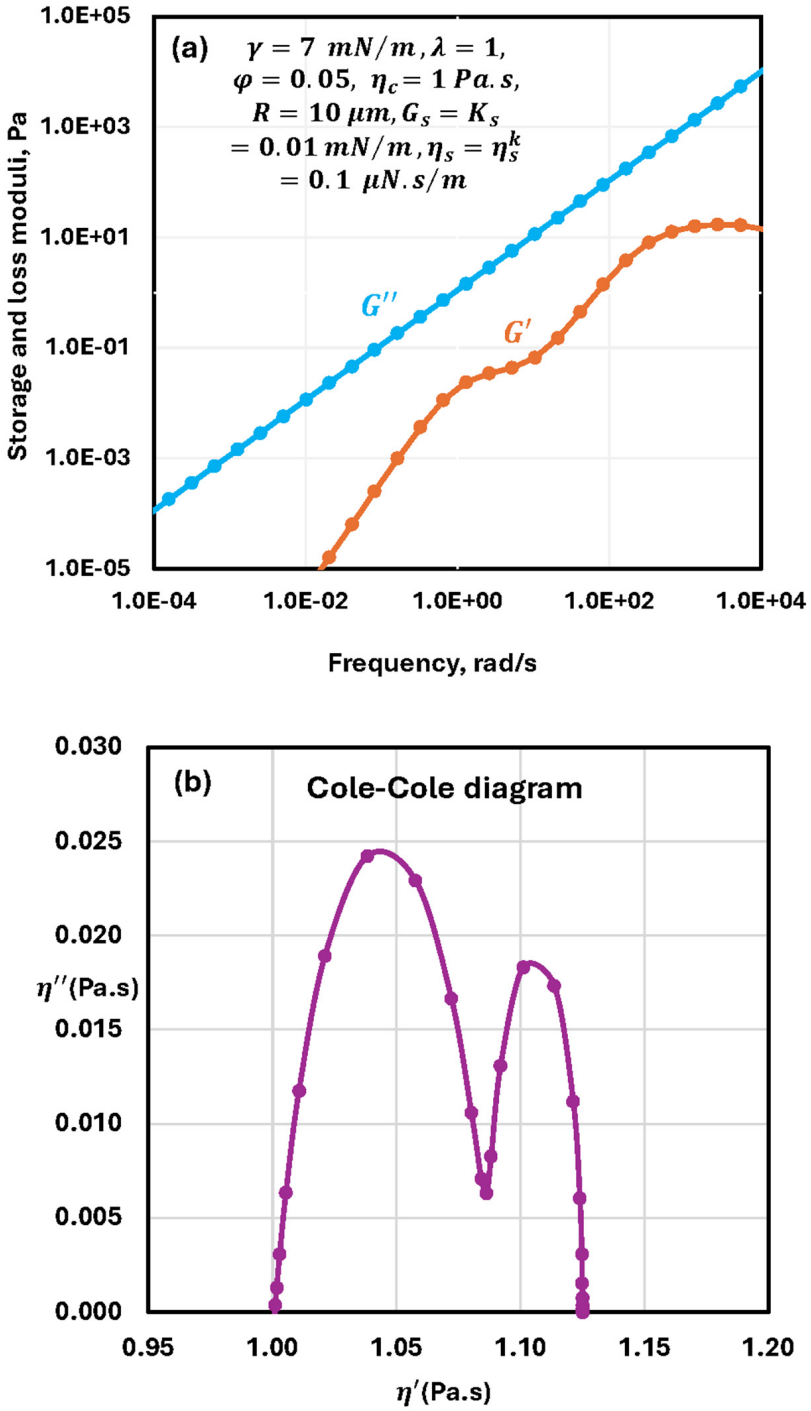


Figure 47. G' and G'' and Cole–Cole diagram of an emulsion composed of droplets coated with viscoelastic film ($G_s = K_s = 0.01$ mN/m).

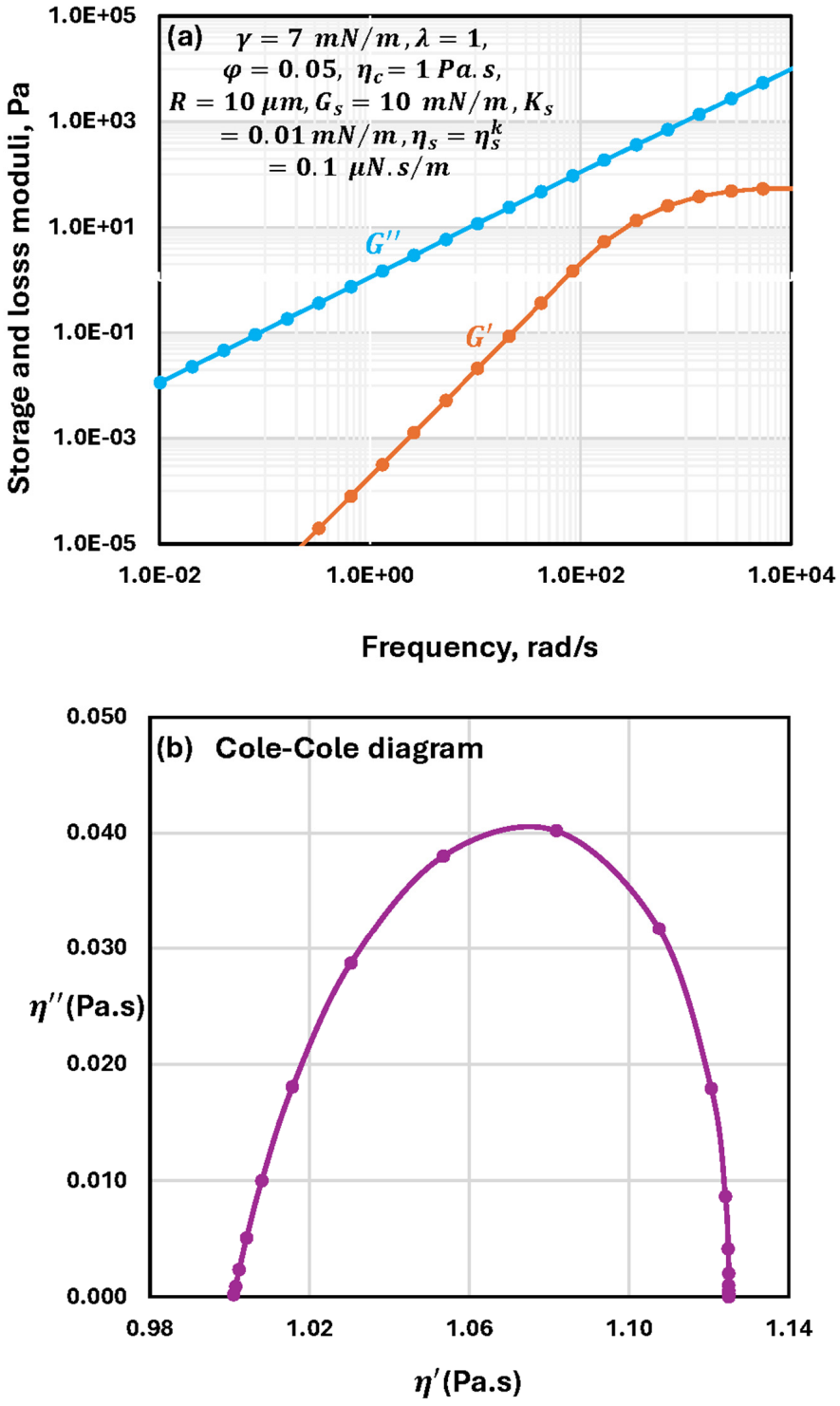


Figure 48. G' and G'' and Cole–Cole diagram of an emulsion composed of droplets coated with viscoelastic film ($G_s = 10$ mN/m, $K_s = 0.01$ mN/m).

9.4. Droplets Covered with Films Possessing Bending Rigidity

The bending rigidity (M), also referred to as the curvature modulus, of a film is defined as [107–111]:

$$M = \frac{Eh^3}{12(1-\nu^2)} \tag{188}$$

where E, ν, and h are Young's modulus, Poisson ratio, and film thickness, respectively. The bending rigidity effect comes into play if the thickness of the film is not extremely

small. The bending rigidity was assumed to be negligible in the films discussed in the preceding sections.

The viscoelastic behavior of emulsions composed of droplets coated with elastic membranes of non-negligible bending rigidity and non-zero dilational modulus was investigated by Seki and Komura [111]. An expression for the bulk stress of a dilute emulsion was developed. The effect of γ was also considered in the analysis. The flow perturbation due to the presence of a single droplet in the continuous phase was first calculated. As the droplets considered were nearly spherical, the rotational part of the shear flow was neglected, and only the pure straining contribution of the flow was considered. At large distances from the droplet, the velocity field prescribed was:

$$\vec{u}_\infty = \overline{\overline{\Gamma}}_\infty \bullet \vec{r} \tag{189}$$

where $\overline{\overline{\Gamma}}_\infty$ is a second-order symmetric tensor given in terms of the elongation rate $\dot{\varepsilon}$ as:

$$\overline{\overline{\Gamma}}_\infty = \frac{\dot{\varepsilon}}{2}\begin{pmatrix} -1 & 0 & 0 \\ 0 & -1 & 0 \\ 0 & 0 & 2 \end{pmatrix} e^{j\omega t} \tag{190}$$

The fluid motion outside and inside the droplet was described by the Stokes equations given below:

$$\nabla^2 \vec{u}_c = \frac{1}{\eta_c}\nabla P_c \quad for \;\; r > R \tag{191}$$

$$\nabla \bullet \vec{u}_c = 0 \quad for \;\; r > R \tag{192}$$

$$\nabla^2 \vec{u}_d = \frac{1}{\eta_d}\nabla P_d \quad for \;\; r < R \tag{193}$$

$$\nabla \bullet \vec{u}_d = 0 \quad for \;\; r < R \tag{194}$$

where subscripts c and d refer to the continuous phase and dispersed phase, respectively. The flow fields inside and outside the droplet were determined by solving Equations (191)–(194). The boundary conditions were:

(i) Far away from the droplet, (r $\longrightarrow \infty$),

$$\vec{u}_c \to \vec{u}_\infty \tag{195}$$

(ii) Continuity of velocity at the surface of the droplet, that is,

$$\vec{u}_c = \vec{u}_d = \vec{u}_m = \frac{\partial \vec{r}}{\partial t} \text{ at } r = R \tag{196}$$

where $\vec{u}_m$ is membrane velocity.

(iii) Force balance at the interface (r = R),

$$\left(\overline{\overline{\sigma}}_c - \overline{\overline{\sigma}}_d\right) \bullet \hat{n} + \vec{F}_n + \vec{F}_t = 0 \tag{197}$$

where $\hat{n}$ is the unit outer normal to the particle surface, $\vec{F}_n$ is the normal restoring force per unit area due to the membrane, and $\vec{F}_t$ is the tangential restoring force per unit area due to the membrane.

Using the flow field calculations, Seki and Komura [111] determined the dipole strength $\overline{\overline{S}}^{0}$ of a single droplet. The dipole strength $\overline{\overline{S}}^{0}$ was defined in Equation (23). The average or bulk stress in a dispersion of identical particles is given by:

$$\left\langle \overline{\overline{\sigma}} \right\rangle = -\langle P \rangle \overline{\overline{\delta}} + 2\eta_c \left\langle \overline{\overline{E}} \right\rangle + \frac{N}{V} \left\langle \overline{\overline{S}} \right\rangle \tag{198}$$

where N/V is the number density of droplets in the emulsion, given as $\varphi / \left(\frac{4}{3} \pi R^3 \right)$; $\langle \overline{\overline{E}} \rangle$ is the average rate of deformation tensor; and $\langle \overline{\overline{S}} \rangle$ is the average value of $\overline{\overline{S}}$ for a reference droplet. Because the interaction between the droplets is negligible in a dilute emulsion, the average $\left\langle \overline{\overline{S}} \right\rangle$ is the same as the $\overline{\overline{S}}^{o}$ value of a single droplet placed in an infinite matrix.

The average stress in the emulsion can also be expressed as:

$$\left\langle \overline{\overline{\sigma}} \right\rangle = -\langle P \rangle \overline{\overline{\delta}} + 2\eta^* \left\langle \overline{\overline{E}} \right\rangle \tag{199}$$

where η^* is the complex viscosity of the emulsion. From Equations (198) and (199), it follows that:

$$\eta^* = \eta_c \left[1 + \frac{3\varphi}{8\pi R^3 \eta_c} \left(\frac{\overline{\overline{S}}}{\overline{\overline{E}}} \right) \right] \tag{200}$$

To simplify the notation, the brackets $\langle\ \rangle$ have been dropped. By substituting the expression for $\overline{\overline{S}}/\overline{\overline{E}}$ in Equation (200), Seki and Komura [111] obtained the following expression for the complex viscosity of a dilute emulsion composed of droplets coated with films characterized by γ, K_s, and M:

$$\eta^* = \eta_c [1 + 5\varphi H^*] \tag{201}$$

where H^* is given by:

$$H^* = \frac{[24 K_s B_s] + [(23\lambda - 16)\ K_s + 4\ (5\lambda + 2) B_s] f + \left[(\lambda - 1)(19\lambda + 16) f^2 \right]}{[48 K_s B_s] + [2(23\lambda + 32) K_s + 40(\lambda + 1) B_s] f + [(2\lambda + 3)(19\lambda + 16) f^2]} \tag{202}$$

where f is $j\omega R \eta_c$ and B_s is given as:

$$B_s = \gamma + \frac{M}{R^2} \left(6 - 2 J_0 R + \frac{1}{2} J_0^2 R^2 \right) \tag{203}$$

where J_0 is the spontaneous curvature of the film. Equation (201) could be re-written in terms of the complex modulus by replacing $\eta^* = G^*/j\omega$. Thus,

$$\frac{G^*}{j\omega \eta_c} = 1 + 5\varphi H^* \tag{204}$$

When $K_s = 0$ and $B_s > 0$, Equation (201) reduces to the following expressions for low-frequency and high-frequency limiting viscosities:

$$\eta_0 = \eta_c \left[1 + \frac{5\lambda + 2}{2(\lambda + 1)} \varphi \right] \tag{205}$$

$$\eta_\infty = \eta_c \left[1 + \frac{5(\lambda - 1)}{(2\lambda + 3)} \varphi \right] \tag{206}$$

Equation (205) is the Taylor viscosity equation [81]. Note that if K_s and B_s are non-zero, the low-frequency viscosity is always:

$$\eta_0 = \eta_c \left[1 + \frac{5}{2}\varphi\right] \tag{207}$$

Equation (207) is the Einstein viscosity equation [85,86].

Figure 49 shows the G' and G'' and Cole–Cole plot of emulsion predicted from Equation (201) for different M (J_0 is taken as zero). The emulsion tends to exhibit two relaxation processes. The high-frequency domain is due to shape relaxation, and the low-frequency domain is due to interfacial relaxation [102].

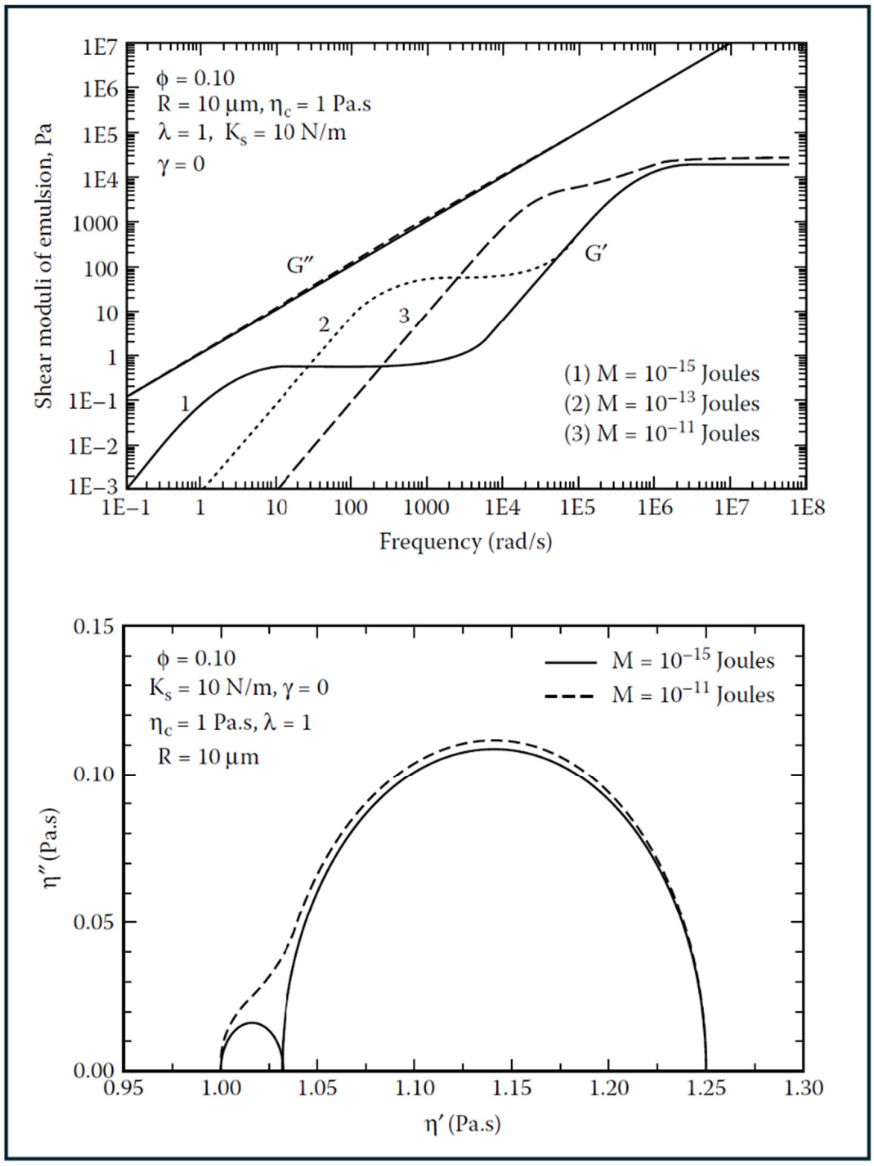


Figure 49. G' and G'' and Cole–Cole diagram for an emulsion of liquid droplets covered with film possessing bending rigidity.

9.5. Droplets Covered with Immiscible Liquid Films

The linear viscoelastic behavior of emulsions composed of droplets coated with liquid films was investigated by Oosterbrook and Mellema [107]. Figure 28 shows a schematic of the droplet covered with an interfacial film of another immiscible liquid of finite thickness.

Oosterbrook and Mellema [107] used the "cell model" approach to derive an expression for the complex viscosity of emulsions. For dilute emulsions, the complex viscosity expression developed by Oosterbrook and Mellema [107] is as follows:

$$\eta^* = \eta_c \left[1 + \varphi\left(\frac{\alpha_0 + \beta_0 H + \mu_0 H^2}{\alpha_0' + \beta_0' H + \mu_0' H^2}\right)\right] \tag{208}$$

where

$$\alpha_0 = 5FD^2\,[96\lambda_{21} + (160\lambda_{31} - 17{,}856\lambda_{21} + 64)D] \tag{209}$$

$$\alpha_0' = 2FD^2[96\lambda_{21} + (160\lambda_{31} - 17{,}856\lambda_{21} + 169)D] \tag{210}$$

$$\begin{aligned}\beta_0 = [40(F+1) \quad & \left(\tfrac{5}{2}\lambda_{31} + 1\right)\lambda_{21}] \\ & +5\left[-(3748 + 3740F)\lambda_{21}\lambda_{31} + 40(F+1)\lambda_{31} + 88(F+1)\lambda_{21}^2 - (1504 + 1568F)\right]\mathrm{D}\end{aligned} \tag{211}$$

$$\begin{aligned}\beta_0' = [40(F+1) \quad & (\lambda_{31} + 1)\lambda_{21}] \\ & +2\left[-(3748 + 3740F)\lambda_{21}\lambda_{31} + 100(F+1)\lambda_{31} + 88(F+1)\lambda_{21}^2 - (3760 + 3728F)\right]D\end{aligned} \tag{212}$$

$$\mu_0 = 5\left[19\lambda_{31}^2\lambda_{21} - 3\lambda_{31}\lambda_{21} - 16\lambda_{21} + D\left(-3572\lambda_{31}^2\lambda_{21} + 38\lambda_{31}^2 + 95\lambda_{31}\lambda_{21}^2 + 543\lambda_{31}\lambda_{21} - 80\lambda_{31} - 32\lambda_{21}^2 - 3008\lambda_{21}\right)\right] \tag{213}$$

$$\mu_0' = 2\left[19\lambda_{31}^2\lambda_{21} + \frac{89}{2}\lambda_{31}\lambda_{21} + 24\lambda_{21} + D(-3572\lambda_{31}^2\lambda_{21} + 95\lambda_{31}^2 + 95\lambda_{31}\lambda_{21}^2 - \frac{16{,}717}{2}\lambda_{21}\lambda_{31} + 120\lambda_{31} + 120\lambda_{21}^2 - 4512\lambda_{21})\right] \tag{214}$$

$$\lambda_{21} = \eta_2/\eta_1 \tag{215}$$

$$\lambda_{31} = \eta_3/\eta_1 \tag{216}$$

$$F = \gamma_{23}/\gamma_{12} \tag{217}$$

$$D = (b - a)/b \tag{218}$$

$$H = jb\eta_1\omega/\gamma_{12} \tag{219}$$

In the limit $D \longrightarrow 0$, the low-frequency viscosity of emulsion becomes:

$$\eta_0 = \eta_c\left[1 + \varphi\left(\frac{\alpha_0}{\alpha_0'}\right)\right] = \eta_c\left[1 + \frac{5}{2}\varphi\right] \tag{220}$$

Thus, at low frequencies, emulsions of droplets covered with thin films of another immiscible liquid behave like suspensions of rigid particles regardless of the viscosity of the inner droplet liquid.

The dynamic moduli of emulsion, along with the Cole–Cole diagram predicted from Equation (208), is shown in Figure 50. The emulsion exhibits two relaxation processes—one due to the thin interfacial film and the other due to the shape of the droplet. The effect of film thickness on the dynamic behavior of the emulsion is shown in Figure 51. With the increase in the film thickness, that is, the decrease in "a" while keeping "b" constant, the larger of the two relaxation times decreases. The merger of the two frequency domains occurs with the increase in the film thickness, as reflected in the Cole–Cole plot [102].

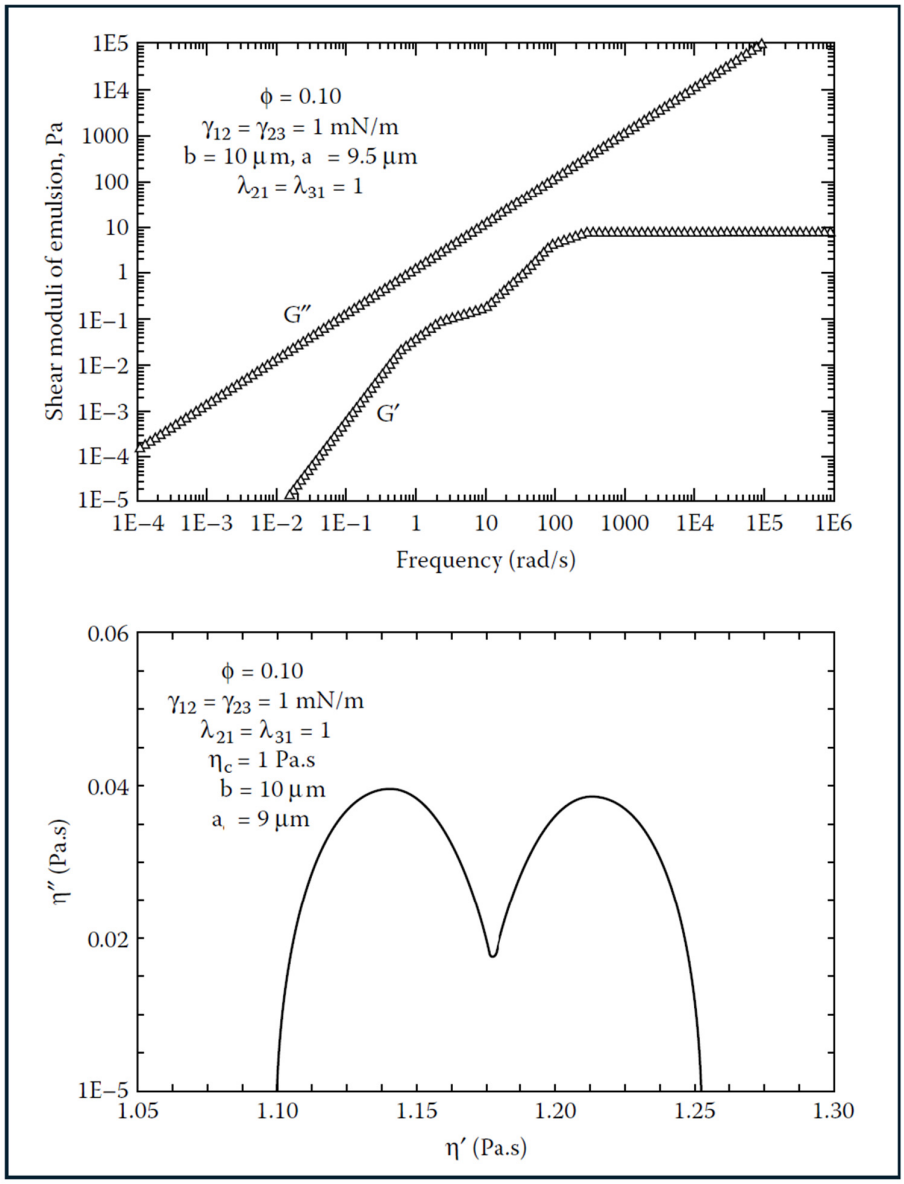


Figure 50. Dynamic moduli and Cole–Cole diagram for an emulsion of double droplets.

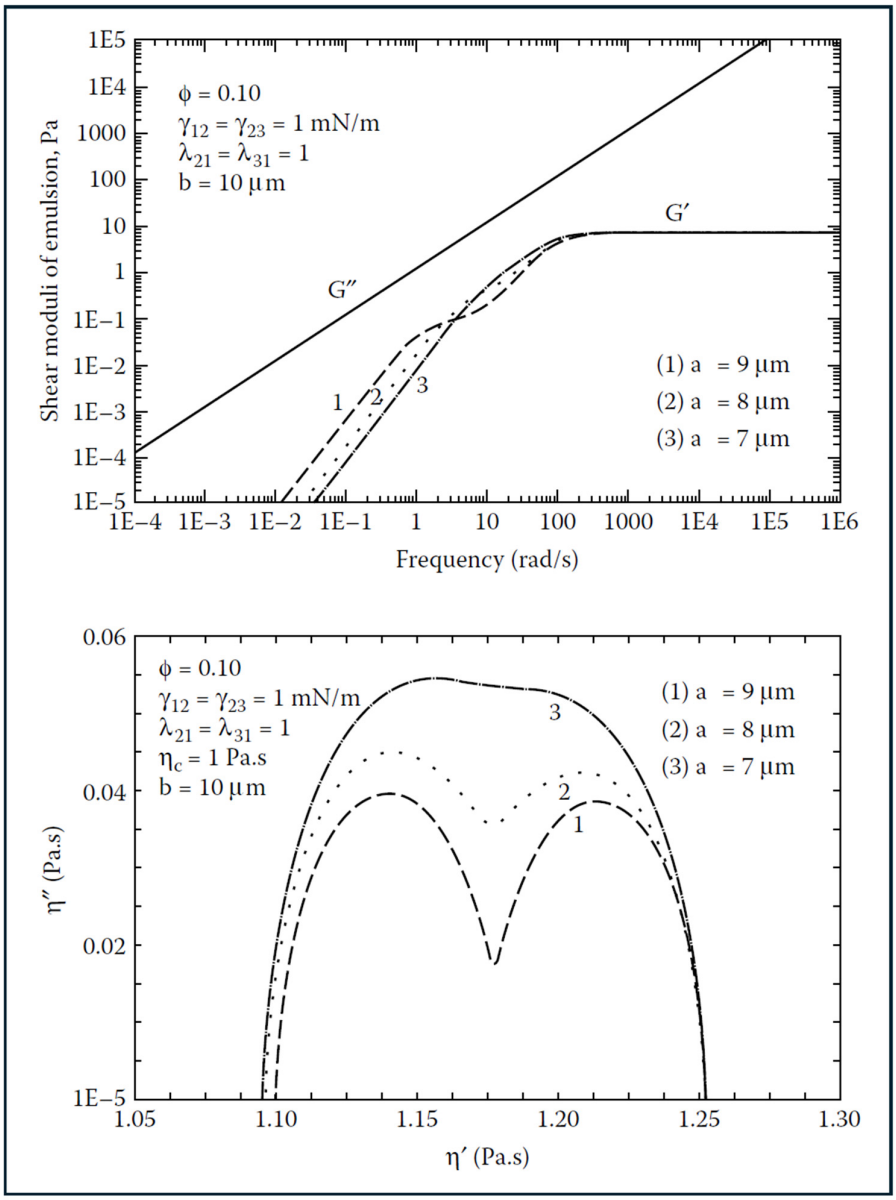


Figure 51. The effect of film thickness on the dynamic moduli and Cole–Cole plot of an emulsion of double droplets.

10. Research Gaps and Future Directions

As demonstrated in this review, our current understanding of dilute emulsion rheology is quite good from a theoretical perspective. However, there are still some serious gaps in the existing knowledge on dilute emulsion rheology.

In the existing literature, there is a general lack of systematic experimental studies available on the rheology of well-characterized dilute emulsions. Consequently, the theories currently available on dilute emulsion rheology remain mostly untested with experimental data. One reason for the lack of experimental studies is that accurate measurements of dilute emulsion rheology require sensitive instruments to detect the changes in the rheological properties with small changes in the droplet concentration. To predict the dynamic rheology of dilute emulsions of additive-laden droplets, interfacial properties such as surface dilational viscosity (η_s^k), surface dilational modulus (K_s), film bending rigidity (M), and spontaneous curvature of interface (J_0), etc., are required. But there is little or no data available on these interfacial properties or how to even measure some of these properties experimentally. The experimental measurements of interfacial rheological

properties are generally lacking. Furthermore, the existing theories about dilute emulsion rheology almost always assume the small deformation of droplets when subjected to bulk flow.

Another serious gap in the existing knowledge on dilute emulsion rheology is that the literature is generally silent on the steady shear rheology of emulsions composed of a non-Newtonian matrix. However, the theory for the linear viscoelasticity of emulsions is well developed for both Newtonian and non-Newtonian matrix phases [106]. To our knowledge, there has been little or no theoretical work done on the development of constitutive rheological laws applicable to the steady shear of dilute emulsions of droplets suspended in a non-Newtonian matrix. This is a serious shortcoming, as emulsions composed of a non-Newtonian matrix are important industrially. Many practical emulsions are formulated or produced consisting of different additives such as surfactants, polymers, clays, nanoparticles, and nanocrystals in the matrix phase. The presence of such additives in the matrix, even in modest amounts, renders the matrix non-Newtonian. The existing well-established rheological constitutive law for dilute emulsions developed by Frankel and Acrivos [67] is restricted to emulsions of a Newtonian matrix.

Our current understanding of the influence of surfactants on dilute emulsion rheology is also inadequate. Further theoretical, numerical, and experimental studies at arbitrary flow strength are needed to fully understand the effects of surfactants on interfacial and bulk emulsion rheology. Most studies that are currently available assume that the surfactant is insoluble in the droplet and matrix phases and restricted to the interface region only. Furthermore, the diffusivity of the surfactant in the interface region is often ignored. The influence of electric charge present on the surface of droplets on the bulk rheology of emulsions needs to be explored further both theoretically and experimentally. The existing models assume small capillary and Peclet numbers (weak flow), neglecting the deformation of droplets. General models applicable at arbitrary flow strengths need to be developed. Furthermore, experimental studies on primary electroviscous effects in emulsions of deformable droplets are scarce. The available studies are mostly restricted to disperse systems of rigid particles.

The practical use of dilute emulsion rheology is limited, as the real industrial emulsions are concentrated systems. Nevertheless, understanding dilute emulsion rheology is indispensable, as it describes different phenomena relevant to emulsion rheology regardless of the concentration of the emulsion system. The greatest advantage of investigating dilute systems is that they are accessible theoretically, whereas concentrated systems are nearly impossible to model rigorously due to hydrodynamic and non-hydrodynamic interactions between the droplets. The models available for concentrated emulsion rheology are at best semiempirical. Most importantly, they are built on dilute emulsion rheological models extended to concentrated systems using approximate techniques such as cell models, self-consisting, and effective medium approaches.

11. Conclusions

- Dilute emulsions of pure oil–water interfaces (no additives) exhibit non-Newtonian rheology such as shear-thinning, non-zero normal stresses, and strain thickening in elongational flow. The rheology is strongly dependent on the viscosity ratio and capillary number.
- The presence of electric charge on the oil–water interface enhances the viscosity of dilute emulsions due to the primary electroviscous effect. For thin electric double layers and high surface potential, the droplets behave like rigid solid particles. This transformation of liquid droplets to solid particles is referred to as the “solidification effect”.

- The presence of surfactants at the oil–water interface can have a strong effect on emulsion rheology, as surfactants introduce Marangoni stresses, in addition to surface shear and dilational viscosities, to the emulsions. Emulsions exhibit non-Newtonian behavior due to the Marangoni phenomenon even when the droplets are spherical and the capillary number is zero. Furthermore, the presence of surfactants can make droplets behave like rigid solid particles and enhance the viscosity.
- When the droplets of emulsions are encapsulated by thin elastic membranes, the droplets behave like rigid solid particles with enhanced viscosity at low shear rates. The membrane-coated droplets undergo deformation and orientation at high shear rates, which results in shear-thinning behavior.
- The viscosity of emulsions of double droplets (droplets covered by a shell of another immiscible liquid) is strongly dependent on the ratio of shell liquid viscosity to matrix fluid viscosity. At high values of this viscosity ratio, the double droplets behave as rigid solid particles regardless of the viscosity of the inner core liquid. Emulsions with a thin outer shell behave as rigid solid particles regardless of the viscosities of the shell and inner core liquids.
- The dynamic rheology of dilute emulsions with a pure oil–water interface (no additives) exhibits a single relaxation behavior reflected in a single plateau of the storage modulus and a single arc in the Cole–Cole diagram. The relaxation behavior is due to the shape relaxation of droplets.
- The dynamic rheology of dilute emulsions with additive-laden oil–water interfaces exhibits two relaxation domains reflected in two plateaus of the storage modulus and two arcs in the Cole–Cole diagram. The two relaxation behaviors are due to the relaxation of the interface and the relaxation of the shape of droplets.
- Experimental measurements of the rheology of well-characterized dilute emulsions are still lacking. The theoretical modeling of the rheological constitutive law of dilute emulsions composed of a non-Newtonian matrix is largely an unexplored area of research. For such systems, there is no parallel treatment available like that of Frankel and Acrivos [67] for emulsions composed of a Newtonian matrix. Systematic experimental studies of interfacial rheology are also lacking in the existing literature. More theoretical and experimental work is needed to fully comprehend the influence of surfactants and surface charge on dilute emulsion rheology.
- This review, for the most part, was limited to analytical solutions of dilute emulsion rheology. The numerical or computational rheology of dilute emulsions was not covered to any significant extent. Several interesting studies are available on the numerical and computational rheology of dilute emulsions, including the effect of surfactants [94,95,101,112–124].

Funding: This research was funded by the NSERC Discovery Grant awarded to R.P.

Data Availability Statement: The raw data supporting the conclusions of this article will be made available by the author on request.

Conflicts of Interest: The author declares no conflicts of interest.

Nomenclature

Greek Symbols

α	parameter given by Equation (77)
α_i	parameters in Equations (86), (87), (89), (90), (92), (106), (151), (152), (168), (169) and (209)
α_i'	parameters in Equations (172), (173), (210)
β_i	parameter in Equations (93), (94), (96), (97), (153), (154), (170), (171) and (211)
β_o'	quantity given by Equation (212)
γ	interfacial tension
γ_{12}	interfacial tension between fluids 1 and 2
γ_{23}	interfacial tension between fluids 2 and 3
$\dot{\gamma}$	shear rate
Γ	surfactant concentration
$\overline{\overline{\Gamma}}_\infty$	second-order tensor given in Equation (190)
δ_i	parameters defined in Equations (98), (123)–(126)
∇	del operator
∇_s	surface gradient operator
∇^2	Laplacian
$\overline{\overline{\delta}}$	unit tensor
$\overline{\overline{\delta}}_s$	surface unit tensor
ε	deformation parameter or permittivity of fluid
ε_m	interfacial mobility parameter defined by Equation (80)
η	shear viscosity
η^*	complex shear viscosity
η'	dynamic shear viscosity
η''	imaginary part of complex shear viscosity
η_i	shear viscosity of ith fluid
η_c	continuous phase viscosity
η_d	dispersed phase viscosity
η_E	elongation viscosity
η_r	relative viscosity
η_o	zero shear viscosity
η_s	surface shear viscosity
η_s^k	surface dilational viscosity
$[\eta]$	intrinsic viscosity, see Equation (83)
$[\eta]_0$	zero shear intrinsic viscosity
$[\eta]_\infty$	infinite shear intrinsic viscosity
$[\eta_C]$	capillary viscosity, see Equation (83)
$[\eta_M]$	Marangoni viscosity
θ	angle between the major axis of the droplet and flow direction
κ^{-1}	thickness of double layer or Debye length
λ	viscosity ratio
$\lambda_\pm$	drag coefficient of ions
μ_o	quantity given by Equation (213)
μ_o'	quantity given by Equation (214)
ν	Poisson ratio
ν_1	relaxation time, Equation (166)
ν_2	retardation time, Equation (167)
$\overline{\overline{\sigma}}$	total stress tensor
$\overline{\overline{\sigma}}_c$	total stress tensor in matrix
$\overline{\overline{\sigma}}^*$	total stress tensor inside the droplet
τ_c	relaxation time of continuous phase
τ_d	relaxation time of dispersed phase

τ_o	time constant given by Equation (56)
τ_1	relaxation time given by Equations (149) and (164)
τ_2	retardation time given by Equations (150) and (165)
$\overline{\overline{\tau}}$	deviatoric stress tensor
τ_{12}	shear stress
$\tau_{11}, \tau_{22}, \tau_{33}$	normal stress components
φ	volume fraction of droplets
$\tilde{\psi}_0$	dimensionless surface potential
ω	frequency of oscillation of stress or strain
$\vec{\omega}_o$	one-half the vorticity of undisturbed flow
Latin Symbols	
a	radius of inner core droplet of double-emulsion droplet
a_o	parameter in Equation (99)
A	surface area
A_o	surface area of a droplet
A'	bounding surface of the region where fluid motion is taking place
$\overline{\overline{A}}$	radial displacement tensor of membrane
A_{12}	component of tensor $\overline{\overline{A}}$
b	radius of outer shell of double-emulsion droplet
b_i	parameters in Equations (99)–(101)
B_s	quantity defined in Equation (203)
$\overline{\overline{B}}$	arbitrary second-order tensor or tangential displacement tensor of membrane
B_{12}	component of tensor $\overline{\overline{B}}$
D	either deformation parameter (Equation (2)) or diffusion coefficient of surfactant or ion or parameter defined in Equation (218)
D^*	complex quantity defined in Equation (181)
D'	quantity given by Equation (186)
D''	quantity given by Equation (187)
D/Dt	Jaumann derivative
e	elementary charge
$\overline{\overline{e}}_s^*$	complex surface strain tensor
E	elasticity
E_G	Gibbs elasticity of interface
$\dot{E}$	rate of energy dissipation in emulsion
$\dot{E}_c$	rate of energy dissipation in matrix alone without droplets
$\overline{\overline{E}}$	rate of strain tensor
$\overline{\overline{E}}_s$	surface rate of strain tensor
E_{12}	component of tensor $\overline{\overline{E}}$
$\overline{\overline{E}}_\infty$	rate of strain tensor of the undisturbed flow far away from the droplet
$\overline{\overline{E}}_\infty'$	dimensionless rate of strain tensor of the undisturbed flow far away from the droplet
$\vec{F}_n$	normal restoring force per unit area
$\vec{F}_t$	tangential restoring force per unit area
$\overline{\overline{F}}$	symmetric and traceless deformation tensor describing the shape of a droplet
$\overline{\overline{F}}'(t)$	dimensionless form of symmetric and traceless deformation tensor $\overline{\overline{F}}$ describing the shape of a droplet
F	parameter defined in Equation (217)
F^*	complex quantity defined in Equation (180)
F'	quantity given by Equation (184)
F''	quantity given by Equation (185)
g	droplet shape variable, defined by Equation (39)

g'	defined in Equation (135)
g''	defined in Equation (136)
G'	storage modulus
G''	loss modulus
G'_c	storage modulus of continuous phase
G'_d	storage modulus of dispersed phase
G''_c	loss modulus of continuous phase
G''_d	loss modulus of dispersed phase
G^*	complex shear modulus, see Equations (129), (139), (174) and (204)
G^*_c	complex shear modulus of continuous phase, see Equations (141) and (143)
G^*_d	complex shear modulus of dispersed phase, see Equations (141) and (143)
G^*_s	complex surface shear modulus
G_s	surface shear modulus
h	function of viscosity ratio λ, see Equation (60), or film thickness
h'	defined in Equation (137)
h''	defined in Equation (138)
H	defined in Equation (219)
H^*	complex quantity defined in Equations (130), (140), (142), (160), (175), (179) and (202)
H'	defined in Equations (133) and (182)
H''	defined in Equations (134) and (183)
I	quantity defined in Equations (103) and (122)
j	complex number
J_o	spontaneous curvature of the film
k	Boltzmann constant
K_s	surface dilational modulus
K^*_s	complex surface dilational modulus
$\overline{\overline{L}}$	symmetric and traceless tensor related to membrane displacement
L_{12}	component of tensor $\overline{\overline{L}}$
M	bending rigidity of film, defined in Equation (188)
$\overline{\overline{M}}$	symmetric and traceless tensor related to membrane displacement
M_{12}	component of tensor $\overline{\overline{M}}$
$m_\pm$	scaled ionic drag coefficient
$\hat{n}$	outward unit normal vector
N_1	first normal stress difference
N_2	second normal stress difference
N_{1r}	reduced first normal stress difference
N_{2r}	reduced second normal stress difference
N^η_{Bo}	shear Boussinesq number
N^k_{Bo}	dilational Boussinesq number
N_{Ca}	capillary number
$N_{Ca,crit}$	critical capillary number
N^S_{Ca}	elastic capillary number defined in Equation (84)
N_{Ma}	Marangoni number defined by Equation (82)
N^s_{Pe}	surface Peclet number defined by Equation (76)
N/V	number density of droplets in the emulsion
p	primary electroviscous coefficient
P	pressure
P_e	Ion Peclet number defined in Equation (65)
P^*	pressure inside the droplet
P_∞	pressure far away from the droplet
$\overline{\overline{P}}_s$	surface stress tensor
$\overline{\overline{P}}^*_s$	complex surface stress tensor

R	droplet radius
r	distance from the droplet center of mass to the droplet surface
$\vec{r}$	position vector
S_i	ith surface spherical harmonic
S_2	second-order surface spherical harmonic
$\overline{\overline{S}}$	dipole strength
$\overline{\overline{S}}^o$	dipole strength of a single droplet located in an infinite matrix
t	time
T	temperature
tr	trace of a tensor
$\vec{u}$	fluid velocity vector
$\vec{u}_c$	fluid velocity vector in continuous phase
$\vec{u}_d$	fluid velocity vector in dispersed phase
$\vec{u}_m$	membrane velocity
$\vec{u}_\infty$	fluid velocity vector far away from the droplet
$\vec{u}^*$	fluid velocity vector inside the droplet
$u_{\text{interface}}$	velocity of droplet interface
V_p	volume of a single double-emulsion droplet
X	surfactant coverage
$\vec{x}$	position vector
x_1, x_2, x_3	position co-ordinates of droplet surface
Z	valence of ion

Appendix A. Derivation of Equations (57)–(59) from Equation (55)

Equation (55) can be re-written as:

$$\left[1+\tau_o\frac{D}{Dt}\right]\overline{\overline{\tau}}=a\left[\overline{\overline{E}}+\tau_o\frac{D\overline{\overline{E}}}{Dt}\right]+b\left[c\frac{D\overline{\overline{E}}}{Dt}+d\times Sd\left(\overline{\overline{E}}\bullet\overline{\overline{E}}\right)\right] \tag{A1}$$

where

$$a=2\eta_c\left[1+\frac{5\lambda+2}{2(1+\lambda)}\varphi\right] \tag{A2}$$

$$b=\varphi\eta_c\left(\frac{\eta_c R}{\gamma}\right) \tag{A3}$$

$$c=-\frac{1}{40}\left(\frac{19\lambda+16}{1+\lambda}\right)^2 \tag{A4}$$

$$d=\frac{3(19\lambda+16)\left(25\lambda^2+41\lambda+4\right)}{140(1+\lambda)^3} \tag{A5}$$

$$\tau_o=\frac{(19\lambda+16)(2\lambda+3)}{40(1+\lambda)}\left(\frac{\eta_c R}{\gamma}\right) \tag{A6}$$

Let the viscometric flow be:

$$\vec{u}=\left(\dot{\gamma}x_2,\quad 0,\quad 0\right) \tag{A7}$$

Consequently,

$$\overline{\overline{E}}=\frac{\dot{\gamma}}{2}\begin{pmatrix}0&1&0\\1&0&0\\0&0&0\end{pmatrix} \tag{A8}$$

$$\frac{D\bar{\bar{E}}}{Dt} = \frac{\dot{\gamma}^2}{2}\begin{pmatrix} -1 & 0 & 0 \\ 0 & 1 & 0 \\ 0 & 0 & 0 \end{pmatrix} \tag{A9}$$

$$\frac{D\bar{\bar{\tau}}}{Dt} = \frac{\dot{\gamma}}{2}\begin{pmatrix} -2\tau_{12} & \tau_{11}-\tau_{22} & 0 \\ \tau_{11}-\tau_{22} & 2\tau_{12} & 0 \\ 0 & 0 & 0 \end{pmatrix} \tag{A10}$$

$$Sd\left(\bar{\bar{E}}\bullet\bar{\bar{E}}\right) = \frac{\dot{\gamma}^2}{12}\begin{pmatrix} 1 & 0 & 0 \\ 0 & 1 & 0 \\ 0 & 0 & -2 \end{pmatrix} \tag{A11}$$

Upon substitution of above quantities into Equation (A1), we get:

$$\begin{pmatrix} \tau_{11} & \tau_{12} & 0 \\ \tau_{21} & \tau_{22} & 0 \\ 0 & 0 & \tau_{33} \end{pmatrix} + \frac{\tau_o\dot{\gamma}}{2}\begin{pmatrix} -2\tau_{12} & \tau_{11}-\tau_{22} & 0 \\ \tau_{11}-\tau_{22} & 2\tau_{12} & 0 \\ 0 & 0 & 0 \end{pmatrix} = \frac{a\dot{\gamma}}{2}\begin{pmatrix} 0 & 1 & 0 \\ 1 & 0 & 0 \\ 0 & 0 & 0 \end{pmatrix} + \frac{a\tau_o\dot{\gamma}^2}{2}\begin{pmatrix} -1 & 0 & 0 \\ 0 & 1 & 0 \\ 0 & 0 & 0 \end{pmatrix} + \frac{bc\dot{\gamma}^2}{2}\begin{pmatrix} -1 & 0 & 0 \\ 0 & 1 & 0 \\ 0 & 0 & 0 \end{pmatrix} + \frac{bd\dot{\gamma}^2}{12}\begin{pmatrix} 1 & 0 & 0 \\ 0 & 1 & 0 \\ 0 & 0 & -2 \end{pmatrix} \tag{A12}$$

Comparing the terms on the left-hand and right-hand sides of Equation (A12) yields the following set of equations:

$$\tau_{11} + \left(\frac{\tau_o\dot{\gamma}}{2}\right)(-2\tau_{12}) = -\frac{a\tau_o\dot{\gamma}^2}{2} - \frac{bc\dot{\gamma}^2}{2} + \frac{bd\dot{\gamma}^2}{12} \tag{A13}$$

$$\tau_{12} + \left(\frac{\tau_o\dot{\gamma}}{2}\right)(\tau_{11}-\tau_{22}) = \frac{a\dot{\gamma}}{2} \tag{A14}$$

$$\tau_{22} + \left(\frac{\tau_o\dot{\gamma}}{2}\right)(2\tau_{12}) = \frac{a\tau_o\dot{\gamma}^2}{2} + \frac{bc\dot{\gamma}^2}{2} + \frac{bd\dot{\gamma}^2}{12} \tag{A15}$$

$$\tau_{33} = \frac{bd\dot{\gamma}^2}{12}(-2) = -\frac{bd\dot{\gamma}^2}{6} \tag{A16}$$

Subtracting Equation (A15) from (A13) gives

$$\tau_{11} - \tau_{22} = 2\tau_{12}\tau_o\dot{\gamma} - \dot{\gamma}^2(a\tau_o + bc) \tag{A17}$$

From Equations (A14) and (A17),

$$\tau_{12} = \frac{a\dot{\gamma}/2}{1+\tau_o^2\dot{\gamma}^2} + \frac{\tau_o\dot{\gamma}^3(a\tau_o+bc)/2}{1+\tau_o^2\dot{\gamma}^2} \tag{A18}$$

From Equation (A18), it follows that:

$$\eta = \frac{\tau_{12}}{\dot{\gamma}} = \frac{1}{1+\tau_o^2\dot{\gamma}^2}\left[\frac{a}{2} + \frac{a}{2}\tau_o^2\dot{\gamma}^2 + \frac{\tau_o bc\dot{\gamma}^2}{2}\right] \tag{A19}$$

Upon substitution of a, b, c, and τ_o into Equation (A19) and simplification, we get:

$$\eta = \frac{\eta_c}{1+\tau_o^2\dot{\gamma}^2}\left\{1 + \left(\frac{5\lambda+2}{2\lambda+2}\right)\varphi + \tau_o^2\dot{\gamma}^2\left[1 + \left(\frac{5\lambda+2}{2\lambda+2}\right)\varphi - \frac{(19\lambda+16)}{(2\lambda+2)(2\lambda+3)}\varphi\right]\right\} \tag{A20}$$

This is the same as the viscosity equation, Equation (57).

From Equations (A17) and (A18), it can be readily shown that:

$$N_1 = \tau_{11} - \tau_{22} = -\frac{bc\dot{\gamma}^2}{1+\tau_o^2\dot{\gamma}^2} \tag{A21}$$

Upon substitution of b and c into Equation (A21), the expression for N_1 becomes:

$$N_1 = \tau_{11} - \tau_{22} = \frac{\eta_c^2\dot{\gamma}^2 R}{40\gamma\left(1+\tau_o^2\dot{\gamma}^2\right)}\left(\frac{19\lambda+16}{1+\lambda}\right)^2\varphi \tag{A22}$$

This is the same as Equation (58).
Subtracting Equation (A16) from (A15) gives

$$N_2 = \tau_{22} - \tau_{33} = \frac{a\tau_o\dot{\gamma}^2}{2} + \frac{bc\dot{\gamma}^2}{2} + \frac{bd\dot{\gamma}^2}{12} - \tau_{12}\tau_o\dot{\gamma} \tag{A23}$$

From Equations (A18) and (A23), it can be readily shown that:

$$N_2 = \tau_{22} - \tau_{33} = \frac{\dot{\gamma}^2}{\left(1+\tau_o^2\dot{\gamma}^2\right)}\left[\frac{bc}{2} + \frac{bd}{4}\left(1+\tau_o^2\dot{\gamma}^2\right)\right] \tag{A24}$$

Upon substitution of b, c, and d into Equation (A23), the expression for N_2 becomes:

$$N_2 = \tau_{22} - \tau_{33} = -\frac{\eta_c^2\dot{\gamma}^2 R}{40\gamma\left(1+\tau_o^2\dot{\gamma}^2\right)}\varphi\left\{\frac{1}{2}\left(\frac{19\lambda+16}{\lambda+1}\right)^2 - \left[\frac{3(19\lambda+16)\left(25\lambda^2+41\lambda+4\right)}{14(\lambda+1)^3}\right]\left(1+\tau_o^2\dot{\gamma}^2\right)\right\} \tag{A25}$$

This is the same as Equation (59).

References

1. Davis, B.W. Applications in the petroleum industry. In *Encyclopedia of Emulsion Technology*; Becher, P., Ed.; Dekker: New York, NY, USA, 1988; Volume 3.
2. Pal, R. Metering of two-phase liquid-liquid emulsions: A state of the art review. *Ind. Eng. Chem. Res.* **1994**, *33*, 1413–1435. [CrossRef]
3. Pal, R. Techniques for measuring the composition (oil and water content) of emulsions-a state of the art review. *Colloids Surf. A* **1994**, *84*, 141–193. [CrossRef]
4. Wong, S.F.; Lim, J.S.; Dol, S.S. Crude oil emulsion: A review of formation, classification and stability of water-in-oil emulsions. *J. Pet. Sci. Eng.* **2015**, *135*, 498–504. [CrossRef]
5. Lissant, K.J. Emulsification and demulsification in oil recovery. In *AIChE Symposium on Improved Oil Recovery by Surfactant and Polymer Flooding*; Shah, D.O., Schechter, P.S., Eds.; AIChE: New York, NY, USA, 1978.
6. Raghavan, R.; Marsden, S.S. Theoretical aspects of emulsification in porous media. *Soc. Pet. Eng. J.* **1971**, *11*, 153–161. [CrossRef]
7. Jenkins, F.W. Oil in water emulsions: Causes and Treatment. In *Water Problems in Oil Production—An Operator's Manual*; Case, L.C., Ed.; Petroleum Publishing Co.: Tulsa, OK, USA, 1977.
8. Lummus, J.L. Water-in-Oil Emulsion Drilling Fluid. U.S. Patent 2,661,334, 1 December 1953.
9. Williams, B.B.; Gidley, J.L.; Schechter, R.S. *Acidizing Fundamentals*; SPE Henry, L. Doherty Series; SPE-AIME: Dallas, TX, USA, 1979.
10. Simon, R.; Poynter, W.G. Down-hole emulsification for improving viscous crude production. *J. Pet. Technol.* **1968**, *20*, 1349–1353. [CrossRef]
11. McAuliffe, C.D.; Simon, R.; Johnson, C.E. Method of Pumping Viscous Crude Oil. U.S. Patent 3,380,531, 30 April 1968.
12. McAuliffe, C.D.; Fullerton; Simon, R.; Whittier; Johnson, C.E. Pumping Viscous Crude. U.S. Patent 3,467,195, 16 September 1969.
13. Beyer, A.H.; Osborn, D.E. Down-hole emulsification for improving paraffinic crude production. In *Proceedings of the 44th Annual Fall Meeting of the SPE and AIME, Denver, CO, USA, 28 September–1 October 1969*; SPE-AIME: Denver, CO, USA, 1969.
14. Zhang, X.; Xiong, L. Effect of adjuvants on the spray droplet size of pesticide dilute emulsion. *Colloids Surf. A Phys. Eng. Asp.* **2021**, *619*, 126557. [CrossRef]
15. Shadakofsky, B.M.; Kulacki, F.A. Boiling of dilute emulsions. Mechanisms and applications. *Int. J. Heat Mass Transf.* **2019**, *141*, 1252–1271. [CrossRef]

16. Zakin, J.L.; Pinaire, R.; Borgmeyer, M.E. Transportation of oils as oil-in-water emulsions. *J. Fluids Eng.* **1979**, *101*, 100–104. [CrossRef]
17. Seymour, E.V. Process for Facilitating Pipeline Flow of Highly Viscous Fluids. U.S. Patent 3,520,313, 14 July 1970.
18. Simon, R.; Poynter, W.G. Pipelining Oil/Water Mixtures. U.S. Patent 3,519,006, 7 July 1970.
19. Simon, R.; McAuliffe, C.D.; Poynter, W.; Jennings, H. Pipelining Crude Oils. U.S. Patent 3,487,844, 6 January 1970.
20. Simpson, W.C.; Sommer, H.J. Transportation of Waxy Oils. U.S. Patent 2,981,633, 25 April 1961.
21. Rimmer, D.P.; Gregoli, A.A.; Hamshar, J.A.; Yildirim, E. Pipeline emulsion transportation for heavy oils. In *Emulsions: Fundamentals and Applications in the Petroleum Industry*; Schramm, L.L., Ed.; Advances in Chemistry Series 231; American Chemical Society: Washington, DC, USA, 1992.
22. Alvarado, D.A.; Marsden, S.S. Flow of oil-in-water emulsions through tubes and porous media. *Soc. Pet. Eng. J.* **1979**, *19*, 269–377. [CrossRef]
23. Binder, G.G.; Clark, N.J.; Russel, C.D. Method of Secondary Recovery. U.S. Patent 3,203,517, 31 August 1965.
24. Decker, R.M.; Flock, D.L. Thermal Stability and application of emulsion composed blocking agents for steam flooding. *J. Can. Pet. Technol.* **1988**, *27*, 69–78. [CrossRef]
25. Torrey, S. *Emulsions and Emulsifier Applications—Recent Developments*; Noyes Data Corporation: Park Ridge, IL, USA, 1984.
26. Friberg, S. *Food Emulsions*; Marcel Dekker: New York, NY, USA, 1976.
27. Lissant, K.J. *Emulsions and Emulsion Technology*; Marcel Dekker: New York, NY, USA, 1974.
28. Bennet, H.; Bishop, J.L.; Wulfinghoff, M.F. *Practical Emulsions—Applications*; Chemical Publishing Co.: New York, NY, USA, 1968.
29. Becher, P. *Emulsions: Theory and Practice*; Krieger Publishing Co.: Malabar, FL, USA, 1977.
30. Lynch, M.J.; Griffin, W.C. Food Emulsions. In *Emulsions and Emulsion Technology*; Lissant, K.J., Ed.; Marcel Dekker: New York, NY, USA, 1974.
31. Friberg, S.E.; Kayoli, I. Surfactant Association Structure, Microemulsions, and Emulsions. In *Foods–An Overview*; El-Nokaly, M., Cornell, D., Eds.; ACS Symposium Series 448; American Chemical Society: Washington, DC, USA, 1990.
32. Schut, J. Meat Emulsions. In *Food Emulsions*; Friberg, S., Ed.; Marcel Dekker: New York, NY, USA, 1976.
33. Graf, E.; Baver, H. Milk and Milk Products. In *Food Emulsions*; Friberg, S., Ed.; Marcel Dekker: New York, NY, USA, 1976.
34. Shepperd, I.S.; Yoell, R.W. Cake Emulsions. In *Food Emulsions*; Friberg, S., Ed.; Marcel Dekker: New York, NY, USA, 1976.
35. Krog, N.J.; Riisom, T.H.; Larsson, K. Applications in the Food Industry. In *Encyclopedia of Emulsion Technology*; Becher, P., Ed.; Marcel Dekker: New York, NY, USA, 1985; Volume 2.
36. Mully, B.A. Medicinal emulsions. In *Emulsions and Emulsion Technology, Part 1*; Lissant, K.J., Ed.; Marcel Dekker: New York, NY, USA, 1974.
37. Davis, S.S.; Hadgraft, J.K.; Palin, K.J. Medical and Pharmaceutical Applications of Emulsions. In *Encyclopedia of Emulsion Technology*; Becher, P., Ed.; Marcel Dekker: New York, NY, USA, 1985; Volume 2.
38. Bennet, H.; Bishop, J.L.; Wulfinghoff, M.F. Cosmetics. In *Practical Emulsions—Applications*; Chemical Publishing Co.: New York, NY, USA, 1968; Volume 2, Chapter 4.
39. Fox, C. Cosmetic emulsions. In *Emulsions and Emulsion Technology, Part II*; Lissant, K.J., Ed.; Marcel Dekker: New York, NY, USA, 1974.
40. Ford, R.E. The use of emulsions in the application of pesticides. In *Theory and Practice of Emulsion Technology*; Smith, A.L., Ed.; Academic Press: London, UK, 1976.
41. Bennet, H.; Bishop, J.L.; Wulfinghoff, M.F. Agricultural Emulsions. In *Practical Emulsions—Applications*; Chemical Publishing Co.: New York, NY, USA, 1968; Volume 2, Chapter 1.
42. Bampfield, H.A.; Cooper, J. Emulsion Explosives. In *Encyclopedia of Emulsion Technology*; Becher, P., Ed.; Marcel Dekker: New York, NY, USA, 1988; Volume 3.
43. Bennet, H.; Bishop, J.L.; Wulfinghoff, M.F. Bituminous Emulsions. In *Practical Emulsions—Applications*; Chemical Publishing Co.: New York, NY, USA, 1968; Volume 2, Chapter 2.
44. Allyn, G. Emulsion paints. In *Emulsions and Emulsion Technology*; Lissant, K.J., Ed.; Marcel Dekker: New York, NY, USA, 1974; Part 1, Chapter 7.
45. Benali, L. Rheological and granulometrical studies of a cutting oil emulsion. *J. Colloid Interface Sci.* **1993**, *156*, 454–461. [CrossRef]
46. Pal, R. Rheology of high internal phase ratio emulsions and foams. *Adv. Colloid Interface Sci.* **2025**, *339*, 103426. [CrossRef]
47. Taylor, G.I. The formation of emulsions in definable fields of flow. *Proc. R. Soc. Lond. A* **1934**, *146*, 501–523. [CrossRef]
48. Cox, R.G. The deformation of a drop in a general time-dependent fluid flow. *J. Fluid Mech.* **1969**, *37*, 601–623. [CrossRef]
49. Chaffey, C.E.; Brenner, H.J. A second-order theory for shear deformation of drops. *J. Colloid Int. Sci.* **1967**, *24*, 258–269. [CrossRef]
50. Brenner, H. Dynamics of neutrally buoyant particles in low Reynolds number flows. *Prog. Heat Mass Transf.* **1972**, *6*, 509–574.
51. Torza, S.; Cox, R.G.; Mason, S.G. Particle Motions in Sheared Suspensions XXVII Transient and Steady Deformation and Burst of Liquid Drops. *J. Colloid Int. Sci.* **1972**, *38*, 395–411. [CrossRef]

52. Barthes-Biesel, D.; Acrivos, A. Deformation and burst of a liquid droplet freely suspended in a linear shear field. *J. Fluid Mech.* **1973**, *61*, 1–21. [CrossRef]
53. Hakami, F.S.; Schowalter, W.R. The effects of shear and vorticity on deformation of a drop. *J. Fluid Mech.* **1980**, *98*, 635–645. [CrossRef]
54. Rallison, J.M. Note on the time-dependent deformation of a viscous drop which is almost spherical. *J. Fluid Mech.* **1980**, *98*, 625–633. [CrossRef]
55. Hinch, E.J.; Acrivos, A. Long slender drops in simple shear flow. *J. Fluid Mech.* **1980**, *98*, 305–328. [CrossRef]
56. Grace, H.P. Dispersion phenomena in high viscosity immiscible fluid systems and application of static mixers as dispersion devices in such systems. *Chem. Eng. Commun.* **1982**, *14*, 225–277. [CrossRef]
57. Acrivos, A. The breakup of small drops and bubbles in shear flows. *Ann. N. Y. Acad. Sci.* **1983**, *404*, 1–11. [CrossRef]
58. Rallison, J.M. The deformation of small viscous drops and bubbles in shear flows. *Ann. Rev. Fluid Mech.* **1984**, *16*, 45–66. [CrossRef]
59. Bentley, B.J.; Leal, L.G. An experimental investigation of drop breakup in steady two-dimensional flows. *J. Fluid Mech.* **1986**, *167*, 241–283. [CrossRef]
60. Stone, H.A. Dynamics of drop deformation and breakup in viscous fluids. *Annu. Rev. Fluid Mech.* **1994**, *26*, 65–102. [CrossRef]
61. Tsakolos, V.T.; Navard, P.; Peuvrel-Disdier, E. Deformation and breakup mechanisms of single drops during shear. *J. Rheol.* **1998**, *42*, 1403–1417. [CrossRef]
62. Guido, S.; Villone, M. Three-dimensional shape of a drop under simple shear flow. *J. Rheol.* **1998**, *42*, 395–415. [CrossRef]
63. Guido, S.; Greco, F.; Villone, M. Experimental Determination of Drop Shape in Slow Steady Shear Flow. *J. Colloid Int. Sci.* **1999**, *219*, 298–309. [CrossRef]
64. Guido, S.; Greco, F. Drop shape under slow steady shear flow and during relaxation. Experimental results and comparison with theory. *Rheol. Acta* **2001**, *40*, 176–184. [CrossRef]
65. Nguyen, T.T.; Hoang, V.T. Modeling droplet deformation and breakup in shear flow using Taylor analogy model. *Chem. Eng. Sci.* **2026**, *320*, 122370. [CrossRef]
66. Schowalter, W.R.; Chaffey, C.E.; Brenner, H. Rheological behaviour of a dilute emulsion. *J. Colloid Interface Sci.* **1968**, *26*, 152–160. [CrossRef]
67. Frankel, N.A.; Acrivos, A. The constitutive equation for a dilute emulsion. *J. Fluid Mech.* **1970**, *44*, 65–78. [CrossRef]
68. Brenner, H. Suspension rheology. In *Progress in Heat and Mass Transfer*; Elsevier: Amsterdam, The Netherlands, 1972; Volume 5, pp. 89–129.
69. Barthes-Biesel, D.; Acrivos, A. The rheology of suspensions and its relation to phenomenological theories for non-Newtonian fluids. *Int. J. Multiph. Flow* **1973**, *1*, 1–24. [CrossRef]
70. Hinch, E.J. The mechanics of fluid suspensions. In *Theoretical Rheology*; Hutton, J.F., Pearson, J.R.A., Walters, K., Eds.; Applied Science Publishers Ltd.: London, UK, 1974.
71. Choi, S.J.; Schowalter, W.R. Rheological properties of nondilute suspensions of deformable particles. *Phys. Fluids* **1975**, *18*, 420–427. [CrossRef]
72. Kennedy, M.R.; Pozrikidis, C.; Skolak, R. Motion and deformation of liquid drops, and the rheology of dilute emulsions in simple shear flow. *Comput. Fluids* **1994**, *23*, 251–278. [CrossRef]
73. Puyvelde, P.V.; Velankar, S.; Moldenaers, P. Rheology and morphology of compatibilized blends. *Curr. Opin. Colloids Interface Sci.* **2001**, *6*, 457–463. [CrossRef]
74. Lucassen-Reynders, E.H. Dynamic interfacial properties in emulsification. In *Encyclopedia of Emulsion Technology*; Becher, P., Ed.; Marcel Dekker: New York, NY, USA, 1996; Volume 4, Chapter 2.
75. Larson, R.G. *The Structure and Rheology of Complex Fluids*; Oxford University Press: New York, NY, USA, 1999; Chapter 9.
76. Stone, H.A.; Leal, L.G. Breakup of concentric double emulsion droplets in linear flows. *J. Fluid Mech.* **1990**, *211*, 123–156. [CrossRef]
77. Reboucas, R.B.; Nikolova, N.N.; Sharma, V. Modeling drop deformations and rheology of dilute to dense emulsions. *Curr. Opin. Colloid Interface Sci.* **2025**, *77*, 101904. [CrossRef]
78. Batchelor, G.K.; Green, J.T. The determination of the bulk stress in a suspension of spherical particles to order c2. *J. Fluid Mech.* **1972**, *56*, 401–427. [CrossRef]
79. Batchelor, G.K. *An Introduction to Fluid Dynamics*; Cambridge University Press: Cambridge, UK, 1967.
80. Nadim, A. A concise introduction to surface rheology with application to dilute emulsions of viscous drops. *Chem. Eng. Commun.* **1996**, *148–150*, 391–407. [CrossRef]
81. Taylor, G.I. The viscosity of a fluid containing small drops of another fluid. *Proc. R. Soc. A* **1932**, *138*, 41–48. [CrossRef]
82. Happel, J.; Brenner, H. *Low Reynolds Number Hydrodynamics*; Noordhoff International Publishing: Leydon, IL, USA, 1973.
83. Einstein, A. Eine neue Bestimmung der Molekuldimension. *Ann. Phys.* **1906**, *19*, 289–306. [CrossRef]
84. Einstein, A. Berichtigung zu meiner Arbeit: Eine neue Bestimmung der Molekuldimension. *Ann. Phys.* **1911**, *34*, 591–592. [CrossRef]

85. Hur, B.K.; Kim, C.B.; Lee, C.G. Functional relationship between volume concentration of dispersed phase and relative viscosity in a liquid-liquid dispersion and emulsion. *J. Ind. Eng. Chem.* **2000**, *6*, 318–324.
86. Han, C.D. *Multiphase Flow in Polymer Processing*; Academic Press: New York, NY, USA, 1981.
87. Wetzel, E.D.; Tucker, C.L. Droplet deformation in dispersions with unequal viscosities and zero interfacial tension. *J. Fluid Mech.* **2001**, *426*, 199–228. [CrossRef]
88. Pal, R. Fundamental rheology of disperse systems based on single-particle dynamics. *Fluids* **2016**, *1*, 40. [CrossRef]
89. Pal, R. Non-Newtonian behavior of suspensions and emulsions: Review of different mechanisms. *Adv. Colloid Interface Sci.* **2024**, *333*, 103299. [CrossRef]
90. Ohshima, H. Primary electroviscous effect in a dilute suspension in a dilute suspension of charged mercury drops. *Langmuir* **2006**, *22*, 2863–2869. [CrossRef]
91. Ohshima, H. Primary electroviscous effect in a moderately concentrated suspension of charged spherical particles. *Langmuir* **2007**, *23*, 12061–12066. [CrossRef]
92. Rubio-Hernandez, F.J.; Carrique, F.; Ruiz-Reina, E. The primary electroviscous effect in colloidal suspensions. *Adv. Colloid Interface Sci.* **2004**, *107*, 51–60. [CrossRef]
93. Russel, W.B. Bulk stresses due to deformation of the electrical double layer around a charged sphere. *J. Fluid Mech.* **1978**, *85*, 673–683. [CrossRef]
94. Vlahovska, P.; Blawzdziewicz, J.; Loewenberg, M. Nonlinear rheology of a dilute emulsion of surfactant-covered spherical drops in time-dependent flows. *J. Fluid Mech.* **2002**, *463*, 1–24. [CrossRef]
95. Blawzdziewicz, J.; Vlahovska, P.; Loewenberg, M. Rheology of a dilute emulsion of surfactant-covered spherical drops. *Phys. A* **2000**, *276*, 50–85. [CrossRef]
96. Mandal, S.; Das, S.; Chakraborty, S. Effect of Marangoni stress on the bulk rheology of a dilute emulsion of surfactant-laden deformable droplets in linear flows. *Phys. Rev. Fluids* **2017**, *2*, 113604. [CrossRef]
97. Edwards, D.; Brenner, H.; Wasan, D. *Interfacial Transport Processes and Rheology*; Butterworth-Hienemann: Boston, MA, USA, 1991.
98. Oldroyd, J.G. The effect of interfacial stabilizing films on the elastic and viscous properties of emulsions. *Proc. R. Soc. A* **1955**, *232*, 567–577. [CrossRef]
99. Oldroyd, J.G. Complicated rheological properties. In *Rheology of Disperse Systems*; Mill, C.C., Ed.; Pergamon Press: London, UK, 1959.
100. Danov, K.D. On the viscosity of dilute emulsions. *J. Colloid Interface Sci.* **2001**, *235*, 144–149. [CrossRef]
101. Pimenta, P.H.N.; Oliveira, T.F. Study on the rheology of a dilute emulsion of surfactant-covered droplets using the level set and closest point methods. *Phys. Fluids* **2021**, *33*, 103306. [CrossRef]
102. Pal, R. *Rheology of Particulate Dispersions and Composites*; CRC Press: Boca Raton, FL, USA, 2007.
103. Barthes-Biesel, D.; Chhim, V. The constitutive equation of a dilute suspension of spherical microcapsules. *Int. J. Multiph. Flow* **1981**, *7*, 493–505. [CrossRef]
104. Drochon, A. Rheology of dilute suspensions of red blood cells: Experimental and theoretical approaches. *Eur. Phys. J. Appl. Phys.* **2003**, *22*, 155–162. [CrossRef]
105. Brunn, P.O.; Roden, T. On the deformation and drag of a type-A multiple drop at low Reynolds number. *J. Fluid Mech.* **1985**, *160*, 211–234. [CrossRef]
106. Palierne, J.F. Linear Rheology of Viscoelastic Emulsions with Interfacial Tension. *Rheol. Acta* **1990**, *29*, 204–214. [CrossRef]
107. Oosterbrook, M.; Mellema, J. Linear Viscoelasticity of Emulsions I. The Effect of an Interfacial Film on the Dynamic Viscosity of Nondilute Emulsions. *J. Colloid Interface Sci.* **1981**, *84*, 14–26.
108. de Bruijn, R.A.; Mellema, J. The linear-viscoelastic behaviour of a dispersion of transversely rigid spherical capsules. *Rheol. Acta* **1985**, *24*, 159–174. [CrossRef]
109. Smenlders, J.B.A.F.; Blom, C.; Mellema, J. Linear viscoelastic study of lipid vesicle dispersions: Hard-sphere behavior and bilayer surface dynamics. *Phys. Rev. A* **1990**, *42*, 3483–3498. [CrossRef]
110. Smenlders, J.B.A.F.; Mellema, J.; Blom, C. Changing mechanical properties of lipid vesicle bylayers investigated by linear viscoelastic measurements. *Phys. Rev. A* **1992**, *46*, 7708–7722. [CrossRef] [PubMed]
111. Seki, K.; Komura, S. Viscoelasticity of vesicle dispersions. *Phys. A* **1995**, *219*, 253–289. [CrossRef]
112. Jaensson, N.O.; Anderson, P.D.; Vermant, J. Computational interfacial rheology. *J. Non-Newton. Fluid Mech.* **2021**, *290*, 104507. [CrossRef]
113. Appleford, T.; Sanjay, V.; Jalaal, M. Rheology of two-dimensional dilute emulsions. *Phys. Rev. Fluids* **2026**, *11*, 033607. [CrossRef]
114. Pozrikidis, C. Numerical investigation of the effect of surfactants on the stability and rheology of emulsions and foam. *J. Eng. Math.* **2001**, *41*, 237–258. [CrossRef]
115. Choi, S.B.; Lee, J.S.; Baik, S.J.; Lee, J.S. Numerical simulations for the rheological characteristics of emulsions under several conditions including temperature, shear rate, surfactant concentration and droplet size. *Micro Nano Lett.* **2014**, *9*, 896–900. [CrossRef]

116. Rosti, M.E.; De Vita, F.; Brandt, L. Numerical simulations of emulsions in shear flows. *Acta Mech.* **2019**, *230*, 667–682. [CrossRef]
117. Skartlien, R.; Sollum, E.; Akselsen, A.; Meakin, P. Direct numerical simulation of surfactant-stabilized emulsions. *Rheol. Acta* **2012**, *51*, 649–673. [CrossRef]
118. Oliveira, T.F.; Cunha, F.R. Emulsion rheology for steady and oscillatory shear flows at moderate and high viscosity ratio. *Rheol. Acta* **2015**, *54*, 951–971. [CrossRef]
119. Narsimhan, V. Shape and rheology of droplets with viscous surface moduli. *J. Fluid Mech.* **2019**, *862*, 385–420. [CrossRef]
120. Aggarwal, N.; Sarkar, K. Rheology of an emulsion of viscoelastic drops in steady shear. *J. Non-Newton. Fluid Mech.* **2008**, *150*, 19–31. [CrossRef]
121. Rosti, M.E.; Takagi, S. Shear-thinning and shear-thickening emulsions in shear flows. *Phys. Fluids* **2021**, *33*, 083319. [CrossRef]
122. Sorgentone, C.; Tornberg, A.K. A highly accurate boundary integral equation method for surfactant-laden drops in 3D. *J. Comput. Phys.* **2018**, *360*, 167–191. [CrossRef]
123. Hsu, S.H.; Chu, J.; Lai, M.C.; Tsai, R. A coupled grid based particle and implicit boundary integral method for two-phase flows with insoluble surfactant. *J. Comput. Phys.* **2019**, *395*, 747–764. [CrossRef]
124. Iqbal, K.Z.; Izbassarov, D.; Brandt, L.; Tammisola, O. Numerical study on rheology of emulsions and bubbly suspensions with elastoviscoplastic matrix fluids in simple shear. *Phys. Rev. Fluids*, 2026, *in press*. [CrossRef]

Disclaimer/Publisher's Note: The statements, opinions and data contained in all publications are solely those of the individual author(s) and contributor(s) and not of MDPI and/or the editor(s). MDPI and/or the editor(s) disclaim responsibility for any injury to people or property resulting from any ideas, methods, instructions or products referred to in the content.